NTNU – Trondheim
Norwegian University of
Science and Technology

Nonlinear Analysis of Fibre Reinforced Concrete Beams

Influence of fibre orientation and density

Øyvind Trygge Moltubakk

Department of Structural Engineering
Faculty of Engineering Science and Technology
NTNU- Norwegian University of Science and Technology

ACCESSIBILITY

OPEN

MASTER THESIS 2014

SUBJECT AREA:	DATE:	NO. OF PAGES:
Concrete Structures	10.06.2014	17+94+27

TITLE:

**Nonlinear Analysis of Fibre Reinforced Concrete Beams:
Influence of fibre orientation and density**

Ikke-lineære analyser av fiberarmerte betongbjelker:
Påvirkning fra fiberretning og densitet

BY:

Øyvind Trygge Moltubakk

SUMMARY:
This master thesis examines nonlinear analysis of fibre reinforced concrete in DIANA, what influence changes in fibre orientation and density have on the load capacity and the load-bearing ability when the displacement grows. The report includes background theory for non-linear analysis to give a better understanding of the analysis. Additionally the report include a literature study, based on earlier research and published material about fibre reinforced concrete and its mechanical properties.

The beams were modeled after the rules in NS-EN 14651. Mostly the analysis were run with a displacement control up to a displacement of 4 mm. Calculations were done to check the contribution from the fibres to the shear capacity. The calculations were based on a set of rules suggested by COIN. Because of the existence of the notch, the first crack will always occur in the mid-section. The results showed that with a good consistency between the normal vector for the crack and the orientation of the fibres, it would be considerable contributions to the shear capacity. With higher density in the critical area, this contribution would become larger. The results from the analysis showed that up to 45 degrees between the normal vector and the fibre orientation the fibres would have a positive effect on the load-bearing capacity also after larger displacement when cracks have occurred.

RESPONSIBLE TEACHER: Max Hendriks

SUPERVISOR(S): Max Hendriks, Elena Vidal Sarmiento

CARRIED OUT AT: Department of Structural Engineering

Abstract

This master thesis examines nonlinear analysis of fibre reinforced concrete in DI-ANA, what influence changes in fibre orientation and density have on the load capacity and the load-bearing ability when the displacement grows. The most important part of the report are the modeling and results from the analysis.

The first part of the report includes background theory for nonlinear analysis to give a better understanding of the analysis. Additionally the report include a literature study, based on earlier research and published material about fibre reinforced concrete and its mechanical properties. Especially the residual tensile strength is interesting, since it is here the fibres become the most useful.

Both modeling and analysis have been done in the FEM-program DIANA. The beams were modeled after the rules in NS-EN 14651. Mostly the analysis were run with a displacement control up to a displacement of 4 mm to make it easier to see what influence the specific types of fibre reinforced concrete had on the load-capacity with increasing displacement. Force-controlled analysis were also tested, but most of the analysis stopped shortly after reaching the maximum load-capacity because of convergence.

Calculations were done to check the contribution from the fibres to the shear capacity. The calculations were based on a set of rules suggested by COIN. Because of the existence of the notch, the first crack will always occur in the mid-section. The results showed that with a good consistency between the normal vector for the crack and the orientation of the fibres, it would be considerable contributions to the shear capacity. With higher density in the critical area, this contribution would become larger. The results from the analysis showed that up to 45 degrees between the normal vector and the fibre orientation, the fibres would have a positive effect on the load-bearing capacity after larger displacements when cracks have occurred.

This thesis shows that through FEM-analysis it is possible to make good models of fibre reinforced concrete. However, more research on strain softening and hardening of FRC, and how to look at local changes, are necessary. In addition a set of design rules should be developed.

i

Sammendrag

Denne masteroppgaven tar for seg ikke-lineære analyser av fiberarmert betong i DIANA, og hvilken innflytelse endringer av fiberretning og densitet har å si for lastkapasiteten og bæringsevnen etter hvert som nedbøyningen øker. Den viktigste delen av rapporten er utførelsen av analysene og resultatene derfra.

Første del av oppgaven består av bakgrunnsteori for ikke-lineære analyser for å gi en bedre forståelse av analysene. I tillegg inneholder rapporten et litteraturstudium basert på tidligere forskning og utgitt materiale om fiberarmert betong, som gir en kort introduksjon til temaet. Dette er etterfulgt av de mekaniske egenskapene til fiberarmert betong. Spesielt er redusert strekkfasthet interessant, siden det er her fibrene kommer mest til nytte.

Både modellering og analysene ble utført i DIANA. Mesteparten av analysene ble gjort med en nedbøyningskontroll hvor man tvang bjelken, modellert etter NS-EN 14651, til en nedbøyning på 4 mm før analysene ble stoppet. Dermed kunne man lettere se hvilken effekt fibrene hadde på betongen etter hvert som belastningen ble større. Det ble også utført lastkontrollerte analyser, men på grunn av konvergens stoppet de fleste analysene like etter maksimum last-kapasitet var nådd.

Det er også gjort beregninger på bidraget fra fibrene til skjærkapasiteten til betongen. Regelverket som er lagt til grunn for beregning av bidraget fra fiberarmeringen til skjærkapasiteten er foreslått av COIN. På grunn av snittet i midten ville det første risset til enhver tid oppstå her. Resultatene viste som ventet at ved god overenstemmelse mellom riss og retning ville det være bidrag vært å ta med i betrakningen for skjærkapasiteten. Ved høyere densitet i kritiske områder ville dette bidraget bli enda større. Resultatene fra analysene viste at ved opptil 45 grader mellom normalvektoren til risset og fiberretningen ville fibrene komme med gode bidrag til lastkapasiteten også ved større nedbøyninger etter at riss har oppstått.

Denne rapporten viser at man gjennom FEM-analyser kan lage gode modeller for å analysere fiberarmert betong. Men mer forskning på området, og utvikling av flere modeller for å se på lokale endringer er derimot nødvendig. I tillegg bør det komme standardiserte metoder for å se på tøyningen etter at den fiberarmerte betongen har nådd strekkfastheten på. For beregninger må et regelverk på plass.

Preface

This report is the end result of a master thesis written at the Department of Structural Engineering at the Norwegian University of Science and Techology (NTNU) the spring of 2014.

After a rough start when learning DIANA, it was interesting to see how the changing properties of the fibres influenced the capacity of the beams. Even though my research is just a small part in looking at the behaviour of FRC, it was inspiring to work with something that is very actual.

I would like to thank my supervisors Max Hendriks and Elena Sarmiento for valuable guidance and help along the way.

Trondheim, 08.06.14

Øyvind Trygge Moltubakk

Contents

List of Figures

List of Tables

Symbols and abbreviations

Latin upper case letters

$C_{Rd,c}$	Factor
$\mathbf{D}$	Displacement vector
E	Young's Modulus
G	Shear modulus
G_f	Fracture energy
F	Force
F_j	Load corresponding to CMOD = $CMOD_j$ (j=1,2,3...)
$\mathbf{K}$	Coefficient matrix
$\mathbf{K}_i$	Tangential stiffness of the structure
L	Length of the beam
M_{Rd}	Moment capacity
$\mathbf{R}$	Load vector
S_f	Tensile force in fibre reinforced concrete
T_c	Compressive force in concrete
$V_{Rd,c}$	Shear capacity
$V_{Rd,cf}$	Shear resistance from fibre reinforced concrete
$V_{Rd,ct}$	Shear resistance from concrete without shear reinforcement

Latin lower case letters

b	Width of the cross-section
b_w	Width of the web
d	Effective depth
$\mathbf{f}_{ext}$	External vector
f_c	Limit compression strength
f_{ck}	Characteristic cylinder compressive strength
f_{cm}	Mean cylinder compression strength
$f_{ftd,res,2.5}$	Design residual tensile strength
$f_{ftk,res,2.5}$	Characteristic residual tensile strength at CMOD = 2.5 mm
$f_{R,j}$	Residual flexural tensile strength at CMOD = $CMOD_j$ (j=1,2,3,...)

f$_{Rk,3}$	Characteristic residual flexural tensile strength at CMOD = 2.5 mm
f$_t$	Limit tensile strength
g	Out-of-balance force factor
h	Height of the cross-section
h$_{el}$	Element size
h$_{sp}$	Distance between the tip of the notch and the top of the specimen
k	Factor
k$_1$	Factor
l	Span length
l$_{ch}$	Characteristic length
t	Thickness
u	Iterative displacement increment
u^c	Predescribed displacement
v$_f$	Volume fraction
w$_1$	Factor
w$_2$	Factor

Greek letters

α	Shear retention factor
γ_{cf}	Material factor for the residual tensile strength
Δ**u**	Displacement increment
δ	Displacement, in millimetres
δ_j	Displacement corresponding to a specific loading
ε	Strain
θ	Angle between the normal vector from the crack and the fibre orientation
μ	Factor
ν	Poisson ratio
ν_{min}	Factor
ρ_l	Factor
σ	Stress
σ_1	Maximum tensile strength
σ_2	Residual tensile strength
σ_{cp}	Axial stress in concrete

Abbreviations

COIN   Concrete Innovation Centre
CMOD   Crack Mouth Opening Displacement
EC2   Eurocode 2
FE   Finite Element
FEA   Finite Element Analysis
FEM   Finite Element Method
FIB   Fédération Internationale du Béton
        /the International Federation for Structural Concrete
FRC   Fibre Reinforced Concrete
MO1   Modified area 1
MO2   Modified area 2
NFEM   Nonlinear Finite Element Method
NR   Newton-Raphson
SFRC   Steel Fibre Reinforced Concrete
SLS   Serviceability-Limit State
ULS   Ultimate-Limit State

Chapter 1

Introduction

In the search of ways to improve the building industry, there is an increased interest for fibre reinforced concrete, which can give the constructions advantages like reduced work time, improved working conditions and more complexed geometry of the casting moulds.

In this master thesis, written at Department of Structural Engineering at NTNU, a version of the bending test for concrete according to NS-EN 14651 is recreated in the finite element program DIANA and analyzed with different properties for fibre reinforced concrete.

The object is to investigate by nonlinear analysis what effect changes in orientation and density have on the load-carrying ability for the beam. Earlier experiments have showed an increased load-bearing capacity after cracking occur, which leads to higher shear capacity for the beams. The method is based on a paper written by Elena Sarmiento [3], where a numerical approach is presented.

The difference in the beams analyzed is their residual tensile strength. The first part only consider the orientation of the fibres, but later on also varying density is included.

The orientation analysis are divided into four parts. At first the orientation is the same in the whole beam. But because of the existence of the notch, required from the test, which make the first crack happen in the mid-span, a modified section is made in the area over the notch. The second part have varying orientations inside the mid-section analyzed keeping the same orientation in the rest of the beam. To see what influence the modified area and the orientation around has to say, the area is exceeded and analyzed as the third approach. At last in the orientation analysis, the beam is modeled with the width divided into two layers to make an approach more close to reality.

The density analysis are divided into two different approaches. In the first one the density varies inside the modified with the same orientation as the rest of the beam, while it in the second one varies with horizontal fibre orientation and 0.5 vol.-% in the rest of the beam.

In addition to the modeling, analysis and results, a literature study including the background for finite element analysis, fibres and their properties are presented. Following is the set-up for the report:

Chapter 2	Background theory for finite element analysis, including incremental and iterative procedures and convergence criteria.
Chapter 3	Introduction to fibres, their behaviour and requirements
Chapter 4	Mechanical properties for fibre reinforce concrete, together with a description of how these properties are governed in the analysis.
Chapter 5	Description of the modeling done in DIANA
Chapter 6	Results from the analysis of the different fibre reinforced concrete beams

Chapter 2

Finite Element Method

2.1 Finite Element Analysis

Finite element analysis (FEA), or so-called Finite Element Method (FEM), is a method for numerical solution of field problems. Those problems are mathematically described by differential equations or by an integral expression. To discretize the mathematical model either description can be used to formulate the finite elements in a mesh, which is a particular arrangement of elements. Numerically, the FE mesh is represented by a system of algebraic equations to be solved for unknowns at nodes. Those nodal unknowns are values of the field quantity and, perhaps also, its first derivatives. [20]

FEA has many advantages. It is applicable to any field problem and has no geometric restrictions. Material properties do not need to be isotropic and may change from element to element, which is a huge advantage when analyzing fibre reinforced concrete and other problems with difficult material behaviour. The same is the case for problems involving difficult geometry.

2.2 Nonlinear Finite Element Analysis

In difference to Linear Finite Element Analysis, successful nonlinear FEA requires more understanding of equation-solving procedures, because a single strategy may not work for all problems. It can take several attempts and changes in strategies to get results that is satisfactory for the analysis.

Nonlinear finite element analysis takes into account the nonlinear material properties in concrete and reinforcement, like cracking and yielding, and the influence of changing geometry on the response. Hence, it is the most accurate prediction of the response in a structure, but it is also very time consuming. [17]

In nonlinear analysis, the nonlinear system of equations must be solved iteratively until equilibrium has been reached. To do this DIANA [2] offers the well-known iteration schemes; Constant and Linear Stiffness, Regular and Modified Newton-Raphson.

All iteration schemes may be combined with Arc-length control methods to adapt the loading during iterations in a load step. An Indirect Displacement control option is available to cope with problems like snap-through and snap-back behaviour. To stabilize the convergence or increase its speed, a Line Search algorithm may be applied. In this thesis, displacement-controlled load is used to force the model to a deflection of 4 mm in the mid-span.

The types of nonlinearity include material nonlinearity, contact nonlinearity and geometric nonlinearity. When a structure is subjected to material nonlinearity the material properties are functions of the state of stress and strain including elasticity, plasticity and creep. Problems in these categories are nonlinear because stiffness, and sometimes load as well, become functions of displacement or deformation.

Briefly explained the nonlinear problems cause that in structural equations, as shown in equation 2.1, coefficient matrix $[\mathbf{K}]$ and perhaps load vector $\{\mathbf{R}\}$ becomes functions of $\{\mathbf{D}\}$. It then becomes impossible to immediately solve for $\{\mathbf{D}\}$, as in equation 2.2, because the information needed to conduct $[\mathbf{K}]$ and $\{\mathbf{R}\}$ is not known in advance. An iterative process is required to obtain $\{\mathbf{D}\}$, and its associated $[\mathbf{K}]$ and $\{\mathbf{R}\}$, such that the product of $[\mathbf{K}] \cdot \{\mathbf{D}\}$ is in equilibrium with $\{\mathbf{R}\}$, see equation 2.3. [20]

$$[\mathbf{K}]\{\mathbf{D}\} = \{\mathbf{R}\} \tag{2.1}$$

$$\{\mathbf{D}\} = [\mathbf{K}]^{-1}\{\mathbf{R}\} \tag{2.2}$$

$$[\mathbf{K(d)}]\{\mathbf{D}\} = \{\mathbf{R(d)}\} \tag{2.3}$$

When the problems are nonlinear, the principle of superposition is not applicable. Each different load case(or step) requires a separate analysis, which make it impossible to scale results in proportion to load or superpose results from different load cases. To solve this set of equations, incremental and iterative procedures are introduced.

2.2.1   Incremental-iterative solution procedure

In nonlinear Finite Element Analysis the relation between force vector, $\{\mathbf{R}\}$, and the displacement vector, $\{\mathbf{D}\}$, becomes nonlinear and the displacement are often dependent on the displacement on earlier stages, e.g. in case of plastic material behaviour. To determine the state of equilibrium, the problems need to be discrete in space with the help from finite elements and in time with increments. To achieve equilibrium at the end of an increment, an iterative solution algorithm is used. The combination is called an incremental-iterative solution procedure. [2]

The choice of the step size for every increment is an important factor in the incremental-iterative process. The optimal choice of incremental step depends on the shape of equilibrium path, the objective of the analysis and the solution algorithm employed.[9]

Incremental procedure

When solving NFEM problems, the load is applied in several load steps, also known as an *incremental load step procedure*. The two most common incremental load step procedures are load control and displacement control. Both procedures increases the applied load for each increment, but they use two different approaches.[19] With load control, the applied load is increased for each increment by directly increasing the external vector $\mathbf{f}_{ext}$. With displacement control, the load is represented with fixed, prescribed displacements, $\mathbf{u}^c$, instead of actual load (Figure 2.1(b)).
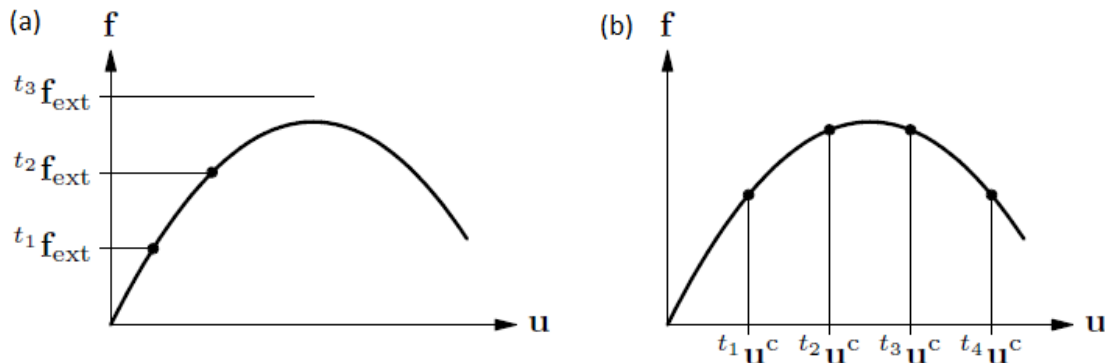
Figure 2.1: Incremental procedure from DIANA User Manual [2]. Figure (a) illustrates load controlled procedure, while (b) illustrate displacement controlled procedure

With load control, the load can only increase for each incremental step. This means that the force control cannot pass limit points. Displacement control, on the other hand, increases the fixed displacement for each incremental step so it can pass limit points, but not turning points. For force-control to overcome the problem and make

the increment pass turning points, Arc-length Control, as shown in figure 2.2, need to be introduced.

Arc-length method

A variation of the iteration algorithm is the Arc-length method. This method adapts the increment size. When using arc-length controlled analysis it is possible to analyze snap-through behaviour, just as for displacement controlled analysis. But where the displacement control fails when it comes to snap-back behaviour, the arc-length method is capable of passing these points, as shown in figure 2.2. When running force-controlled analysis it is therefore an advantage to apply arc-length.
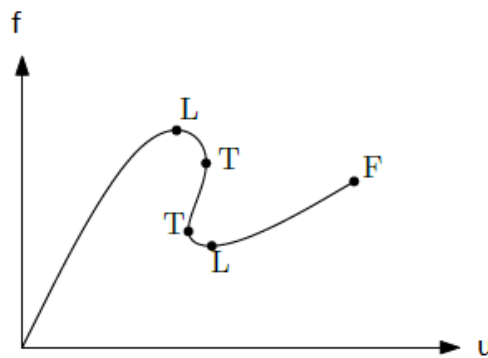
Figure 2.2: Snap-back with limit (L), turning (T) and failure (F) points [19]

Iterative procedure

DIANA offers various solution procedures needed to solve the system of equations of a finite element model. To solve the set of equations for each incremental step, the solution procedure need to iterate until convergence is achieved. One of most commonly used methods is the procedure used in this thesis, the Newton-Raphson method (NR).

The two most general subclasses are *Regular* and *Modified* Newton-Raphson method. Both method uses *Line search iterations* to determine the iterative increment of the displacement vector (Figure 2.4). The difference between them is the point where the stiffness matrix is evaluated.

With Regular NR iteration the stiffness matrix is evaluated for every iteration, illustrated in figure 2.3(a). The prediction of line search iteration is therefore based on the last known situation, equilibrium state or not. Because of this Regular NR is quite computational expensive, but it uses few iterations to reach convergence to the final solution.

An alternative to Regular NR is Modified Newton-Raphson, figure 2.3(b). In Modified NR the stiffness matrix is only updated one time for each increment, at the beginning. This means that the prediction is always based on a converged equilibrium state, and usually Modified NR converges slower to equilibrium than Regular. This leads to more iterations, but every iteration is faster than for Regular NR [2].

Figure 2.3: Iterative procedures: Regular Newton-Raphson(a) and Modified Newton-Raphson(b). $\mathbf{g}$ is the out-of-balance force factor and $\Delta\mathbf{u}$ is the displacement increment [2]

In a Newton-Raphson method, the stiffness matrix $\mathbf{K}_i$ represents the tangential stiffness of the structure, and can be derived from figure 2.3 as the following:

$$\mathbf{K}_i = \frac{\partial \mathbf{g}}{\partial \Delta \mathbf{u}} \tag{2.4}$$

Line search iteration

In structures with high nonlinearities, like cracking, a common problem is that the iteration process is not going to converge since the prediction is too far from equilibrium. Line search algorithms can increase the convergence rate and are especially useful if the ordinary iteration process fails. [2]

Figure 2.4: Line Search Iteration [2]

7

2.2.2 Convergence

When the results are satisfactory the iteration process need to be stopped. For this purpose, there are several different convergence criteria, e.g. force norm, displacement norm, energy norm or residual norm. For each increment the iterations continue until convergence is achieved, or maximum numbers of iterations occur. Figure 2.5 shows the items used to set up the various norms. Both detection of divergence and convergence are based on the same norm.
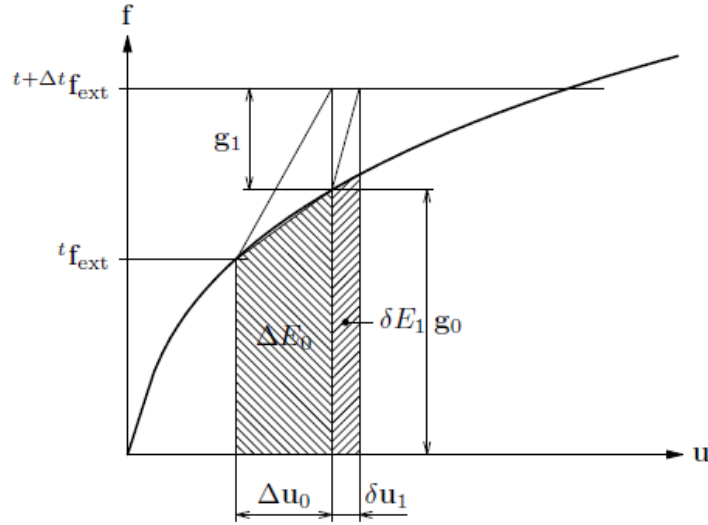
Figure 2.5: Norm items [2]

For the analysis in this report the displacement norm and the force norm are used. The force norm is the Euclidian norm of the out-of-balance vector $\mathbf{g}$, while the displacement norm is the Euclidian norm of the iterative displacement increment $\mathbf{u}$. To check convergence, the force norm after the current iteration is checked against the norm of the initial unbalance $\mathbf{g}_0$. The displacement norm, on the other hand, is checked against the norm of the displacement increments in the first prediction of the increment. [2]

$$\text{Force norm ratio} = \frac{\sqrt{g_i{}^T \cdot g_i}}{\sqrt{g_0{}^T \cdot g_0}} \tag{2.5}$$

$$\text{Displacement norm ratio} = \frac{\sqrt{\delta u_i{}^T \cdot \delta u_i}}{\sqrt{\Delta u_0{}^T \cdot \Delta u_0}} \tag{2.6}$$

Chapter 3

Fibre Reinforced Concrete

3.1 Concrete

Concrete is a composite material, and is a mixture of coarse gravel (pebble), sand, cement, water, admixtures and mineral additives, such as pozzolans. Fine and coarse aggregates make up approximately 70% of the volume, while the remaining 30% are considered as cement paste. Coarse aggregate is defined as crushed or natural particles of rock with diameter larger than 4 mm.[6] Figure 3.1 gives an overview over the composition of concrete. Because concrete is a plastic material in the fresh phase, there is virtually no limit to the architectural design for a concrete structure.[21]
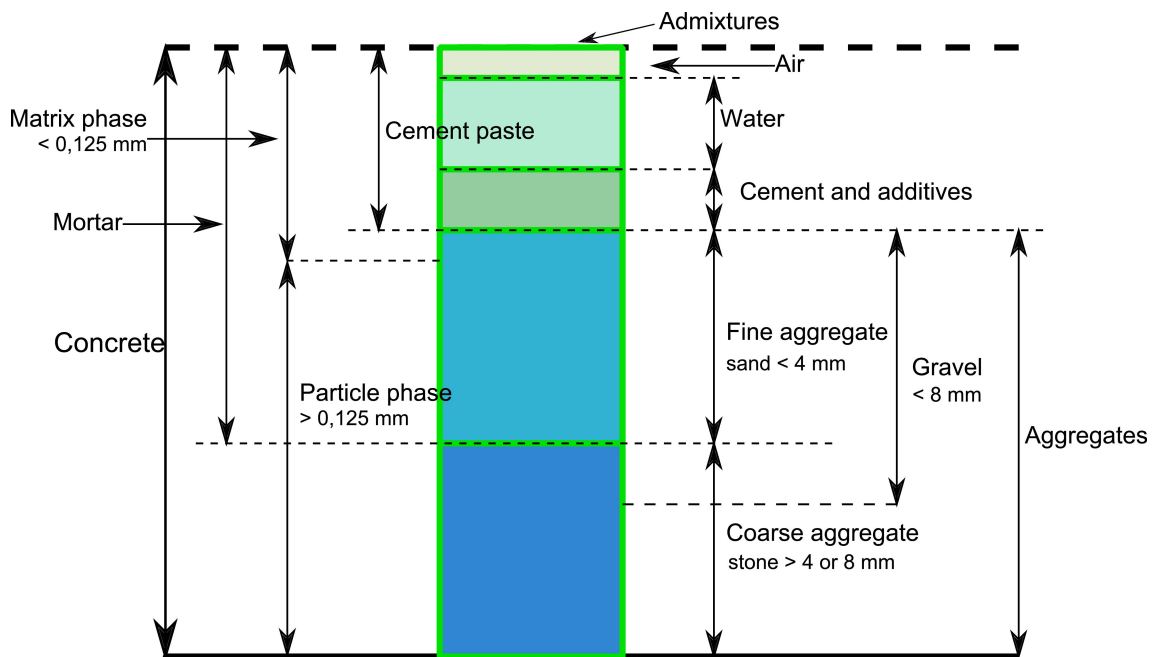
Figure 3.1: Composition of concrete [6]

9

Concrete has a completely nonlinear stress-strain behavior in compression, and have excellent properties when it is subjected to that. The ability to resist tensile stresses, on the other hand, are really poor, and concrete has therefore a very low tension strength compared to compression.

Reinforced concrete

Concrete cracks at relative small tensile strains, leading to a rapid decrease in capacity. That makes concrete a brittle material [21]. To compensate for this, and make the concrete able to resist tensile stresses, steel reinforcement, which can tolerate large tension forces, is normally placed in the tensile zone. That give what is known as reinforced concrete, and like for non-reinforced concrete it is a material with highly nonlinear behaviour. The reinforcement steel added reduce crack widths, and gives the construction a ductile behaviour and increased strength. Concrete helps with both corrosion- and fire protection for the steel.

Today, reinforced concrete is one of the most important building materials in constructions. Economy, suitability, workability and durability of the material are some of the advantages that makes it attractive. For a reinforced concrete structure to be successful the construction need to be strong and secure, behave as predicted, have good durability and a low cost.[24]

3.2 Fibre reinforced concrete

As already mentioned, concrete is a brittle material with low tensile strength. Therefore, it is needed to add some kind of reinforcement, usually steel bars, to improve its tensile qualities. Another way to improve the tensile strength is to add reinforcement fibres. Fibre reinforced concrete (FRC) can be defined as concrete reinforced with relatively short, discrete, discontinuous fibres instead of large unidirectional continuous steel bars (traditional steel reinforcement).

The use of fibre reinforcement will normally not affect the strain at cracking either, but the fibres are capable to transfer stresses across cracks, leading to a significant improvement of the residual strength. Another benefit of fibres is reduced crack width and spacing. Concrete carries flaws and micro-cracks in the material and at the interfaces even before an external load is applied. Under an applied load, these micro-cracks unite and larger, possibly critical, cracks occur. The fibres tend to bridge the cracks and thereby control the crack development and prevent the occurrence of large crack widths. [1]

Even at low fibre contents, the addition of fibres significantly increases the post-cracking toughness and ductility of the concrete. With sufficient amount of fibres

the residual strength may also be increased and become larger than the cracking strength. But this will require a high volume percentage of fibres to get any substantial increase.[21] The enhanced post-cracking tensile softening behaviour and crack control of concrete, may lead to significant improvements in the behaviour of the resulting structural members, both in ULS and SLS. [10]

Use of FRC for structural applications therefore holds the potential for reducing, or even eliminating, the conventional bar reinforcement, which in turn may lessen the congestion of reinforcement, get decreased height of the structure and lead to designs that are more efficient. Compared with non-reinforced concrete considerable reduction in thickness can be obtained with SFRC.

However, in Norway today, fibres are only used for structural parts where reinforcement is not statically required. The use is mainly limited to walls and slabs on grade where only a minimum amount of reinforcement according to EC2 [12] is needed for crack control. In such structures, fibre reinforcement might be able to replace the traditional reinforcement completely, and may be a more cost effective alternative, even though the material cost is somewhat larger than for traditional reinforcement. This is caused by the decreasing amount of work to be done before casting.

The biggest advantages for FRC compared to traditional reinforcement are presented by COIN 29-2011[4] as:

- Reduced working hours

- Transportation throughout the floor

- Larges jointless areas

- Smaller and less cracks

- Considerably reduction in thickness compared to non-reinforced concrete when used in roads and airports

General requirements for the fibres

For fibres to be effective in a concrete mix, Löfgren[8] has proposed that they should have the following properties:

- A tensile strength much higher than the one in the matrix (two or three orders)

- A bond strength between the matrix and the fibre of at least the same order as the tensile strength in the matrix, preferably higher.

- At least three times as high elastic modulus in tension for the fibres than the matrix.

- A ductility high enough so fibres do not fracture due to fibre abrasion or bending.

- The same order of the Poisson ratio and the coefficient of thermal expansion of the fibres for both fibres and matrix. Higher Poisson ratio of the ratio may lead to debonding due to lateral contraction of the fibres.

- Additionally, the fibres must be durable and able to withstand the high alkaline environment.

3.2.1 Steel fibres

There are many different types of fibres that can be used in fibre reinforced concrete, but most common is steel and synthetic fibres. The fibres of interest in this thesis are steel fibres, which are the most used and best examined fibre type. Table 3.1 presents typical steel fibre properties.

Length	60 mm
Diameter	0.75 mm
E-modulus	190-210 GPa
Tensile yield strength	200 - 2600 MPa
Specific gravity	7,85 $g/_{cm^3}$
Ultimate elongation	$0,5 - 5\%$ ̧
Fibres/kg	4600 (example)
Surface	Round, smooth with end hooks (example)

Table 3.1: Physical fibre properties [8]

The fibres are classified after which basic materials they are produced from [4]. The most common type is class I, cold-drawn wire.

Class	Type
I	Cold-drawn wire
II	Cut sheet
III	Melt extracted
IV	Shaved cold drawn wire
V	Milled from blocks

Table 3.2: Classifications by COIN 29-2011 [4]

The steel fibres may have different shapes, usually with deformed end to ensure good bonding. The most usual design is with end hooks, which give a more ductile fracturing than most of the other fibre shapes. Typical diameter of steel fibres are 0.5 to 1 mm and the length are between 25 and 60 mm. In this thesis 0.75 mm and 60 mm, respectively.
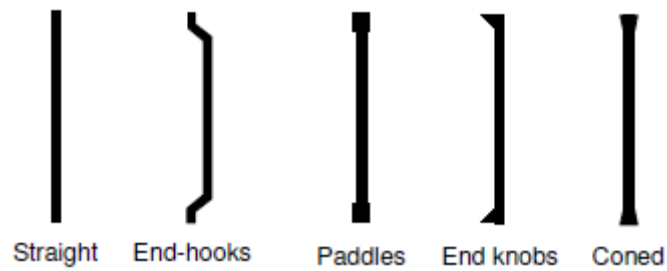
Figure 3.2: Example of fibre geometry [8]

The steel fibres will not become active until crack openings of a certain size appear, but they will gain full strength at smaller CMODs(Crack mouth opening displacement) than other fibre reinforcement.

An disadvantage is the aesthetic prospect. Because of the random distribution, some of the fibres will be at the top of the surface of the structure. These might rust so that the surface gets discoloured. [18]

The physical properties of the steel fibres that are considered to have the most influence on the performance in concrete are according to general design (Concrete society, 2007) [7]:

- Bond and anchorage mechanism
- Fibre length and diameter
- Dosage (kg/m^3)
- Tensile strength
- Elastic modulus

13

Chapter 4

Mechanical Properties

4.1 Introduction

The stress-strain relation for non-reinforced concrete has nearly linear elastic response up to about 30% of the compressive strength, before it exhibits strain softening until failure by crushing, because micro-cracks are developed.[8] When fibres are added into the concrete mix, they generally improve several mechanical properties of the FRC, depending on the volume fraction, bond and fibre distribution. [23]

When adding fibres especially the increase in post-cracking toughness and ductility are advantageous. The fibres can resist micro-cracks from developing into larger cracks either from external loads or from drying shrinkage. When the material becomes ductile, the fibres that span the cracks that have formed will give the concrete a residual load-carrying capacity. By increased toughness means that the area under the stress-strain curve is significant larger than for non-reinforced concrete. It can be defined as the energy absorption capacity of the material. [10]

Based on the same fundamentals as the design for traditionally reinforced concrete, the design of SFRC according to the RILEM $\sigma - \epsilon$ -design method (Hooks law) defines a load-deflection or load-CMOD relationship, where the load at predefined deflections/CMODs is the base for determining the concrete's residual or equivalent flexural strength. [7]

f_c [MPa]	f_t [MPa]	E [GPa]	G_f [Nm/m^2]	l_{ch} [mm]
20-80	1.5-5.0	25-40	>500	>1000

Table 4.1: Mechanical properties for fibre reinforced concrete [8]

In table 4.1 the mechanical properties proposed by Löfgren [8] are presented. The characteristic length, first presented by Hillerborg (1976)[26], can give an indication of the brittleness in the material, and is defined as:

$$l_{ch} = \frac{E_c \cdot G_f}{f_t^2} \tag{4.1}$$

Orientation and distribution of fibres

To investigate how the orientation and distribution of the fibre influence the load-carrying capacity is the main goals of this thesis. The first study in the analysis is to look at how different orientations affect the load-carrying ability of the FRC, while the second part of the analysis is to look at local changes in density.

The orientation of fibres in FRC is very important for the capacity and mechanical performance. The fibres are most effective when they are normal to the cracks and crack occurs in the middle of the fibre. This will not happen for all fibres in most FRC structural elements, and it's important to allow for this when designing. The COIN-report 29-2011 [4] gives a theoretical formula for residual tensile strength and is later described in section "Residual tensile strength".

Figure 4.1 describe some way of looking at distribution in the FRC. Figure 4.1**a** can be used to describe the first part of the thesis where all the fibres are homogenous in one direction.
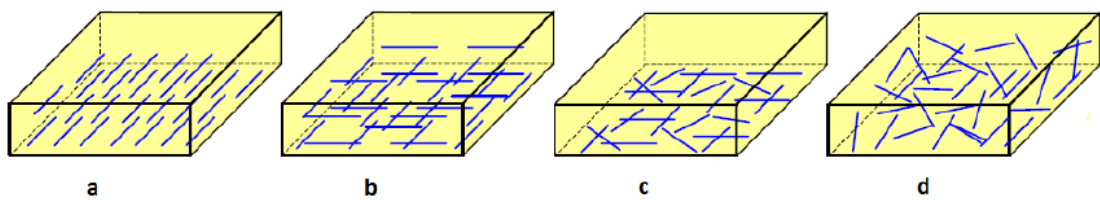
Figure 4.1: Different distributions of discontinuous fibres [8]

a   Biased 1-D fibre orientation
b   Biased 2-D fibre orientation
c   Plane random fibre orientation
d   Random fibre orientation

4.2 Strength classes

SFRC is classified by its compressive strength as for plain concrete, based on an assumption that the ratio between the compressive and tensile strength is the same. In addition, SFRC is classified due to its residual tensile strength at a crack width of 2.5 mm. The strength classes are given in table 4.1 and 4.2 in COIN Project Report 29-2011, where an example of the classification is presented; **B30-R1.5** is fibre reinforced concrete with characteristic cylinder compression strength of 30 N/mm^2 and 1.5 N/mm^2 characteristic residual tensile strength at 2.5 mm crack width. [4]

4.3 Compressive strength

The main concrete property utilized in structures is the compressive strength. It has therefore been the most important quality criterion. Often, in codes and design rules, the other properties are expressed in terms of the compressive strength [6].

A general conclusion is that conventional steel fibres at moderate dosages ($< 1\%$) first start affecting the properties of concrete after maximum stress is reached. The compressive behaviour of structural FRC can therefore be expressed in terms of the characteristic cylinder compressive strength, f_{ck}, in the same manner as for ordinary concrete [12]. However, since the structure becomes more ductile, it may increase the failure strain and the strain at crack localization. As illustrated in figure 4.2, the effect from fibre on the compressive strength is highly dependent on fibre type, amount and the concrete matrix. [8]
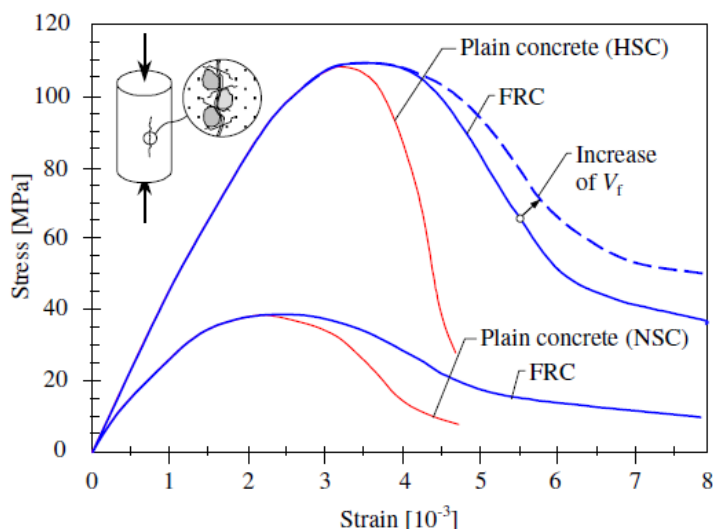
Figure 4.2: Behaviour of concrete and FRC in compression [8]

Compression test from the lab

At NTNU today, there is a lot of ongoing research about FRC. Figure 4.3 shows the setup for a compression test, and figure 4.4 shows how the fibre reinforced concrete looks after being subjected to it. By looking closer at the left picture in figure 4.4, you can see how the fibres that operate normal to the crack have tried to counteract the crack development.
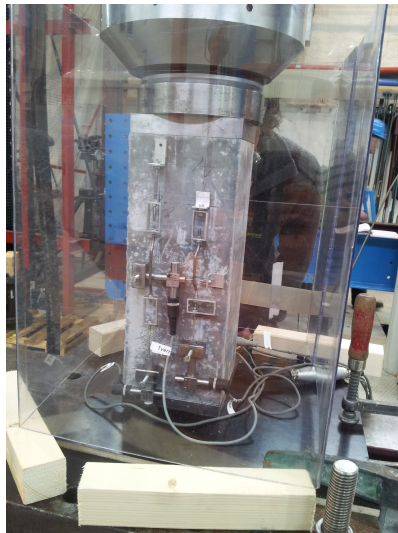
Figure 4.3: Test setup for compression test of SFRC
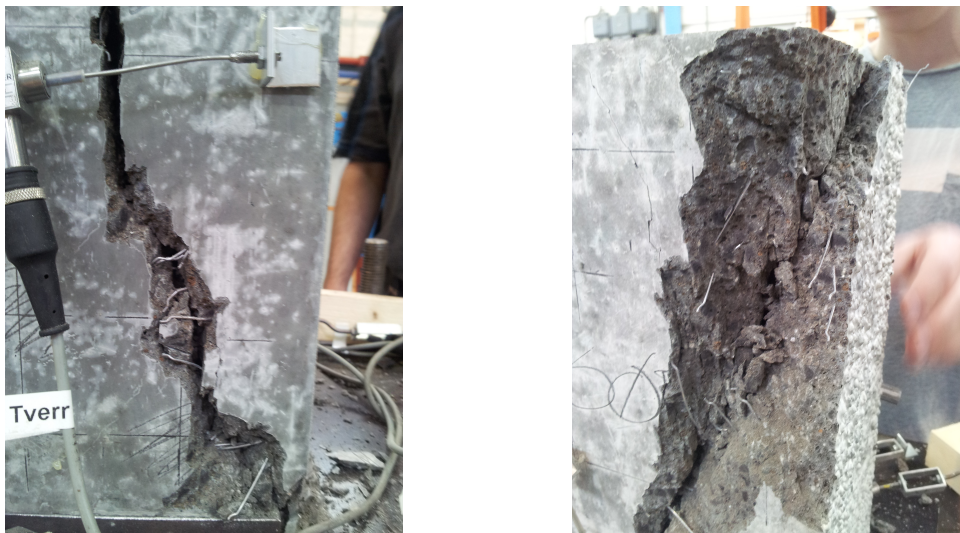
Figure 4.4: After cracking

4.4 Tensile strength

Up to 2.0 vol.-% fibre content, it is assumed that only the tensile properties of the concrete are altered by the inclusion of fibres. Therefore, the most effected parameter is the tensile strength, or more specific the tensile fracture behaviour. While the tensile load-carrying abilities of the plain concrete are almost none after a crack width of about 0.3 mm, the FRC will be able to carry significant loading also after cracking. [8]

This means that FRC has a more ductile behaviour than plain concrete, and give the concrete a residual capacity after the stress-strain diagram has reached its peak. This more ductile behaviour is created because the fibres across the cracks will be able to carry more load than other weak zones in the concrete. New cracks will therefore develop in the brittle matrix. When enough cracks are formed, the fibres will have plastic deformations until ultimate failure is reached when the fibres are completely drawn out of the concrete matrix. [18]

4.4.1 Residual tensile strength

As already mentioned, one thing standing out about FRC is the relatively stable tensile strength with increasing crack widths after cracking. This property is what is known as residual tensile strength.

The post-crack tensile strength of FRC is very dependent on the distribution and orientation of fibre. They are again governed by factors like the casting process, the concrete mix, the size and geometry of the specimen, its boundaries and potential obstacles like reinforcement bars[7]. Because of this affection, the characteristic residual tensile strength at $2.5\,mm$ crack width is in COIN reports chosen as the material parameter governing the effect of fibres.[4] The characteristic residual tensile strength is derived from the flexural tensile strength at $2.5\,mm$ crack width, $f_{R,3}$, established from flexural tests on notched prisms according to NS-EN 14651, fully described in section "Three-point bending test". [14]

4.4.2 Strain softening in FRC

Strain softening is defined as the loss of load-carrying capacity of concrete after it has reached the maximum load [25]

FRC, even with small volume fractions (<1 vol.-%), can be attracted as a strain-softening material [8]. Tensile response of strain-softening FRC can be simplified to idealized stress-strain models as shown in figure 4.5. This model shows very clearly

the difference between the brittle strain softening (RED) and the more ductile behaviour(BLUE). If the softening diagram becomes very steep after exceeding the tensile strength, the material is said to behave brittle. Nevertheless, if the post-peak curve approaches the strain axis slowly, the material has a ductile behaviour. The properties of the concrete, geometry and boundary conditions has a large impact on how the concrete will react after cracking.

Some of the tension softening failures DIANA offers are brittle, linear softening in tension, hereunder fracture energy based and ultimate strain based, and Multi-linear diagram in tension. The last two, linear tension softening and multi-linear diagram in tension, are more described in the chapter "Finite Element Modeling".

4.4.3 Strain hardening in FRC

When the residual tensile strength becomes higher than the tensile strength at cracking, the structure is affected to what is known as strain hardening. After the first crack, the tensile strength continues to grow while multiple cracks occur until failure. This is illustrated in figure 4.5 as the green line.
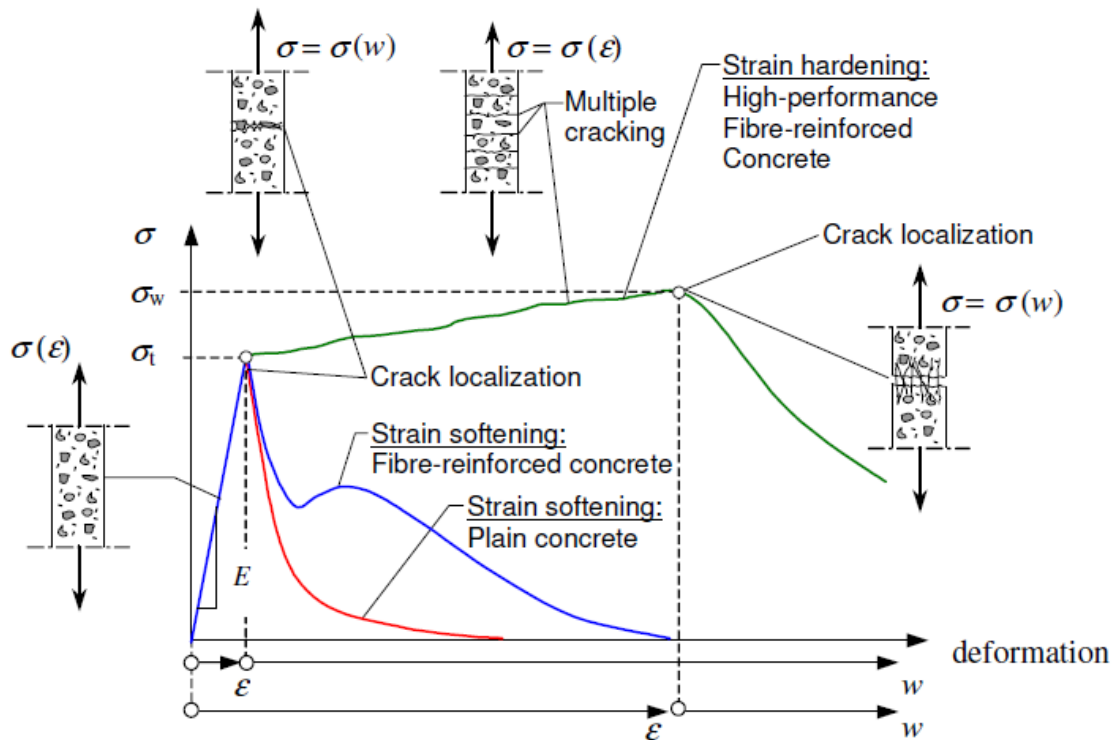
Figure 4.5: Tensile behaviour by Löfgren [8]. After cracking, the tensile zone can still be able to carry stress equal to residual tensile strength. Simplified, tensile zone may be characterized as an area with uniform stress distribution with the stress equal to the design residual strength.

Chapter 5

Finite Element Modeling

The modeling and analysis in this thesis have been done using DIANA, which is a Finite Element Analysis Software with material, element and procedure libraries based on advanced database techniques. Especially for concrete analysis DIANA is appealing, and furthermore for models with smeared or discrete cracking. DIANA's strongest points lie in its nonlinear capabilities, which include material models for plasticity, cracking, elasticity and many more. [2]

5.1 Introduction

The basis for this thesis is a paper written by Sarmiento, Hendriks and Kanstad [3] at the Department of Structural Engineering at NTNU about modeling and numerical analysis of FRC. The modeling is based on the three-point bending test in NS-EN 14651, which describe the test method for fibre reinforced concrete.

In *Chapter 4* - "Smeared Cracking in a Notched Beam" for the *Concrete and masonry analysis*-part of the Diana online documentation [2], there is an example presented with quite similar design to the model created in this thesis. That was a great help in order to understand the modeling. Further on, the paper "Modeling of tension behaviour in fibre reinforced concrete", written by Elena Sarmiento, was very useful.

When modeling, there is always a careful balance needed between the level of detailing and the complexity of the problem, the desired output and the "accuracy" of the results. The pros and cons always have to be considered carefully when choosing models and elements. [8]

5.2 Finite element model

The geometry in the Diana model is derived from the paper written by Sarmiento, Hendriks and Kanstad [3]. The beams in that paper were tested according to a three-point bending test described in NS-EN 14651 [14], and the modeling in this report is therefore based on that test. That guideline also give the restrictions when it comes to geometry for the beam and the fibres.

5.2.1 Three-point bending test

The principle of the test is to find residual flexural tensile strength for the concrete determined from values determined from load-CMOD or load-deflection curves.

Where Norwegian sawn beam test [13] uses two point loads, the test described in NS-EN 14651 only uses one point load in the centre of the span to create bending moment. The roller on top must be able to rotate about its axis. The testing beam also has a notch in the bottom of the mid-span. The setup for the test is shown in figure 5.1.[14][18]
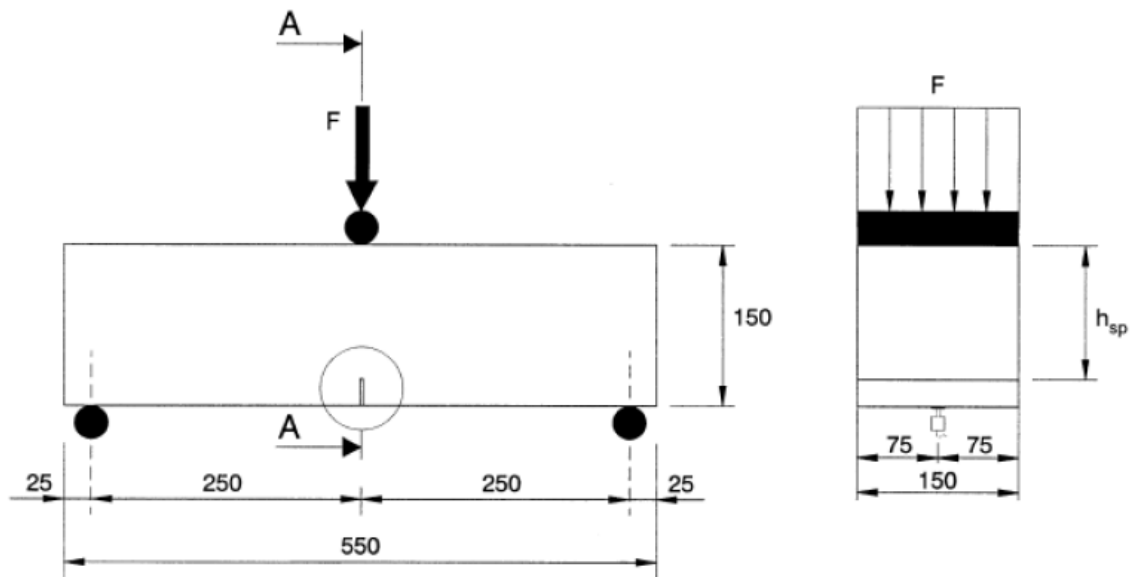
Figure 5.1: Test setup for the NS-EN 14651 bending test [14]

The distance between the centres of the supporting rollers (i.e. span length) shall always be equal to 500 mm. Figure 5.2 shows the static model for the beam investigated in this thesis.
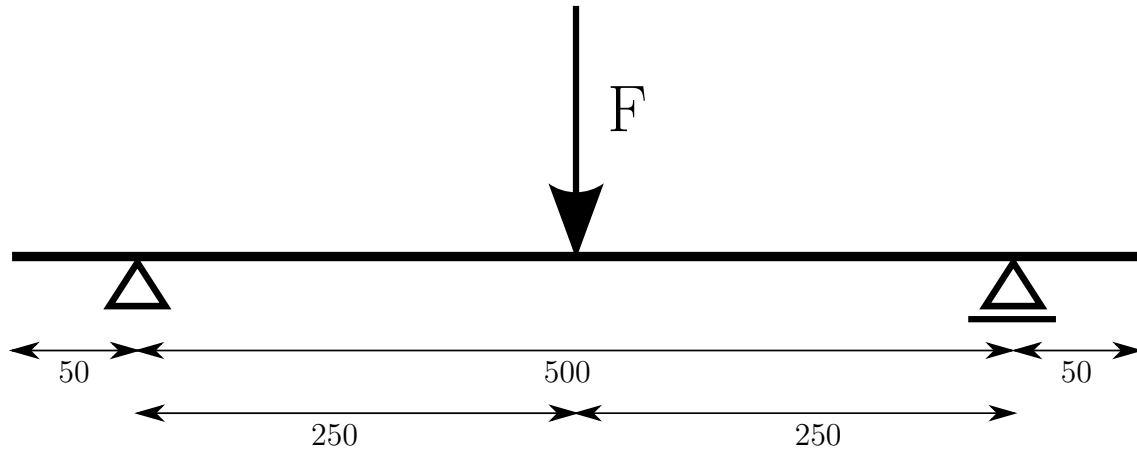
Figure 5.2: Static model

In difference to the test setup in NS-EN 14651, this beam has a length of 600 mm. The width and depth are the same, 150 mm, confirming the requirements in EN 12390 [16] of prisms with a nominal size (width and depth) of 150 mm and a length L larger than 550 mm and smaller than 700 mm. [14] All the lengths for the geometry of the model are given in figure 5.3.
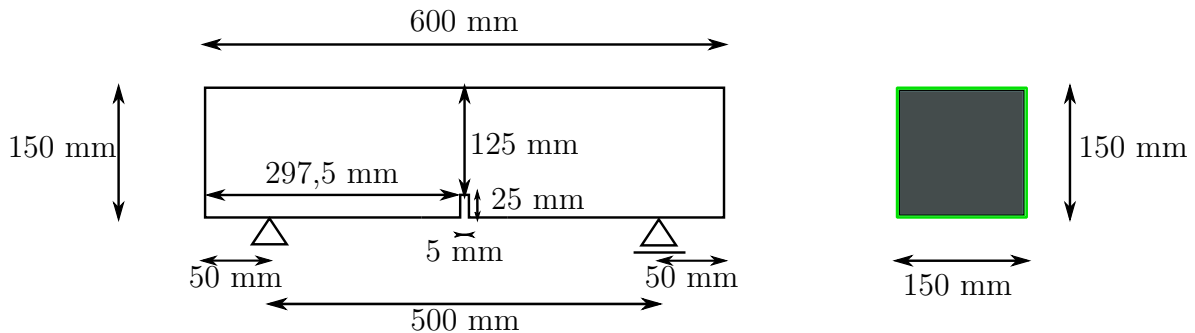
Figure 5.3: The model for the analysis, with lengths

Notch

The presence of the notch in the beams guarantees that the cracking will happen in the mid-span section. At this point, the cross-section is the smallest (height reduced to 125 mm) and the bending stresses are highest.

The notch is made by sawing the test specimen, cured according to EN 12390-2 [15]. The width of the notch should be equal to, or smaller than, 5 mm, and the depth 25 mm $\pm$ 1 mm. In this thesis the width of the notch is 5 mm and the distance h_{sp} is 125 mm, which give an height of 25 mm for the notch.

22

Outcome of the test

The test gives a Load-CMOD-curve (Crack Mouth Opening Displacement), but the standard states that the relation between the deflection and the CMOD is given as[14]:

$$\delta = 0.85 \cdot CMOD + 0.04 \tag{5.1}$$

Determination of the residual flexural tensile strength, $f_{R.j}$ in equation 5.2, is done in terms of areas under the load-deflection curve obtained by the CMOD or the displacement-controlled bending test [7]. Its value is further translated into a characteristic residual tensile strength, $f_{ftk,res2.5}$.

$$f_{R.j} = \frac{3 \cdot F_j \cdot l}{2 \cdot b \cdot h_{sp}^2} \tag{5.2}$$

where
$f_{R.j}$ is the residual flexural tensile strength corresponding with CMOD = $CMOD_j$ or $\delta = \delta_j$, in N/mm² (j=1,2,3,4);
F_j is the load corresponding with CMOD = $CMOD_j$ or $\delta = \delta_j$, in N;
l is the span length, in millimetres;
b is the width of the specimen, in millimetres;
h_{sp} is the distance between the tip of the notch and the top of the specimen, in millimetres;

By equating the moments from the two stress distributions in figure 5.4, the following expression is provided:

$$f_{Rk,3} \cdot \frac{bh^2}{6} = f_{ftk,res,2.5} \cdot b \cdot 0.9h \cdot 0.5h \tag{5.3}$$

which again can describe the characteristic residual tensile strength as:

$$f_{ftk,res,2.5} = 0.37 f_{Rk,3} \tag{5.4}$$
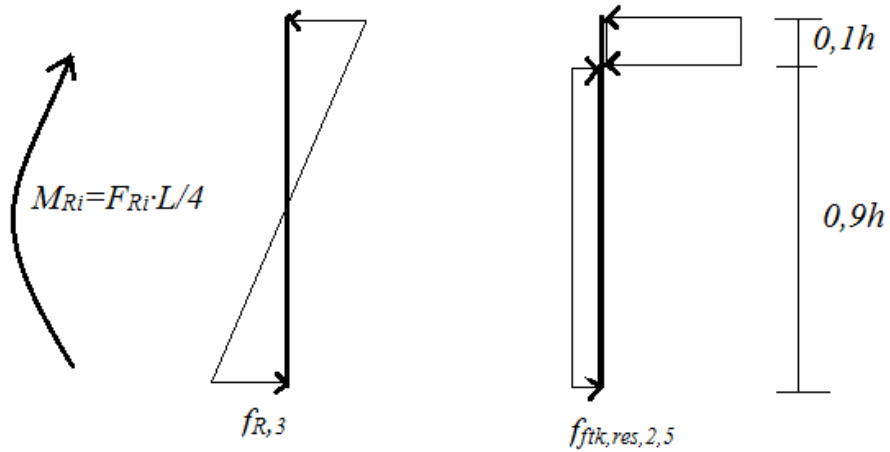
Figure 5.4: Illustration of the relation between flexural residual tensile strength and characteristic residual tensile strength [4]

5.3 Geometry

Analysis section	
Units defintion	
Model type:	$\rightarrow$ Structural 2D
Length:	$\rightarrow$ Millimeter
Mass:	$\rightarrow$ Kilogram
Force:	$\rightarrow$ Newton
Time:	$\rightarrow$ Second
Temperature:	$\rightarrow$ Kelvin

Table 5.1: Analysis and units
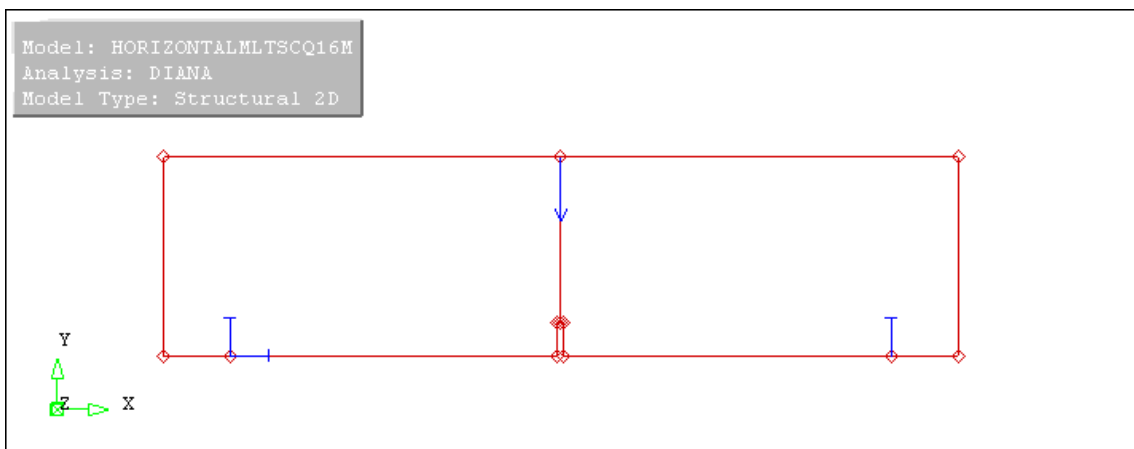
Figure 5.5: Geometry of the notched beam showing constraints and the point load from DIANA

24

5.3.1 Geometry definition

To define the geometry, seven points ,P1 to P7, are defined, as illustrated in figure 5.6. By using these points, seven straight, coherent lines are constructed and gathered with a set named LEFT. These lines defines the surface S1 and is defining the left-hand side part of the model.

Figure 5.6: Points for geometry definition of the left side of the model

5.3.2 Meshing

There were two element types that were possible for these analysis. The first one were four-node quadrilateral isoparametric plane stress elements based on linear interpolation and Gauss integration, called Q8MEM. The other one were CQ16M elements, which are eight-node quadrilateral isoparametric plane stress elements, based on quadratic interpolation and Gauss integration. By default, DIANA applies 2x2 Gauss integration scheme. The meshing type recommended by the user manual [2] for nonlinear analysis is CQ16M. That is the mesh used in the paper by Sarmiento, Hendriks and Kanstad as well [3]. The best alternative, and the one chosen, is therefore CQ16M.
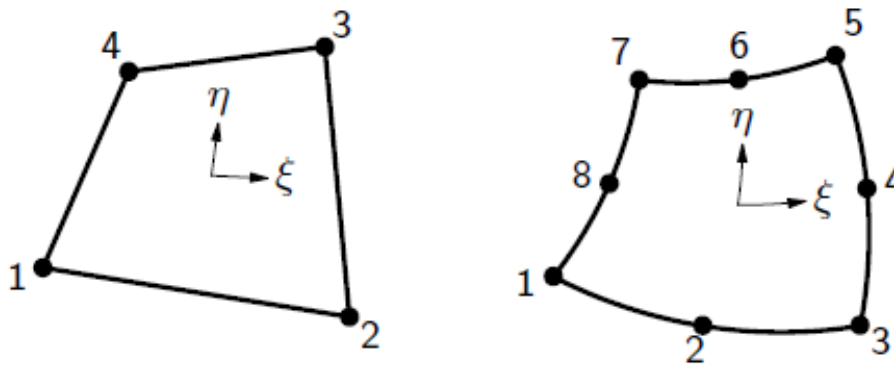
Figure 5.7: Q8MEM (left) and CQ16M (right) - elements [2]

The mesh is created with an average element size of 12.5 mm. The command PAVING allows creating a quadrilateral free mesh on any type of surface and is therefore well suited to mesh the left surface of the model.
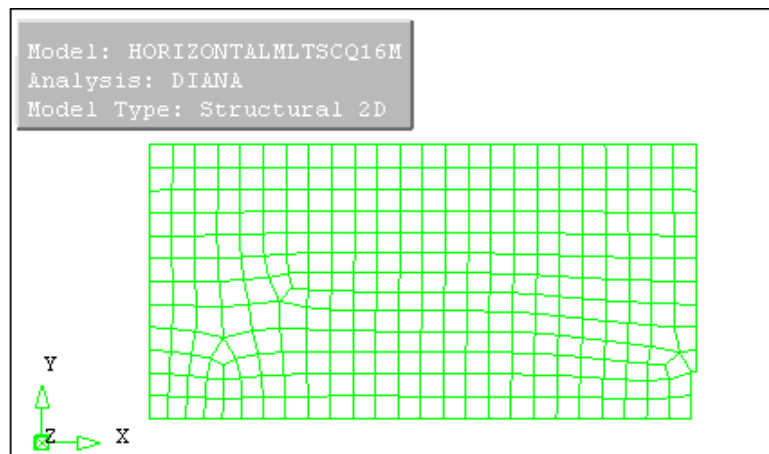
Figure 5.8: Mesh of the left side geometry

5.3.3 Expansion to full model

By mirroring surface S1 to a vertical line at X=300 mm the model is completed. The completed model is shown in figure 5.5 without the mesh and in figure 5.9 with the mesh.

5.3.4 Boundary conditions

The beam is supported with two pin supports, both constrained in Y-direction with an additional constraint in X-direction for the left point, as indicated in figure 5.2 and figure 5.9.

As a default DIANA also add a constraint where the loading is applied.
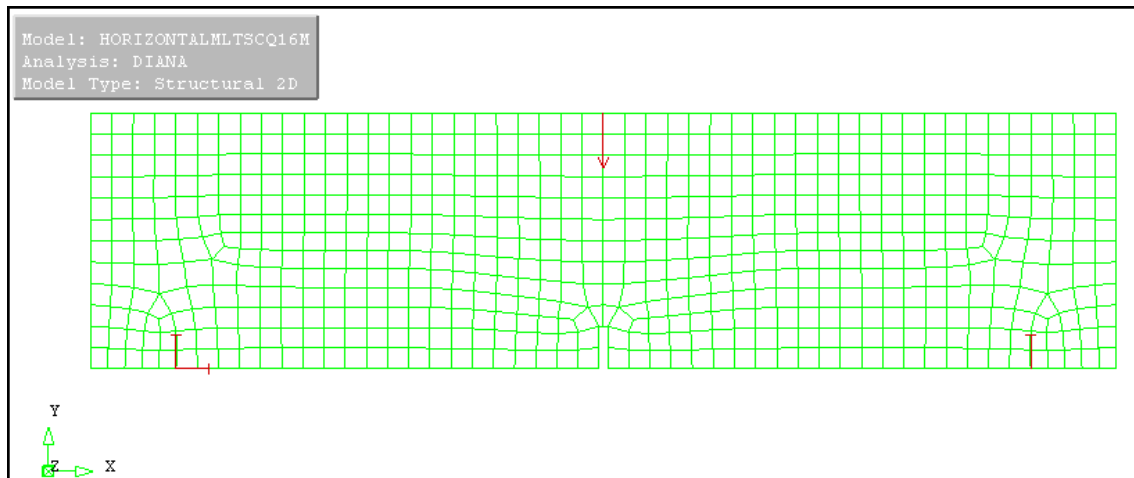
Figure 5.9: Boundary conditions and loads

5.3.5 Loading

Two options have been considered in terms of loading, displacement controlled and force-controlled. To find the optimal choice of load steps, as discussed in section "Incremental-iterative solution procedure", is very important for the outcome of the analysis.

Displacement-controlled

Principally displacement-controlled analysis are used in this thesis. This is done by adding a displacement loading of δ = -1 mm at the top of the mid-span of the beam. When running the analysis, user specified load steps are used to reach 4 mm deflection. To obtain satisfactorily results, fittings with different load steps were tried out:

Try	User specified load steps	Displacement max load	Load step
1st	1E-05 0.1(40)	0.2	3
2nd	1E-05 0.05(40) 0.1(20)	0.15	4
3rd	1E-05 0.05 (80)	0.15	4
4th	1E-05 0.01(30) 0.05(24) 0.1(25)	0.13	14

Table 5.2: Variations of load steps to reach 4 mm deflection

There was no doubt that the fourth try gave the best results. That is the one used to compare the results, and the one used in further analysis with density as well. The solution procedure used is presented in table 5.3

Iteration method	Full Newton - Raphson
Control increment	Displacement control
Load	-1[mm]
Step size	User specified
Max iterations	150
Convergence Norm	Displament and Force 0.01
No convergence	Terminate

Table 5.3: Solution procedure, displacement-controlled analysis

Force-controlled

The force-controlled analysis were used in order to investigate if the displacement-controlled results corresponded with the force-controlld. The loading used was a vertical force F = -1000 N.

As mentioned in chapter "Finite Element Method" when the load is applied as force, the arc-length control is required. Unless, the models are going reach convergence because of instabilities in the load-deflection curve at a small load level.

A lot of fittings gave the chosen variations as presented in table 5.4, and the solution procedure for the force-controlled analysis is shown in table 5.5.

User specified load steps	
Horizontal	1E-05 10(10) 5(30) 2(40)
30 degrees	1E-05 2(5) 1(10) 0.5(65)
45 degrees	1E-05 2(10) 1(30) 0.5(40)
60 degrees	1E-05 1(15) 0.5(65)
Vertical	1E-05 1(5) 0.5(70)

Table 5.4: User specified loadstep, force-controlled analysis

Iteration method	Full Newton - Raphson
Control increment	Force control
Load	-1000[N]
Step size	User specified
Max iterations	Varies
Convergence Norm	Displament and Force 0.01
No convergence	Terminate

Table 5.5: Solution procedure, force-controlled analysis

5.4 Material models

The parameters the fibre reinforcement are based on properties from a paper written by Elena Sarmiento named "Accounting for the fibre orientation on the structural performance of flowable fibre reinforced concrete" [3]. The properties are listed in table 5.6.

f_{cm}	65 [MPa]
E_{cm}	38000 [MPa]
σ_1	3.8 [MPa]
ε_1	0.1 ‰
ε'_2	1.5 ‰
Volume fraction	0.5 %

Table 5.6: Input parameters from the paper

5.4.1 Linear properties

The linear behaviour was modeled as a simple beam with the following requirements for all cases. The behaviour was elastic, isotropic with properties as in table 5.7. In DIANA only two inputs were required: E-modulus and Poisson ratio. The E-modulus is assumed to be the same for all cases.

Material name: MACONLIN		
Linear elasticity	→ Isotropic	
	Young's modulus	E= 38000 N/mm^2
	Poisson's ratio	$\nu = 0.2$

Table 5.7: Material properties for linear analysis

Physical property name: PHCONCRE		
Plane stress	→ Regular	
	Thickness	t = 150 mm

Table 5.8: Physical properties

5.4.2 Nonlinear properties

The nonlinear behaviour of the material were modeled with a rotating smeared crack model. Total Strain Rotating crack is used for both for non-reinforced concrete and the fibre reinforced concrete. For non-reinforcement concrete fracture energy based and ultimate strain based cracking are used to get a basis for comparison, while the

fibre reinforced concrete uses a cracking in DIANA called "Multi-linear diagram in tension". Examples of the input for the diagrams are shown in appendix E, and the nonlinear prooperties are more described in section "Modeling of tension behaviour".

5.5   Cracking

Cracking can be described as a combination of tension cut-off, tension softening and shear retention criteria.[2] Cracking occurs when the principle tensile stress exceeds the limit tensile stress, f_t, in this thesis also known as σ_1. After cracking, the concrete tensile strength softens, governed by fracture energy. This is also known as tension softening. [19]
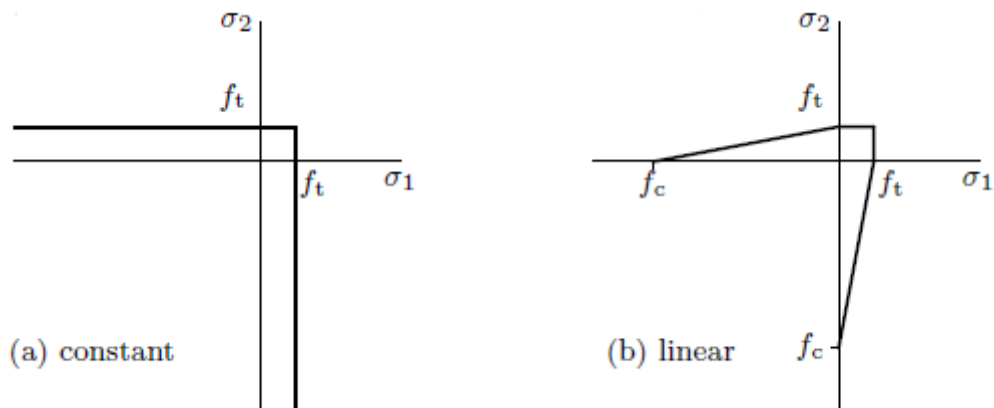
Figure 5.10: Tension cut-off criterias in DIANA [2]

There are two main approaches for modeling of cracking in concrete: the discrete crack and the smeared crack approach. Here, only the smeared cracking is evaluated.

5.5.1   Smeared cracking

For brittle materials, like concrete, various smeared cracking models are available to simulate the cracking. The models based on total strain uses a nonlinear elasticity relationship to describe the cracking and crushing behaviour of the material, and is recommended by the user manual. [2]

The effect of cracking in FRC leads to smeared cracking, which does not separate the mesh, but assumes that the crack is smeared over the element. That reduces the limit tensile strength within this area, and keeps the element mesh continuous after cracking. [19]

Two different types for the smeared cracking model, which both are based on the orthotropic stress-strain law that accounts for concrete after cracking ($\sigma \geq f_t$), have been developed: the Fixed crack model and the Rotating crack model [22]:

$$
\begin{bmatrix} \sigma_1 \\ \sigma_2 \\ \tau_{12} \end{bmatrix} = \begin{bmatrix} 0 & 0 & 0 \\ 0 & E & 0 \\ 0 & 0 & 0 \end{bmatrix} \begin{bmatrix} \varepsilon_1 \\ \varepsilon_2 \\ \gamma_{12} \end{bmatrix} \tag{5.5}
$$

Fixed crack model introduces a shear retention factor, α, to reduce the shear modulus (G), but by introducing the Rotating crack model this assumption can be avoided. The Rotating crack model only evaluates the principal stresses and introduces a tangential stiffness [22]:

$$
\begin{bmatrix} \sigma_1 \\ \sigma_2 \\ \tau_{12} \end{bmatrix} = \begin{bmatrix} \mu E & 0 & 0 \\ 0 & E & 0 \\ 0 & 0 & \frac{\sigma_1 - \sigma_2}{2(\varepsilon_1 - \varepsilon_2)} \end{bmatrix} \begin{bmatrix} \varepsilon_1 \\ \varepsilon_2 \\ \gamma_{12} \end{bmatrix} \tag{5.6}
$$

A huge advantage of this model is that new cracks only can occur in the normal direction of an existing crack.

5.5.2 Crack modeling

The cracking used in this thesis is the Total Strain Rotating Crack model. The model takes into account that the crack direction may change during the analysis, in difference to fixed crack models. Three different version of the crack model have been used for the tension failure. For non-reinforced concrete, both ultimate strain and fracture energy based have been used. For FRC the one based on Multi-linear tension softening has been used. That is because of the behaviour of FRC after cracking, which need to be modeled through a stress-strain-diagram with properties decided on the forehand.

Both compressive and pre-cracking response is assumed to be similar to plain concrete since the fibres main contribution first occur after cracking. The compression behaviour is therefore modeled as "linear-ideal plastic", shown in figure 6.2, for all models. [3]

Peaks and drops in the load-displacement-curves represent typical areas where the fibres are partly pulled out before they are (almost) completely drawn out when the curve drop down to almost none load-bearing capacity.

5.6 Modeling of tension behaviour of the fibre reinforced concrete

As mentioned, the behaviour of the FRC is described with the rotating crack model. This model describes the tensile and compression behaviour with a stress-strain relationship. The input of this model comprises the basic properties describing the linear-elastic behaviour before cracking/maximum tensile strength is reached and the definition of the behaviour in tension, shear and compression, which govern the response of nonlinear behaviour. Table 5.9 shows the input information for the FRC in the thesis.

Material name: MACONC		
Linear elasticity	→ Isotropic	
	Young's modulus	E= 38000 N/mm^2
	Poisson's ratio	$\nu = 0.2$
Static nonlinearity	→ Concrete and brittle materials	
	→ Total strain rotating crack	
	→ Direct input	
	→ Multi-lin. diagram in tension	
	→ Ideal in compression	
	→ No lateral confinement behav.	
	→ No lateral cracking reduction	
	→ No Poisson ratio	
	File stress-strain diagram	HORIZONTALF1.dat
	Compressive strength	f$_{cm}$ = 65 N/mm^2

Table 5.9: Material properties for nonlinear analysis

The nonlinear tensile behaviour of the fibres are modeled with "Multi-linear diagram in tension", which means that the behaviour is completely defined by the user. In other words, it allows prescribing the points in the stress-strain curve. [22] The different fibre properties are based on simplified calculations from values in the paper[3]. When choosing this type of property it is possible to give the model strain hardening properties in tension.

The fibre reinforcement are defined through a $\sigma - \epsilon$ -design method based on known factors. The resulting stress-strain relation of this rigid-plastic approach for the residual tensile strength is presented in figure 5.11. To implement this in DIANA dat-files, like "HORIZONTALF1.dat" in table 5.9 are created. In the curves five points have been generated.
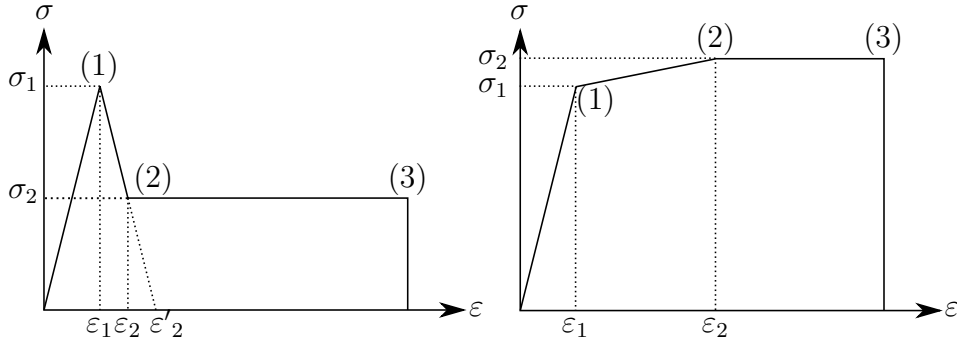
Figure 5.11: Tension softening and hardening modeled behaviour

First point is defined at $(\sigma, \varepsilon) = (0,0)$, where the tensile behaviour begins. The second point is based on Hooks law, equation 5.7, and a linear-elastic behaviour until maximum tensile strength is reached.

$$E = \frac{\sigma}{\varepsilon} \tag{5.7}$$

All of the values up to this point are found in table 5.6 as E_{cm}, σ_1 and ε_1, which means that for all orientations the tensile strength of the FRC is assumed to be 3.8 N/mm^2.

The residual tensile strength (Point (2) on the left hand side in figure 5.11) is based on calculations from a fibre efficiency parameter from the paper[3], more described in the chapter about the analyses. The point where the residual tensile strain is reached in tension softening is based on the formula:

$$y = 4.07 - 2713.33x \tag{5.8}$$

where y represents ε and x represents σ based on the fibre efficiency parameter. This relationship is based on the two points (0.1, 3.8) and (1.5,0), and a linear line between them. The first term represent the tensile strength of the FRC, and the latter term is where the concrete reach failure at ε'_2 in the paper, illustrated in figure 5.11.

The fourth and the fifth point, locate as point (3) in the figure 5.11, are based on an assumption that the maximum elongation for fibre reinforced concrete is reached where:

$$\varepsilon = \frac{CMOD_{0.5}}{h_{el}} = \frac{0.5}{12.5} = 0.04 \tag{5.9}$$

If the tensile strength after cracking exceeds (strain hardening), it is assumed that it will reached it full capacity at $\varepsilon = 4.0$ ‰, represented by point (2) on the right side of figure 5.11. In total, this can give the two relationships illustrated in figure 5.11 for developing the stress-strain curves for tensile strength.

33

Chapter 6

Analysis and Results

6.1 Design codes for FRC

The COIN Project report 29-2011 [4] design approach is based on the residual tensile strength at $2.5\,mm$ crack width. Its value is derived from the residual flexural strength at $2.5\,mm$ crack opening established from three-point bending tests on small notched FRC prisms.

6.1.1 Ultimate limit state

According to NS-EN 1990 [11], concrete with only fibre reinforced concrete can only be used in reliability class 1.

Material factor for the residual tensile strength is given as:

$$\gamma_{cf} = 1.5 \tag{6.1}$$

which give a design stress for the residual stress of:

$$f_{ftd,res,2.5} = \frac{f_{ftk,res,2.5}}{\gamma_{cf}} \tag{6.2}$$

Moment capacity of SFRC

For FRC you can simplify calculate the capacity by assuming residual tensile strength to have influence over a height of 0.8h, and that the internal moment distance is 0.5h, see figure 6.1. The moment capacity is then given as:

$$M_{Rd} = 0.4 \cdot f_{ftd,res2,5} \cdot b \cdot h^2 \tag{6.3}$$
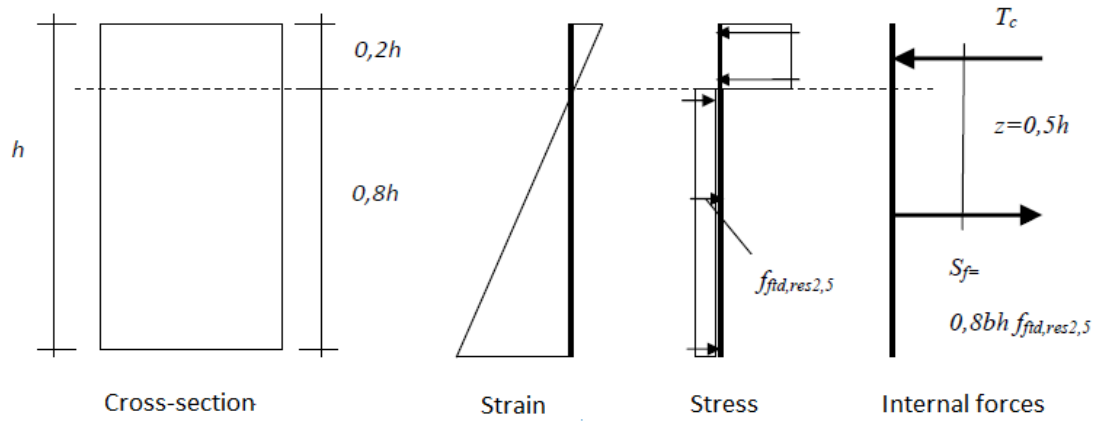
Figure 6.1: Stress- and strain distributions for rectangular cross-sections of FRC exposed to pure bending from COIN 29-2011 [4]

Shear resistance of SFRC

COIN, technical report 63 and FIB's Model Code are the three different methods to calculate the shear resistance of fibre reinforced concrete. In COIN, the shear resistance of SFRC cross-sections can be calculated as a combination of clause in EC2 6.2.2(1) [12] for ordinary concrete and an additional fibre contribution term according to section 6.2.6 in COIN 29-2011 [10]. The total resistance is given as:

$$V_{Rd,c} = V_{Rd,ct} + V_{Rd,cf} \tag{6.4}$$

where the first term on the right-hand side is the design value for the shear resistance for beams without need for shear reinforcement in EC2 6.2.2(1):

$$V_{Rd,ct} = [C_{Rd,c}k(100\rho_l f_{ck})^{1/3} + k_1\sigma_{cp}]b_w d \geq (\nu_{min} + k_1\sigma_{cp})b_w d \tag{6.5}$$

and the latter term takes into account the effect of fibres:

$$V_{Rd,cf} = 0.6 f_{ftd,res,2.5} b_w h \tag{6.6}$$

6.1.2 Serviceability limit state

Fibre is very favorable when it comes to both crack distance and crack widths in FRC with traditional reinforcement. Even small amount of fibres could limit the scale of cracks in a great extent. That will cause the concrete to be almost free for visible cracks in serviceable limit state (SLS).

6.2 What to investigate

In this thesis, the goal was to look at how variations in fibre orientation and density influenced the capacity of fibre reinforced concrete beams. The analysis were based on available results from the mentioned paper. The following list give a brief overview and introduction of the investigations done in DIANA:

1. The first analysis is of non-reinforced concrete to get a reference of its behaviour to compare FRC with later.

2. Analysis of FRC with changed fibre orientation

    2.1. Variations in element size of the mesh to see what influence that would have on the results.

    2.2. Displacement-controlled analysis of the same fibre orientation, homogenous distributed, in whole beam. Horizontal, 30 degrees, 45 degrees, 60 degrees and vertical orientation the ones considered.

    2.3. Force-controlled analysis of the beams from 2.2.

    2.4. Since the cracking happen in the mid-span, an area was made to see what changed fibre orientation in the mid-span, keeping another fibre orientation in the rest had of influence on the behaviour.

    2.5. To check what an increased area of the mid-span section with different properties than the rest of the beam had to say, a new, larger area in the mid-span was made to see what influence that would have.

    2.6. To get the modeling more close to reality a model with two layers of 75 mm in the 2D-view was made to see what influences that would have on the load-bearing capacity.

3. Analysis with local changes in density

    3.1. Density changes in the mid-section within the same orientation as the rest of the beam

    3.2. Density and orientation changes in the mid-section. Horizontal fibre orientation in the rest of the beam.

6.3 Non-Reinforced Concrete

6.3.1 Non-reinforced concrete analysis

To get a reference for what to expect from the analyses of FRC, analysis on non-reinforced concrete have been investigated. The non-reinforced concrete is modeled with two different cracking models. The first one is fracture energy based cracking and the other one is ultimate strain based cracking. Both are what we call linear smeared cracking.
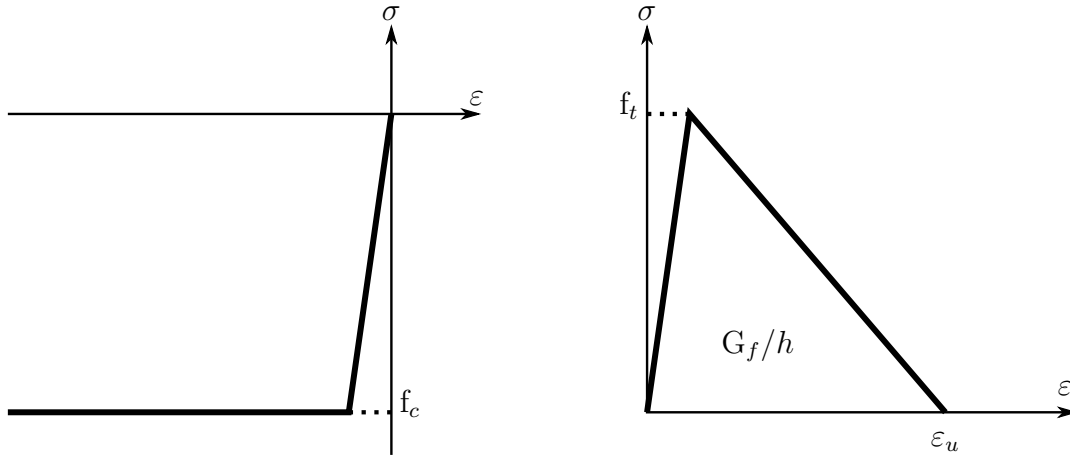
Figure 6.2: Linear tension softening for non-reinforced concrete. Linear-Ideal Plastic in compression on the left side. Linear smeared cracking in tension on the right.

In the ultimate strain based model only the ultimate strain is specified, while the fracture energy is computed correct in each element according to the element size and the given ultimate strain. In the fracture energy based model, on the other hand, the fracture energy and average element size is given and the ultimate strain are being calculated according to those values.

The crack bandwidth is chosen as the length of the side of an element. In this case, the bandwidth is set to 12.5 mm.

$$h_{el} = \sqrt{\frac{A_{concrete}}{n_{elements}}} = 12.5mm \qquad (6.7)$$

When a linear softening behaviour is assumed, the relationship between fracture energy (G_f) and ultimate strain (ε_2) is given as [3]:

$$\frac{G_f}{h_{el}} = \frac{1}{2} \cdot \sigma_1 \cdot \varepsilon_2 \qquad (6.8)$$

Since ε_2 is based on the paper, which operates with a value of 1.5 ‰, the fracture energy becomes:

$$G_f = \frac{1}{2} \cdot \sigma_1 \cdot \varepsilon_2 \cdot h_{el} = \frac{1}{2} \cdot 3.8 \cdot 0.0015 \cdot 12.5 = 0.036 \qquad (6.9)$$

The tables below give the input information for non-reinforced concrete. Fracture energy based cracking require six inputs which is mentioned in table 6.1. Ultimate strain based cracking require five inputs as in table 6.2

Material name: MACONC		
Linear elasticity	→ Isotropic	
	Young's modulus	E= 38000 N/mm^2
	Poisson's ratio	$\nu = 0.2$
Static nonlinearity	→ Concrete and brittle materials	
	→ Total strain rotating crack	
	→ Direct input	
	→ Linear softening in tension	
	→ Fracture energy based	
	→ Ideal in compression	
	→ No lateral confinement behav.	
	→ No lateral cracking reduction	
	→ No Poisson ratio	
	Tensile strength	$f_t = 3.8$ N/mm^2
	Mode I-Fracture energy	$G_f = 0.036 N/mm^2$
	Crack bandwidth	h = 12.5
	Compressive strength	$f_{cm} = 65$ N/mm^2

Table 6.1: Material properties for Fracture energy based

Material name: MACONC		
Linear elasticity	→ Isotropic	
	Young's modulus	E= 38000 N/mm^2
	Poisson's ratio	$\nu = 0.2$
Static nonlinearity	→ Concrete and brittle materials	
	→ Total strain rotating crack	
	→ Direct input	
	→ Linear softening in tension	
	→ Ultimate strain based	
	→ Ideal in compression	
	→ No lateral confinement behav.	
	→ No lateral cracking reduction	
	→ No Poisson ratio	
	Tensile strength	f$_t$ = 3.8 N/mm^2
	Mode I-Ultimate tensile strain	ϵ_2= 0.0015
	Compressive strength	f$_{cm}$ = 65 N/mm^2

Table 6.2: Material properties for Ultimate strain based

6.3.2 Comparison of the different crack models for non-reinforced concrete

Cracking	Load [kN]	Displacement [mm]	Load step
Fracture energy based	11.594	0.04	5
Ultimate strain based	11.638	0.04	5

Table 6.3: Non-reinforced concrete - maximum load
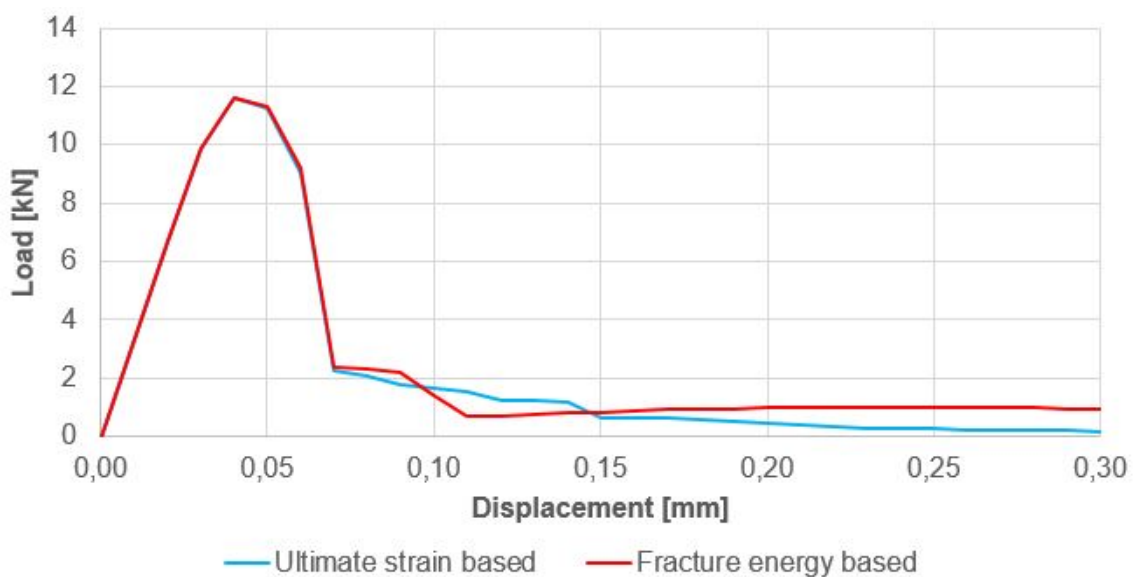
Figure 6.3: Load-displacement curve for non-reinforced concrete

Both have the brittle failure, which is expected. Since both are based on the same principle, it was expected that the results should be similar. That gives an indication that the modeling is correct. To prove that the Von Mises at max load are quite similar with 16.8 and 16.9 N/mm², respectively, for the two different models.

On the forehand it is expected that concrete alone as almost the same properties as the vertical fibre direction, which reached a maximum loading of 12.923 kN at 0.05 mm displacement. Both approaches therefore give a good model to compare non-reinforced concrete with SFRC, illustrated in figure 6.3.
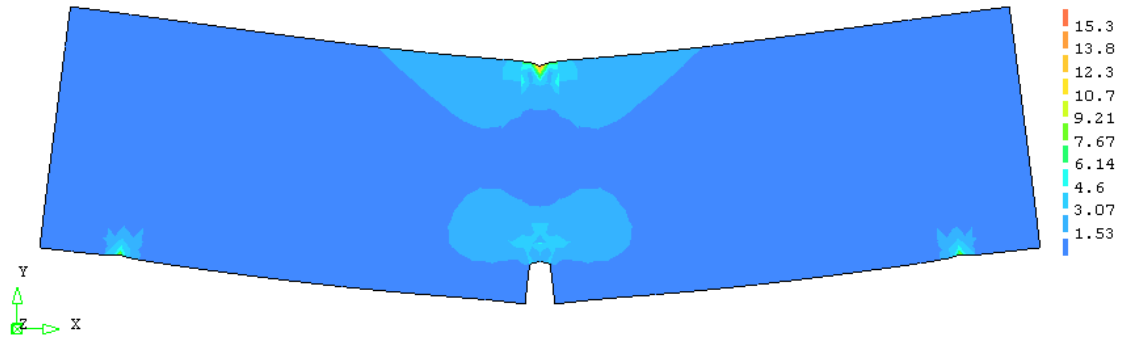
Figure 6.4: Von Mises plot for maximum loading

To get a good overview, figure 6.5 is added to show how the fibre-reinforced behaviour is compared to non-reinforced concrete. This also include a fracture energy, G_f, of 0.154 calculated from equation 6.10, which is the one *fib*[5] operate with. That clearly overrate the capacity compared to the properties used for FRC in this thesis.

$$G_f = 73 \cdot f_{cm}^{0.18} [\text{N/m}] \tag{6.10}$$
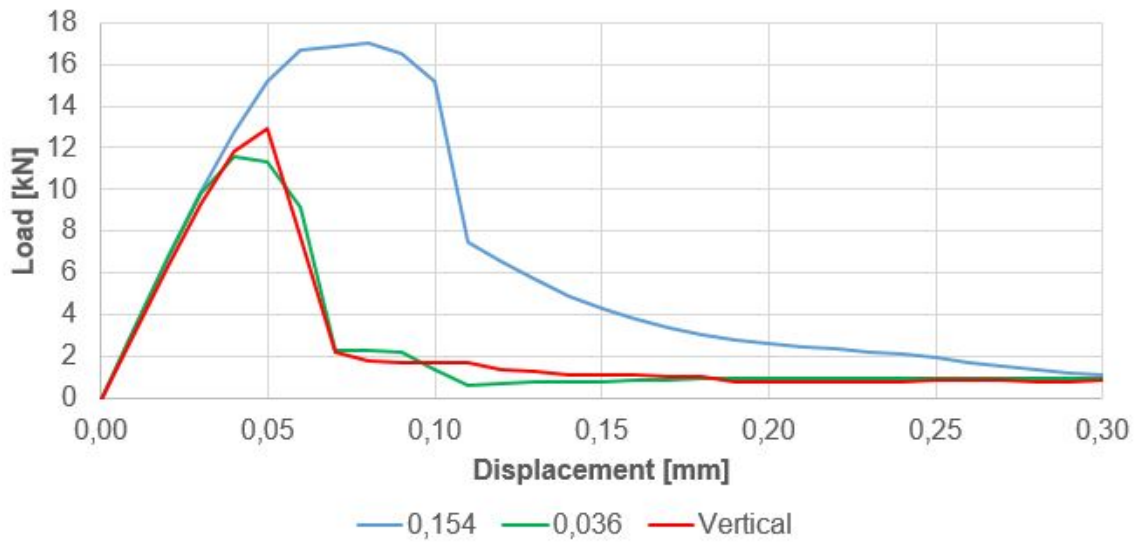
Figure 6.5: Comparison between the different fracture energies and vertical fibre orientation

6.4 Variations in element size

A challenge when running nonlinear analysis is to find a satisfactory approach. Three different element sizes for the mesh were therefore tried out and considered; 10, 12.5 and 25 mm. The mesh were changed to see if the element size had any considerable influence on the results. All element types had QU8 CQ16M elements.
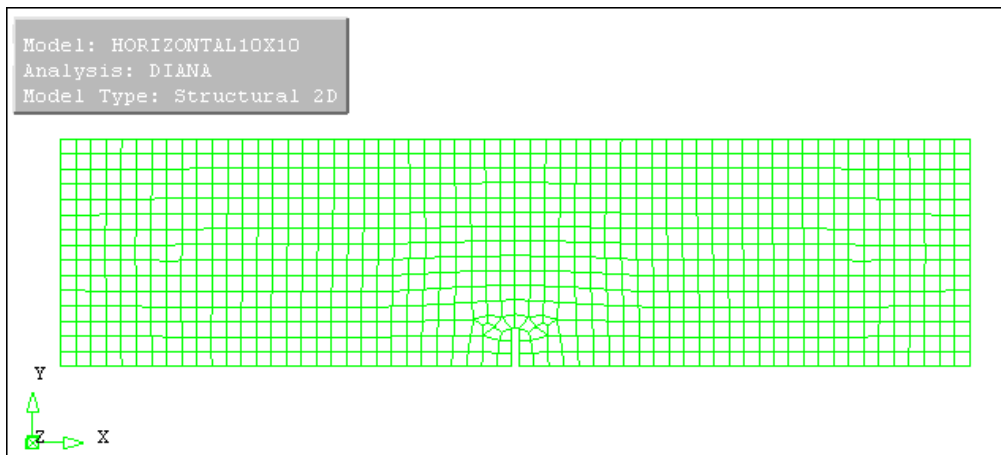
Figure 6.6: 10x10
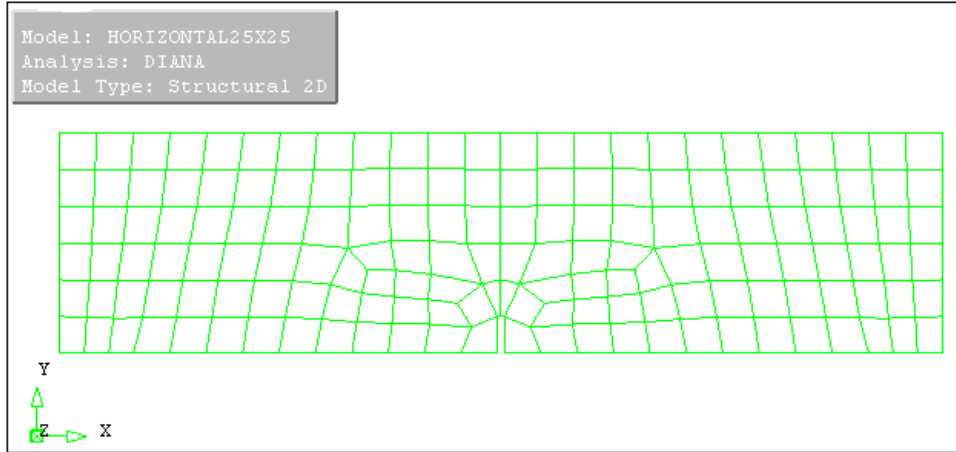
Figure 6.7: 25x25

Element size	Load [kN]	Displacement [mm]	Load step	Load 2.2 mm [kN]
10x10	39.154	0.55	36	32.354
12.5x12.5	40.117	0.6	37	31.714
25x25	41.566	0.8	41	29.858

Table 6.4: Maximum load-capacity and load-bearing capacity after 2.2 mm displacement - changes in mesh

As indicated in the graph, give the 25 mm element size a higher maximum load-capacity because of the courser mesh, but it also has the most unstable curve as the displacement grows. Both 12.5 and 10 mm element size give similarly shape and results. 12.5 mm has fewer elements, is therefore less computational expensive and fits the geometry very well.

Looking at residual tensile strength at a deflection of 2.2 mm corresponding to CMOD of 2.5 mm the role is switched. Here the 10 mm element size have the highest capacity and similar results to 12.5 mm, which is an example that a finer mesh give better results when looking at the development of the load-displacement curve. 12.5 mm element size was the one chosen to be used in the thesis.
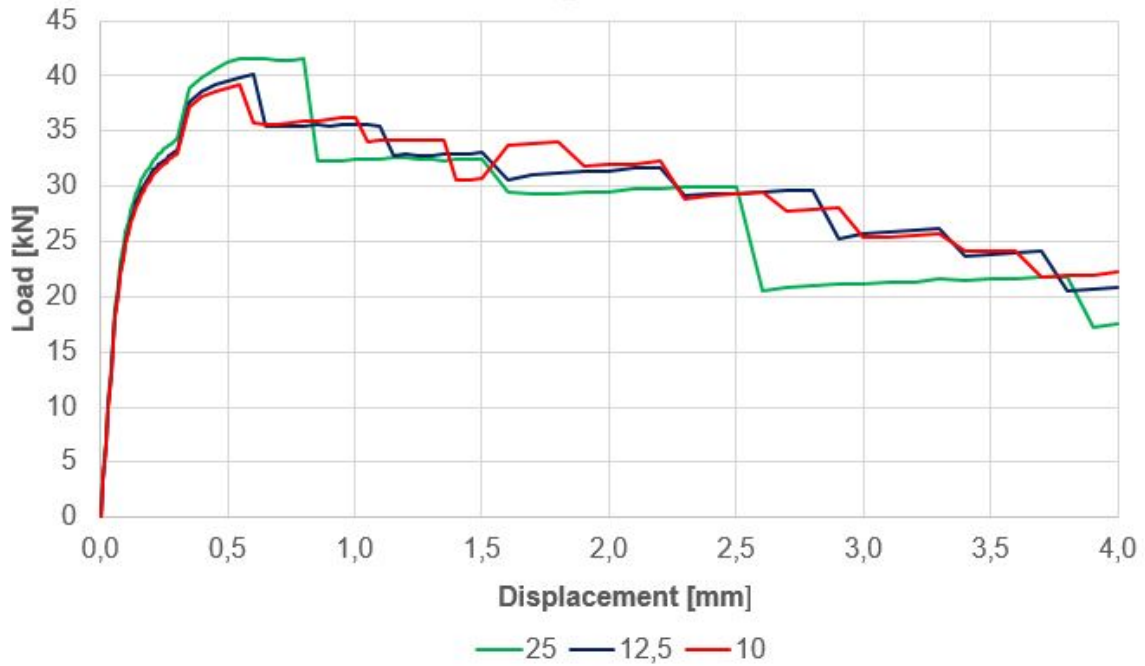
Figure 6.8: Load-displacement curves for different meshing

6.5 Same fibre orientation, homogenous distributed, in the whole beam

For the first FRC-analysis, only fibre orientations from 0 to 90 degrees in the 2D-view of the beam are taken into account and considered. The fibre orientations are horizontal (0 degrees), 30 degrees, 45 degrees, 60 degrees and vertical (90 degrees). It is assumed that the cracks are vertical, and therefore it is expected that the fibres acting normal to the cracks, i.e. horizontal, will give the highest capacity. The results from the analysis are compared with each other and cracking for non-reinforced concrete.
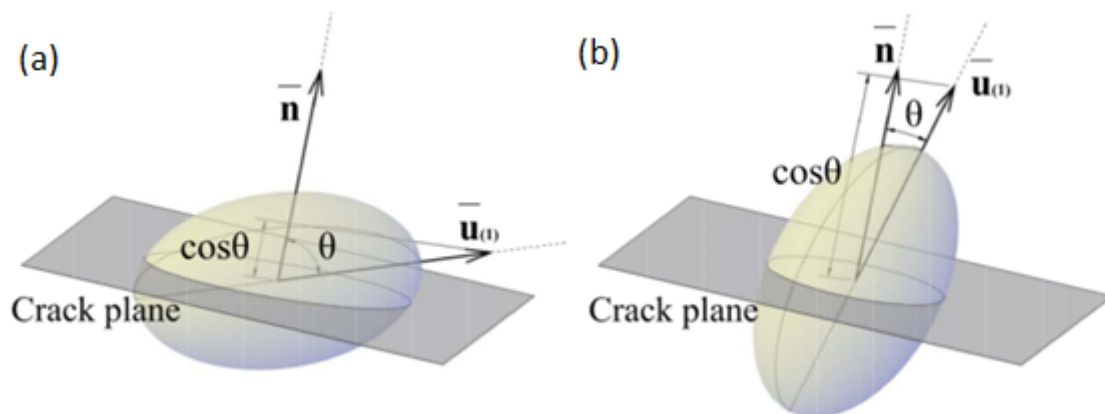
Figure 6.9: Crack plane illustration[3], (b) is the preferred fibre orientation
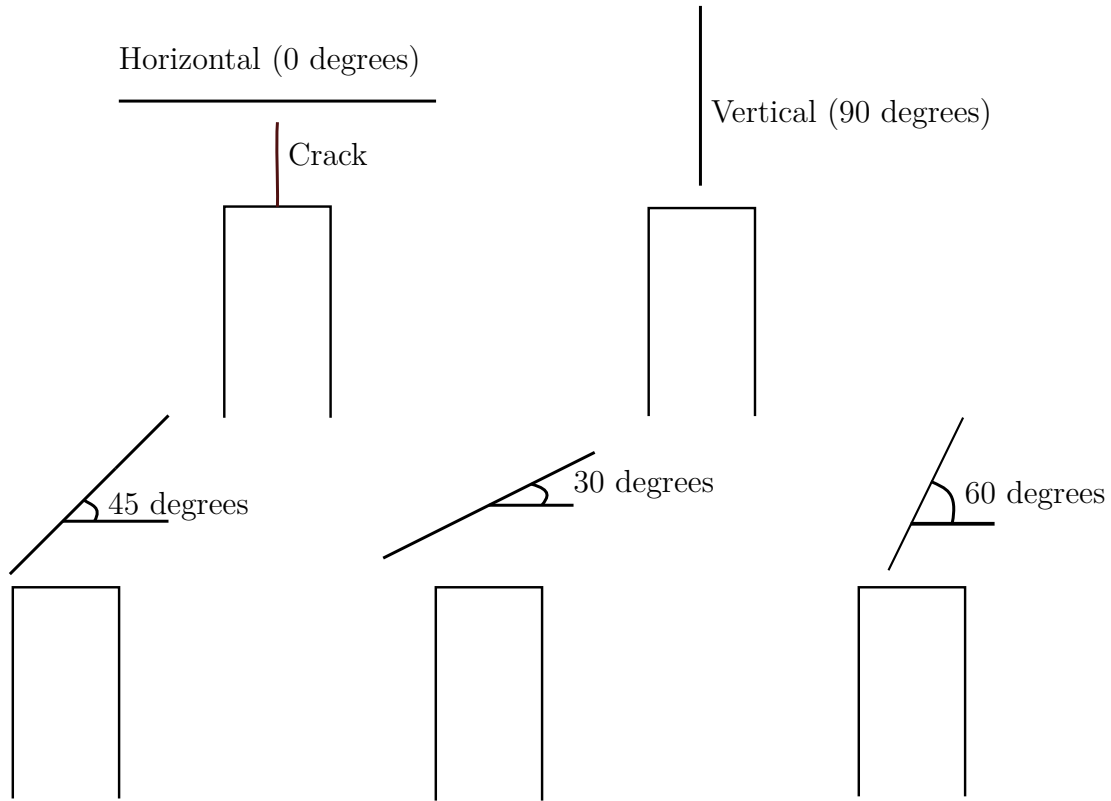
Figure 6.10: The orientations given. It is assumed that crack occur in the middle of the notch as shown on the upper left figure.

As shown in figure 6.9 the fibres in the real world would act like ellipsoids over an area. In this report, they are modeled as a behaviour over the whole beam or within an area in the mid-span, as in section 6.5 "Orientations changed in the mid-section of the beam".

A fibre efficiency parameter, based on experimental tests by Sarmiento [3], has been developed. The first term govern the orientation, the second part the influence from local changes density.

$$\mu = w_1 \cdot \cos(\theta) + w_2 \cdot \frac{v_f}{\bar{v}_f} \tag{6.11}$$

For the first part of the analasis only the orientation of the fibre (w_1) is considered.

$$w_1 = 1 \tag{6.12}$$

$$w_2 = 0 \tag{6.13}$$

making the fibre efficiency parameter as simple as:

$$\mu = \cos(\theta) \tag{6.14}$$

As shown in figure 6.11, all the different fibre orientations reach a tensile strength of 3.8 MPa before they start to loose their strength. In table 6.5 the residual tensile

strength for the different orientations are given.

Fibre direction	θ	μ	σ_2 [N/mm^2]
Horizontal (0 degrees)	0	1.000	3.8
30 degrees	30	0.866	3.3
45 degrees	45	0.707	2.7
60 degrees	60	0.500	1.9
Vertical (90 degrees)	90	0.000	0.0

Table 6.5: Residual tensile strength different orientations
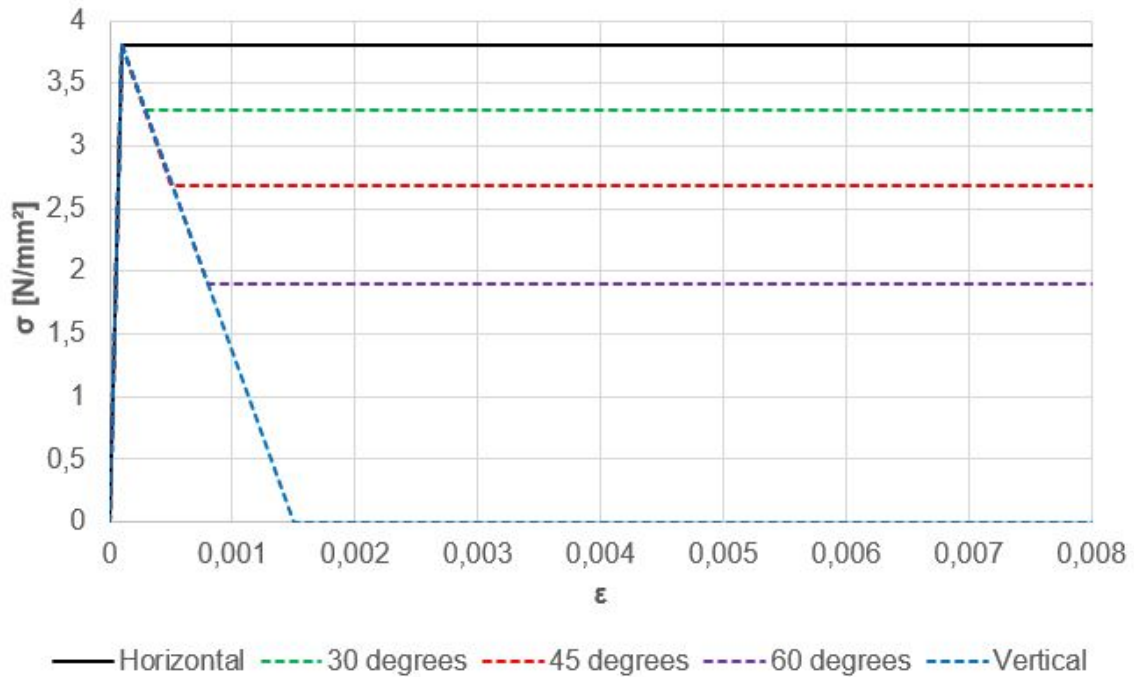
Figure 6.11: Tensile strength for the different orientations

Displacement controlled

Orientation	Load [kN]	Displacement [mm]	Load step	Increase [%]
Horizontal	40.117	0.6	37	344.7
30 degrees	27.201	0.24	25	233.7
45 degrees	23.083	0.45	34	198.3
60 degrees	18.490	0.45	34	158.9
Vertical	12.923	0.05	6	111

Table 6.6: Displacement at max load

After a deflection of 0.3 mm the non-reinforced concrete had almost none load-bearing capacity. So especially the load-bearing capacity after this point is significantly increased for all fibre orientations than vertical. In according to what is expected from the analysis of load-carrying capacity it is not surprising that horizontal fibres gave the best results. That also states that the model works the way it should do.

Another thing is that the FRC reach a much higher displacement before it start losing load-bearing capacity. Especially the horizontal fibre direction can resist huge deflections in this scale, and continue to have a high load-bearing capacity after the maximum load is reached. To show this a percentage increase in maximum load-bearing capacity is added in the table. As one can see, horizontal fibre orientation has almost 3.5 times as high capacity than non-reinforced concrete.
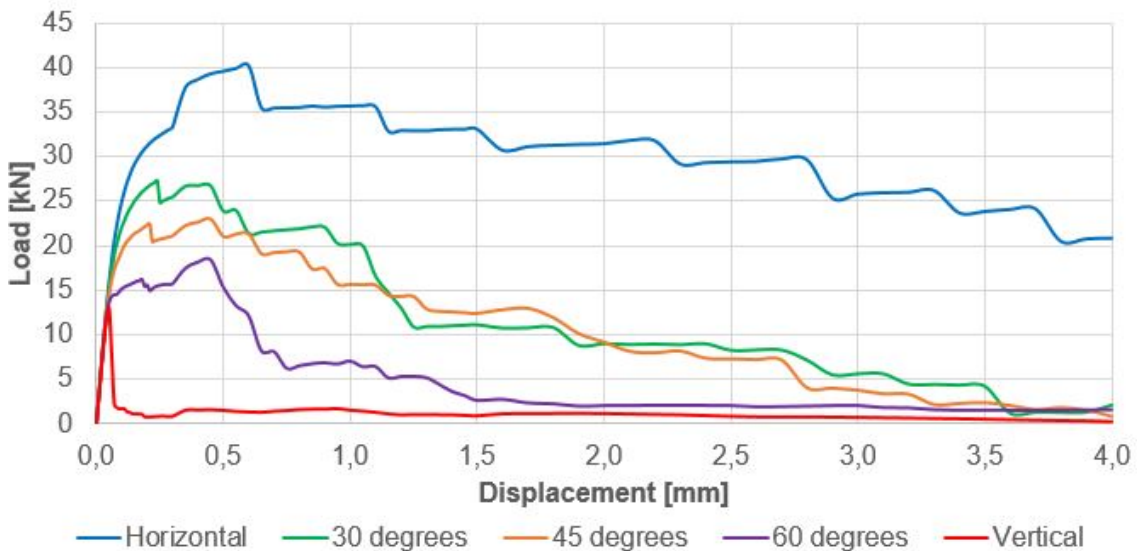
Figure 6.12: All orientations - same nonlinear properties in the whole beam

Figure 6.13 shows the displacements when the maximum load-capacity in the load-displacement curve for 45 degrees fibre orientation is reached. The stress plot shows how the stresses from the load works in the beam. The most affected area is at the top under the loading. The strain shows the increase of cracking over the notch. From these three plots, one can see that the critical area is in the mid-section.
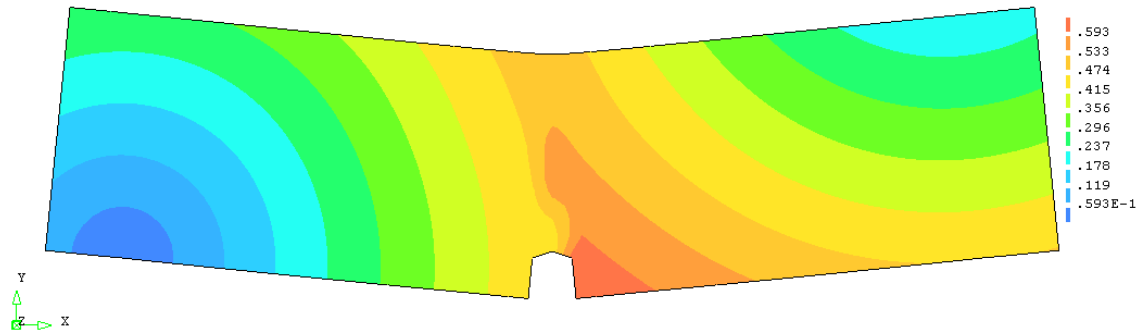
Figure 6.13: 45 degrees - Load step 34 - Displacement
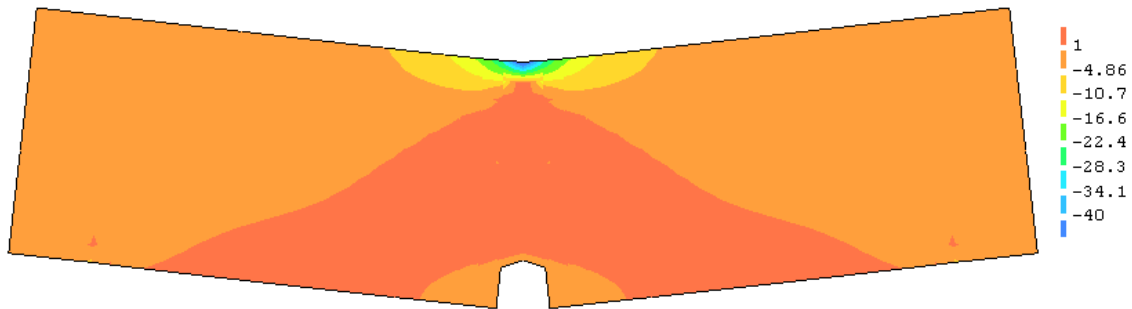
Figure 6.14: 45 degrees - Loadstep 34 - Displacement - Stress σ_{xx}
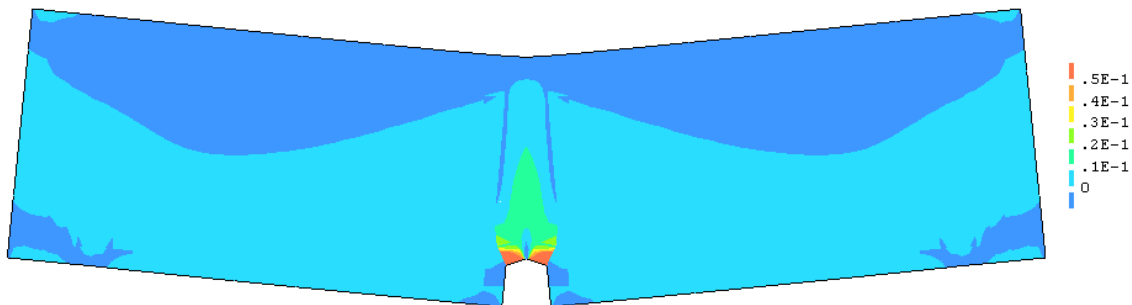
Figure 6.15: 45 degrees - Loadstep 34 - Displacement - Strain ε_{xx}

Capacity calculations

The relationship between δ and CMOD from NS-EN 14651 [14] states that:

$$\delta = 0.85 \cdot CMOD + 0.04 = 2.17 \tag{6.15}$$

The formula from NS-EN 14651 [14] to calculate the flexural residual tensile strength is given as:

$$f_{R.j} = \frac{3 \cdot F_j \cdot l}{2 \cdot b \cdot h_{sp}^2} \tag{6.16}$$

where F_j is the load-capacity at 2.17 mm displacement which corresponds to 2.5 mm CMOD. Here it is assumed that the results for 2.17 mm displacement can be assumed the same as the results from 2.2 mm displacement.

Orientation	Horizontal	30 degrees	45 degrees	60 degrees	Vertical
Load 2.2 mm [kN]	31.714	8.945	8.018	2.122	1.077

Table 6.7: Load at 2.2 mm displacement corresponding to CMOD of 2.5 mm, F_j

The contribution to the shear capacity from non-reinforced concrete based on simplified calculations according to EC2 [12] is given as:

$$V_{Rdc} = 26.184 kN \tag{6.17}$$

Orientation	Horizontal	30 degrees	45 degrees	60 degrees	Vertical
F_j [kN]	31.714	8.945	8.018	2.122	1.077
f_{R3} [N/mm^2]	10.148	2.862	2.566	0.679	0.345
$f_{ftd.res2.5}$ [N/mm^2]	2.503	0.706	0.633	0.167	0.085
M_{Rd} [kNm]	3.379	0.953	0.854	0.226	0.115
V_{Rdcf} [kN]	33.794	9.532	8.544	2.261	1.148
→ V_{Rd} [kN]	59.978	35.715	34.728	28.445	27.331

Table 6.8: Capacity calculations for the same fibre orientation in the whole beam based on formulas in the design codes

As one can see in the table perceptible contributions to the shear capacity are achieved with the fibre orientations horizontal (normal to crack), 30 degrees and 45 degrees.

Comparison with paper

In the paper which give the basis for the thesi,s the residual tensile strength is found based on the experimental results of f_{R3} using the formula:

$$\sigma_2 = \frac{f_{R3}}{3} \tag{6.18}$$

Orientation	Horizontal	30 degrees	45 degrees	60 degrees	Vertical
σ_2 [N/mm^2]	3.38	2.98	2.67	0.71	0.36

Table 6.9: Residual tensile strength, σ_2 based on formula from the paper

Based on the results from orientation analysis, the modeled value for the residual tensile strength for horizontal fibre orientation is overestimated with 3.8 N/mm^2 as its residual strength compared to 3.38 from the calculations afterwards. Same goes for 30 degrees, which was modeled with a residual tensile strength of 3.3 N/mm^2. 45 degrees on the other hand correspond very well. Modeled with 2.7 N/mm^2, and a result after analysis and calculations of 2.67 N/mm^2, is a good consistency. The chosen residual tensile strength for 60 degrees is totally overestimated with 1.9 N/mm^2

compared to 0.71 N/mm^2 based on calculations from the analysis. Vertical fibre orientation (which had a linear cracking modeled) gets a higher residual strength in the calculation, but that was expected. Worth mentioning is that in the paper both the fibre orientation and density are considered when calculating σ_2.

Force-controlled analysis

A lot of fittings were done to try and make a force-controlled analysis as close to the displacement-controlled as possible. They were presented in the chapter "Finite Element Modeling". The results for maximum load-capacity are presented in table 6.10.

Orientation	Load [kN]	Deflection [mm]	Load step
Horizontal	35.78	0.5417	35
30 degrees	27.90	0.2743	12
45 degrees	22.18	0.2071	80
60 degrees	16.43	0.1994	9
Vertical	9.21	0.0302	16

Table 6.10: Force-controlled analysis
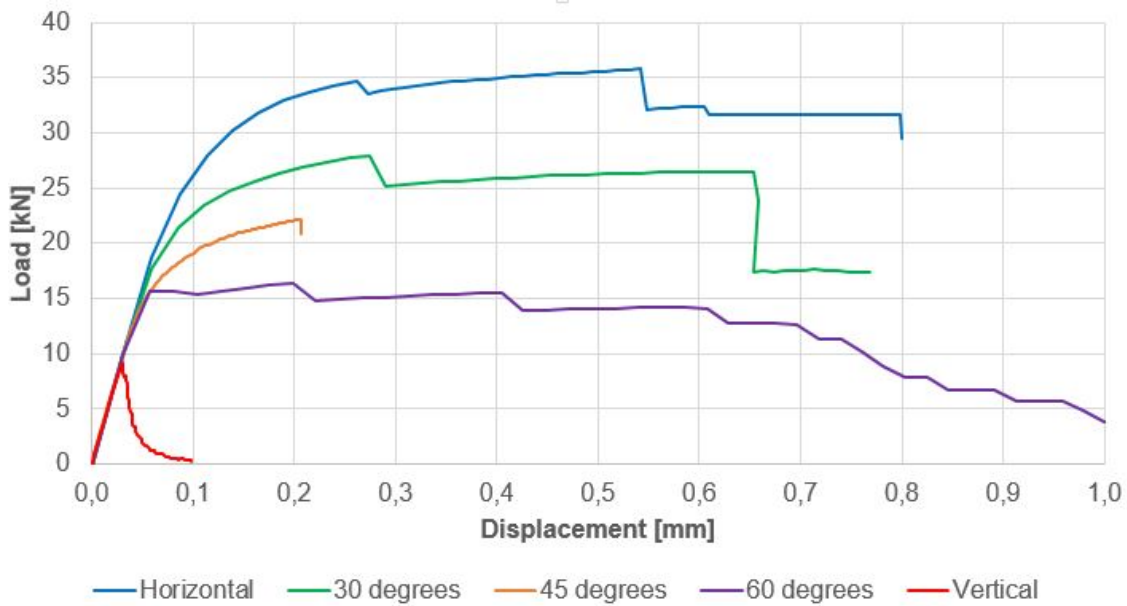
Figure 6.16: Force-controlled analysis

Comparison between force-controlled and displacement-controlled

The results on the load-capacity for all, except vertical fibre direction where the FRC have a brittle failure, show a good load-bearing capacity after the cracking start to occur. This was also expected, since the displacement-controlled analysis showed the same.

For horizontal fibre orientation, displacement-controlled at the same load step (0.54 mm) gave a load of 39.8 kN, which is over 4 kN higher than for the force-controlled analyze. Up to 0.3 mm the load-displacement curves are quite similar. Maximum from the displacement-controlled 40.117 kN were reached at 0.6 mm displacement. As one can see from figure 6.17, that is because the displacement-controlled analysis overcome a point at 0.3 mm, which the force-controlled cannot, and from there it get an increased load-bearing capacity.
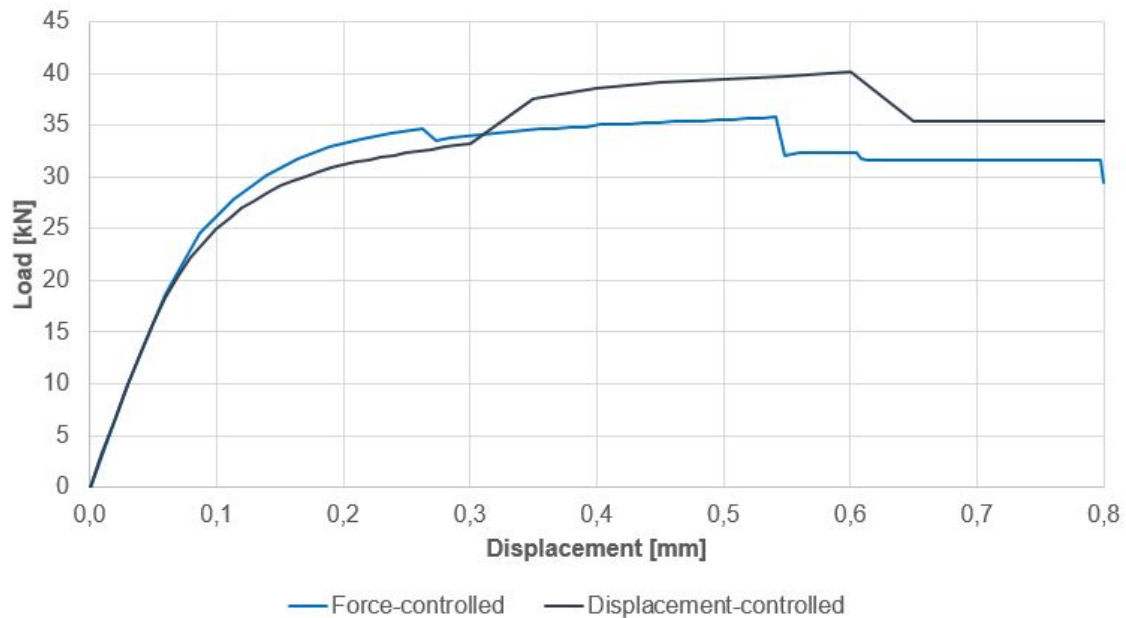
Figure 6.17: Horizontal, force control compared with displacement control

When looking at 30 degrees the results are quite similar. Actually has the force-controlled one higher capacity than the displacement controlled one, which had a maximum capacity of 27.2 kN at 0.24 mm displacement. At the same load step (0.27 mm) the load capacity from displacement-controlled is 25.1 kN. Figure 6.18 shows similar capacities, with a stable load-carrying ability until the force-controlled analyze suffer a a steep drop from a crack occurrence.
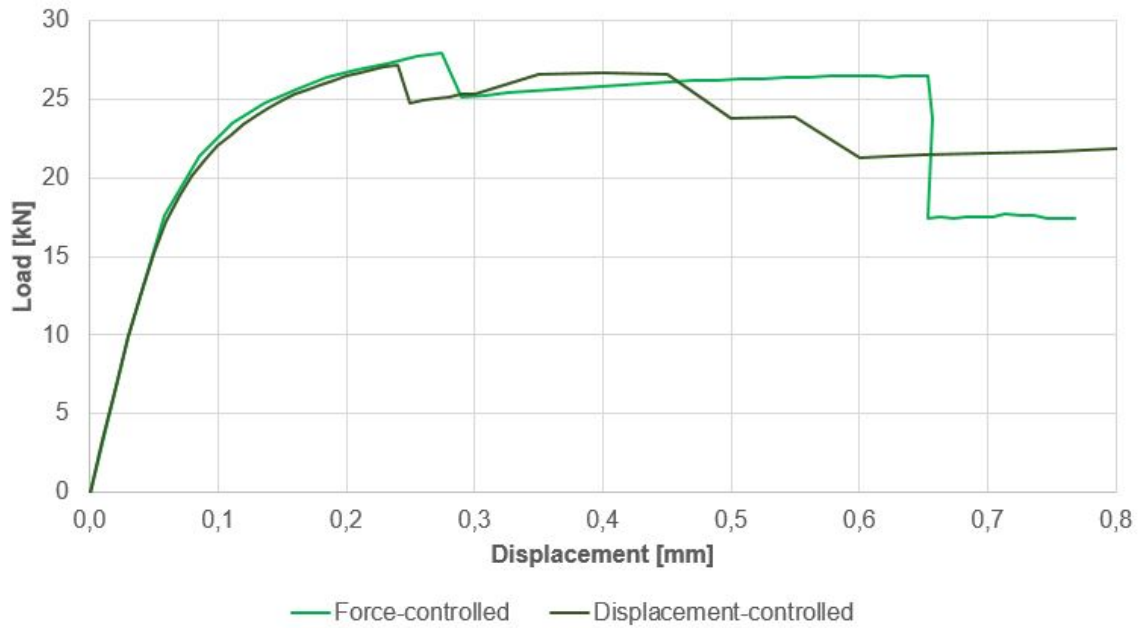
Figure 6.18: 30 degrees, force control compared with displacement control

45 degrees has definitely the best correspondence between the analysis. However, it was also the one that reached convergence first for the force-controlled analysis, only one load step after reaching maximum capacity. At 0.21 mm displacement-controlled analysis gives a load-capacity of 22.5 kN, which is very similar to the one in the force-controlled. The development of the curves are shown in figure 6.19. Since the displacement-controlled continue to develop, it reaches it maximum capacity of 23.083 kN at 0.45 mm displacement.
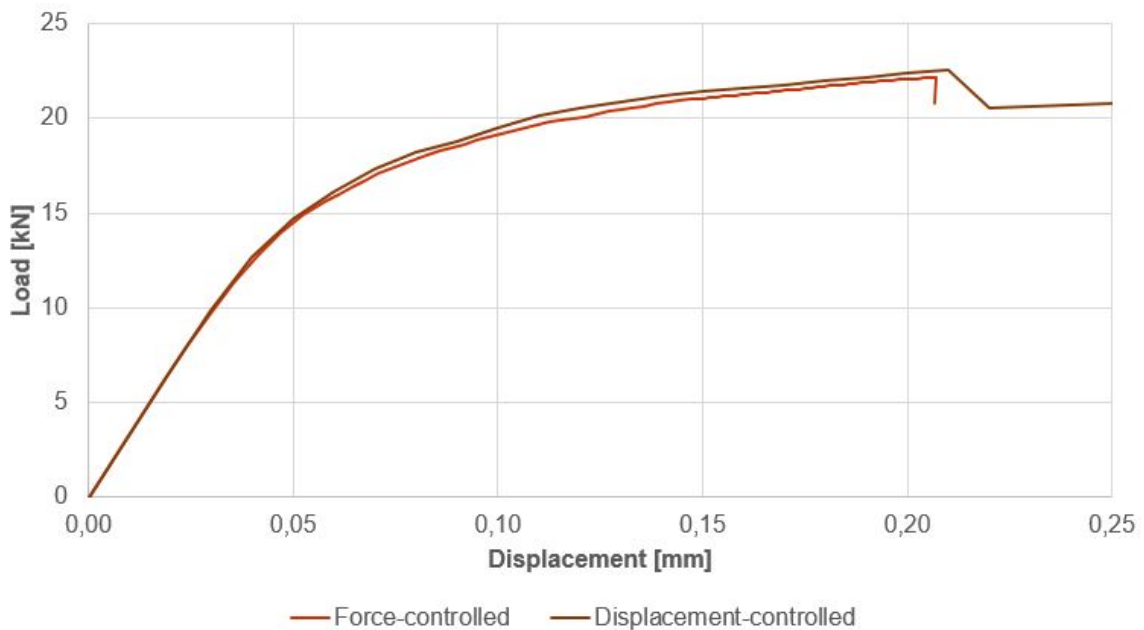
Figure 6.19: 45 degrees, force control compared with displacement control

51

60 degrees was the force-controlled analysis which went furthest, and therefore gave the best basis for comparison for an increasing displacement up to 1 mm deflection. When displacement-controlled analysis reached 0.2 mm the load is 15.658 kN, which is a bit lower than the force-controlled one. But as one can see in figure 6.20 their development up to this point are quite similar. After reaching 0.2 mm the force-controlled analysis start to have ductile behaviour, while the displacement-controlled overcome the critical point and reach maximum at 0.45 displacement before suffering a much more critical loss in capacity.
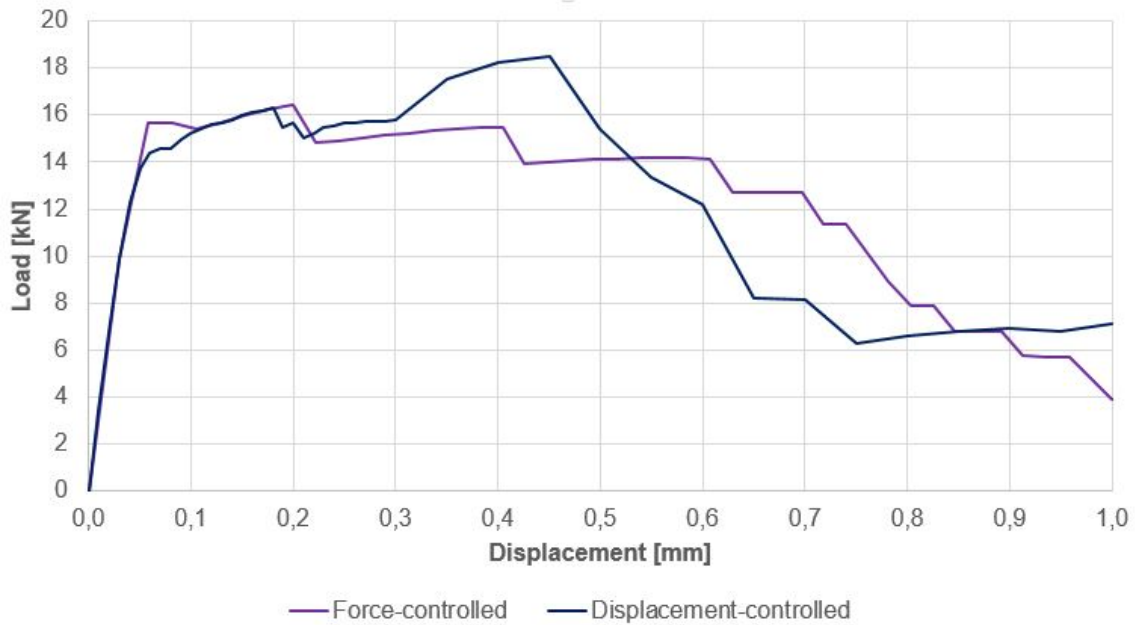
Figure 6.20: 60 degrees, force control compared with displacement control

For vertical fibre orientation, displacement-controlled analysis at 0.03 mm displacement gives 9.3 kN. That is similar to the maximum of 9.21 kN from the force-controlled at the same point. Up to maximum load the development is exactly the same. But, in difference, the curve from displacement-controlled analysis continue to grow up to a displacement of 0.05 mm where the load-capacity is 12.923 kN. Both have the brittle failure that were expected because of their orientation.
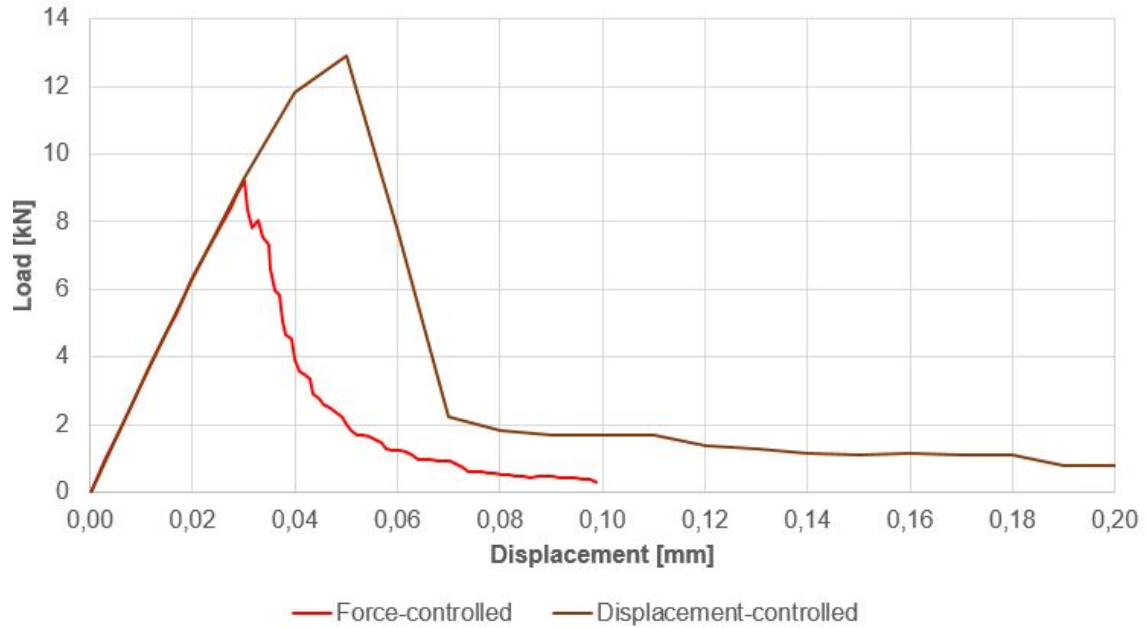
Figure 6.21: Vertical, force control compared with displacement control

Similar for all, except vertical fibre orientation, is that the load-displacement curve up to 0.2-0.3 mm deflection is the same. From there, the force-controlled analysis is stopped when it reach a convergence criteria.

Stress and strain at the same loads similar for both analysis for 45 degrees. The two plots for stress and strain for force-controlled (Annex I) confirming the statement that critical section for the beam is over the notch in the mid-span.

Crack development at several load levels

Because of the existence of the notch the crack pattern consists of a single crack in the mid-section. A point of interest will therefore be to look at the crack development. In the following figures the deformed beam and the displacement is displayed together with the equivalent Von Mises stresses [22]. This is done to give a better understanding of the crack development in the beams.

Before showing the results at the different load steps, it is interesting to observe figure 6.23, which corresponds to the maximum load in force-controlled analysis of 45 degrees fibre orientation and figure 6.22, which corresponds to the same displacement as the point where the force-controlled analyze reaches maximum. For displacement-controlled the Von Mises stress is 37.4 N/mm^2 for 0.2 mm displacement and 38.1 N/mm^2 for 0.21 mm displacement. Both displacements have a similar Von Mises distribution. The maximum for the force-controlled is 37.7 N/mm^2 at 0.207 mm displacement.

Since the displacement-controlled analysis can pass snap-through behaviour and pass limit points that analysis will reach a maximum load-bearing capacity at 0.45 mm displacement with a corresponding Von Mises stress of 56.3 N/mm². The reason why 45 degrees fibre orientation is chosen because it has a slowly decrease in load-bearing capacity until it almost has none left at 4 mm displacement. That symbolizes a ductile cracking. Therefore, this is the most interesting case to look into the crack development from. Because of the idealized situation with a concentrated at a single node, the analyze produce high concentrated stresses at the top of the beam. The increasing Von Mises stress is a result of higher compressive forces concentrated in a small area. [22]
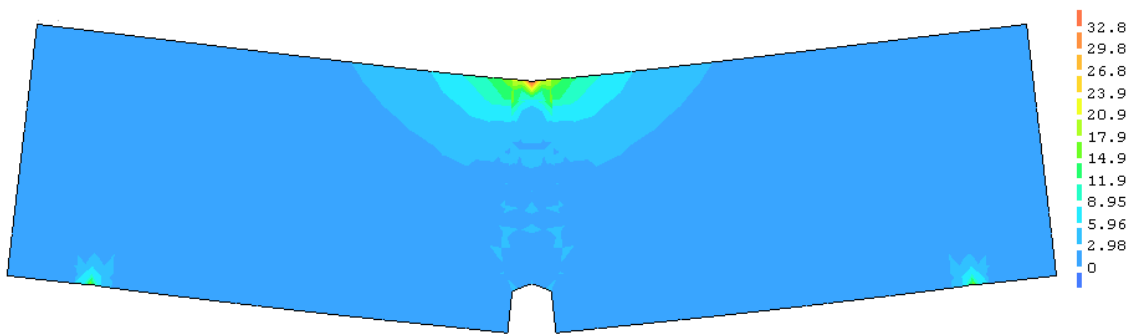
Figure 6.22: Crack and Von Mises stress for the displacement-controlled analysis, corresponding to a displacement of 0.2 mm - 45 degrees
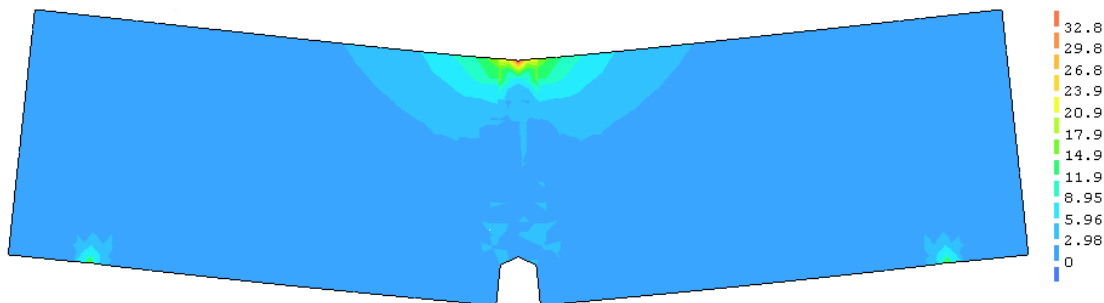
Figure 6.23: Crack and Von Mises stress for the force-controlled analysis just before convergence - 45 degrees

When showing the results at different load levels for the crack and Von Mises stress, the contour levels for the stress limited to 10 N/mm², so that it is possible to observe the stress development in the beam and not only in the cracked section. Since the force-controlled analysis reaches convergence when it gain the maximum load-capacity, only the displacement-controlled cracking for the 45 degrees fibre orientation is shown.

From figure 6.24 one can see that stresses increases up to load step 40, where the crack start arising. The load steps plotted are 2, 5, 10, 30, 40, 50, 55, 60, 65, 70, 75 and 80. The stresses is concentrated to the top of the mid-span. The crack development is increasing for each step, and one can clearly see how the crack appears in the mid-span.

56
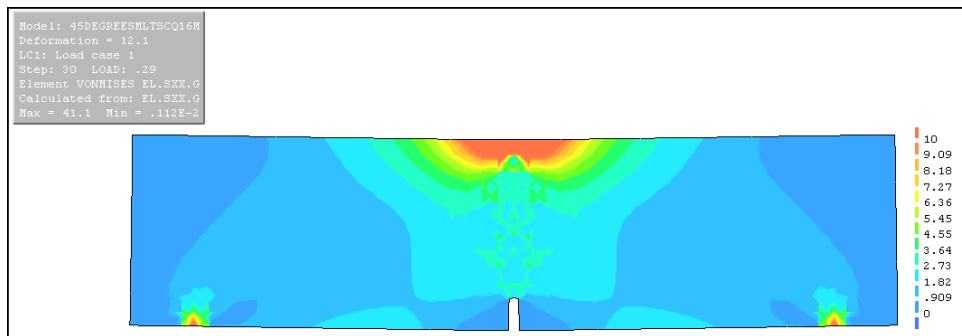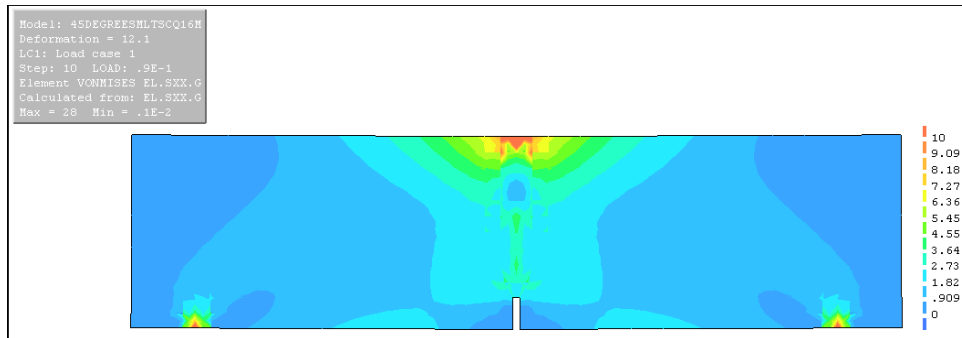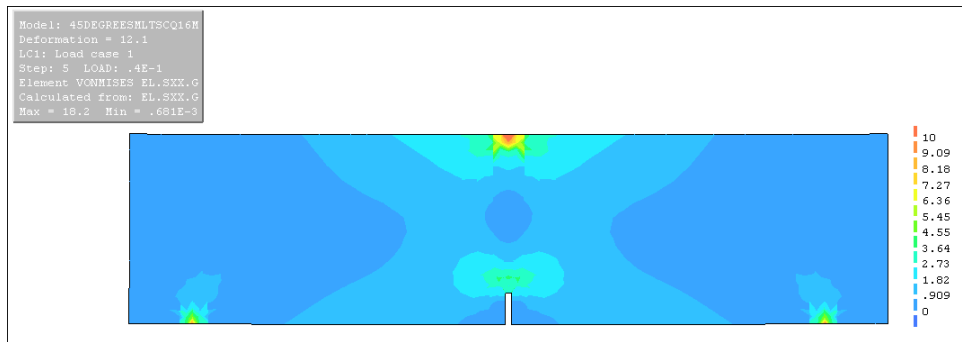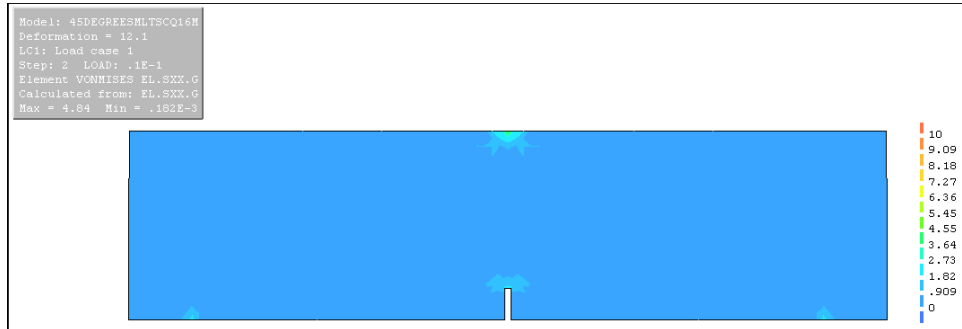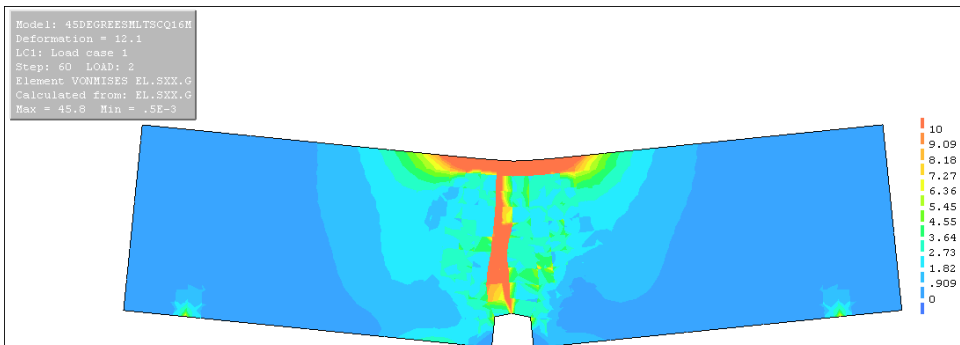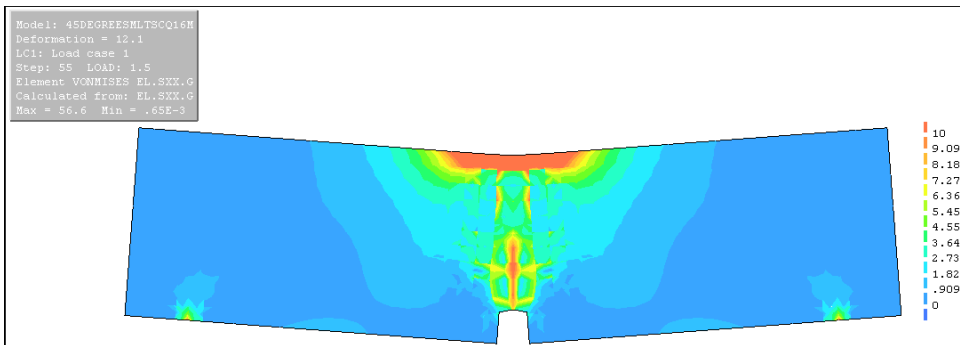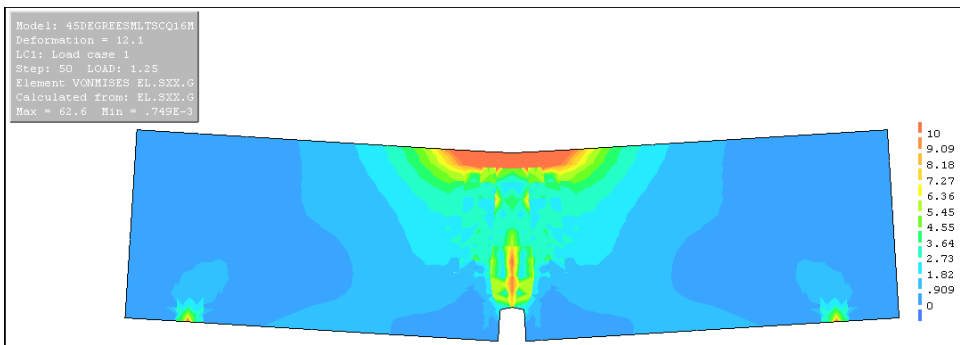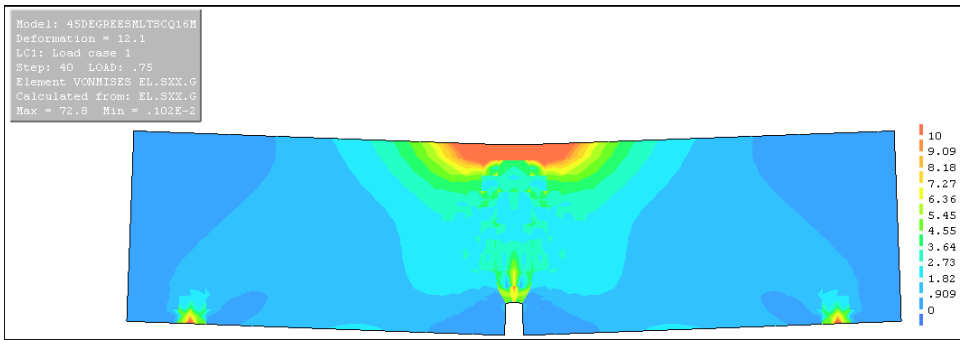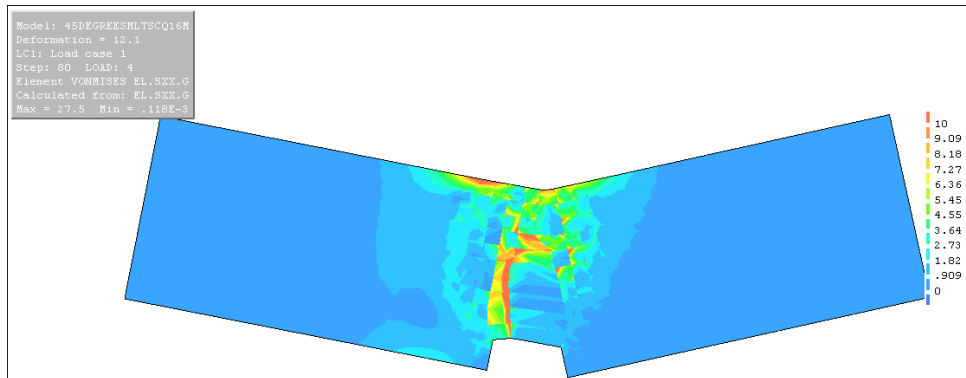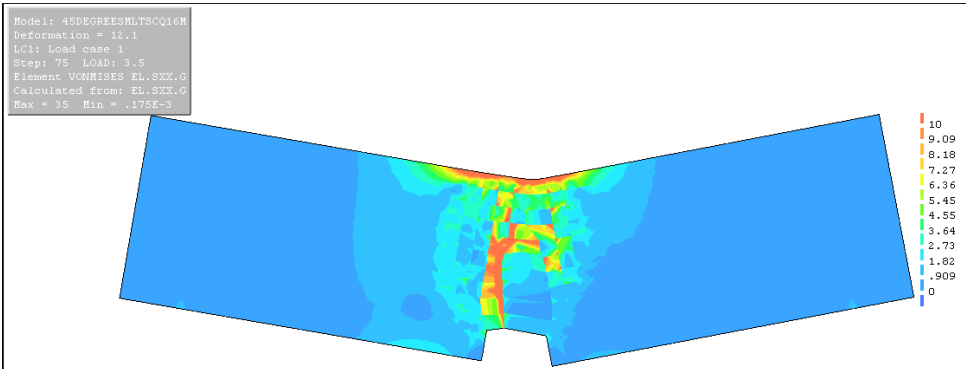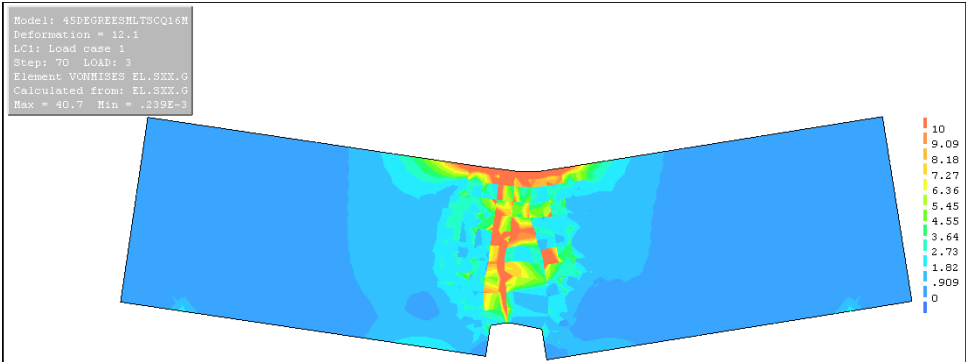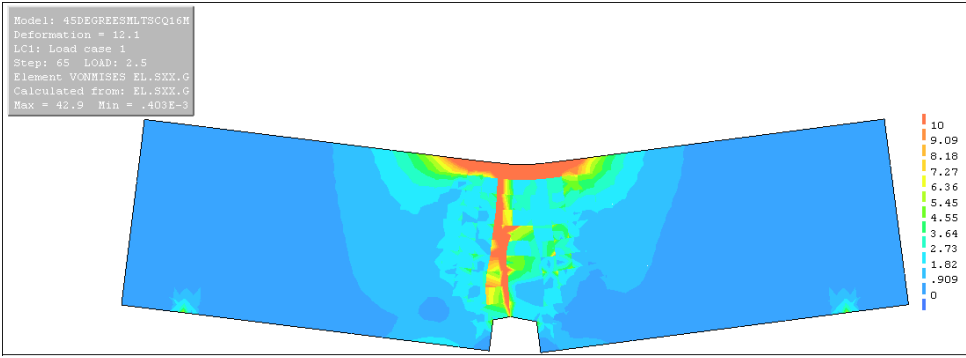
Figure 6.24: Crack development and Von Mises stresses

6.6 Orientations changed in the mid-section of the beam

Since the existence of the notch make the first cracking occur in the mid-span, it is of interest to look at this specific area and changes within it. Therefore, a modified area, as shown in figure 6.25, is modeled in the mid-span of the beam to be able to make changes within this area. This is, of course, a very simplified method to see what influence the fibre orientation in the mid-span have on the load-bearing capacity of the beam.

The tensile behaviour, kept the same as for the fibre orientations in the previous section, now varies within the modeled modified area in the beams. In this area, shown in figure 6.25, the specific orientation chosen is assumed homogenous distributed.
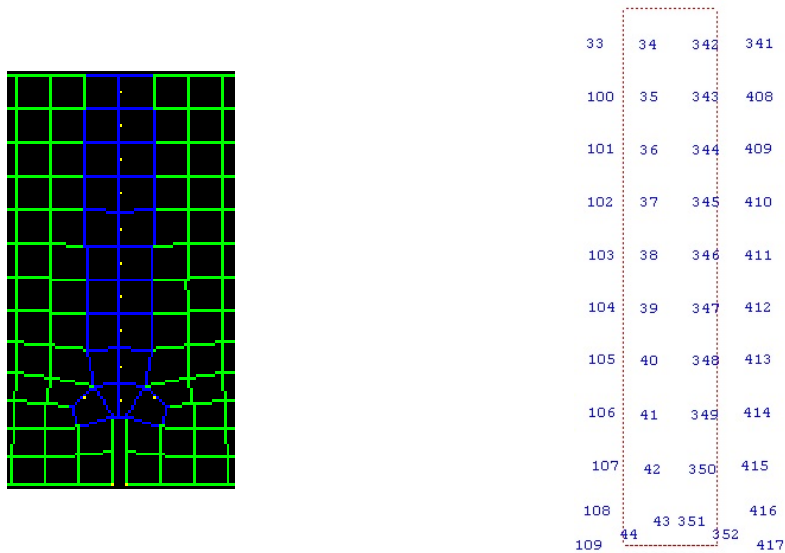
Figure 6.25: The modified area in the mid-section in DIANA. Elements 34-44 and 342-352 represent MO1

6.6.1 Changes within horizontal fibre orientation

The first attempt was with horizontal fibre orientation outside the modified area. The results for horizontal fibre orientation in the mid-section is therefore the same as in the first orientation analysis.

The results for 30 degrees in the mid-section gives the same maximum load-capacity as the one with 30 degrees in the whole beam, but the load-bearing capacity at 2.2 mm is a lot smaller. 8.945 kN when homogenous in the whole beam is almost twice as much as the results from this analyze. 45 degrees, 60 degrees and vertical

have quite similar results as for homogenous in the whole. All three has a bit lesser maximum load-capacity, but 60 degrees has a higher load-capacity at 2.2 mm. The results from these analysis are similar to the beams with same fibre orientations in whole beam for almost every of the fibre orientations except for 30 degrees. That may indicate that the horizontal fibres in the rest of the beam are not able to prevent the crack in the mid-section from growing.

Orientation	Load [kN]	Displacement [mm]	Load step	Load 2.2 mm [kN]
Horizontal	40.117	0.6	37	31.714
30 degrees	27.201	0.24	25	4.928
45 degrees	23.051	0.45	34	7.174
60 degrees	18.436	0.45	34	2.629
Vertical	11.498	0.04	5	0.804

Table 6.11: Horizontal, changes within modified area

Orientation	Horizontal	30 degrees	45 degrees	60 degrees	Vertical
f_{R3} [N/mm^2]	10.148	1.577	2.296	0.841	0.257
$f_{ftd.res2.5}$ [N/mm^2]	2.503	0.389	0.566	0.208	0.063
M_{Rd} [kNm]	3.379	0.525	0.764	0.280	0.086
V_{Rdcf} [kN]	33.794	5.251	7.645	2.801	0.857
$\rightarrow V_{Rd}$ [kN]	59.978	31.435	33.828	28.985	27.040

Table 6.12: Capacity calculations for changes in orientation in the modified area for horizontal fibre orientation around, based on formulas in the design codes.
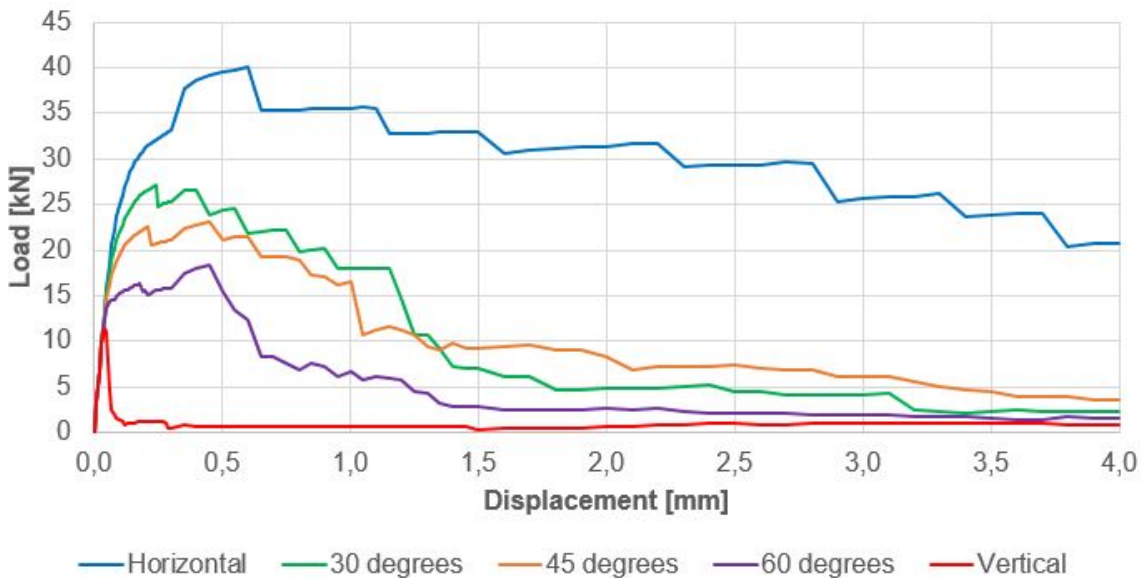
Figure 6.26: Load-displacement curves when the orientation is changing within modified area, horizontal fibre orientation in the rest of the beam.

6.6.2 Changes within 30 degrees fibre orientation

Here the fibre orientation outside the modified area is assumed to be 30 degrees.

The behaviour is as expected for all fibre directions, and also here the main difference is the load-bearing capacity at a displacement loading of 2.2 mm. As a difference from the previous case, the analyze with horizontal fibres in the middle has a remarkable decrease in the load-bearing capacity with a growing displacement, but it is still the one with highest capacity with increased loading. An interesting thing as well is the steep drop in load-bearing capacity for the horizontal fibre orientation from a displacement load of 1.3 mm to 1.35 mm. The quick loss of capacity, by all means, indicates a critical crack occurrence. Even so, the contribution from the horizontal and 30 degrees fibre orientations to the shear capacity from the calculations are still quite good.

Orientation	Load [kN]	Displacement [mm]	Load step	Load 2.2 mm [kN]
Horizontal	35.198	0.75	40	10.321
30 degrees	27.201	0.24	25	8.945
45 degrees	23.035	0.45	34	2.377
60 degrees	18.498	0.45	34	2.395
Vertical	11.498	0.04	5	0.1

Table 6.13: 30 degrees, changes within modified area

Orientation	Horizontal	30 degrees	45 degrees	60 degrees	Vertical
f_{R3} [N/mm^2]	3.303	2.862	0.761	0.766	0.032
$f_{ftd.res2.5}$ [N/mm^2]	0.815	0.706	0.188	0.189	0.008
M_{Rd} [kNm]	1.100	0.953	0.253	0.255	0.011
V_{Rdcf} [kN]	10.998	9.532	2.533	2.255	0.107
$\to V_{Rd}$ [kN]	37.182	35.715	28.716	28.736	26.290

Table 6.14: Capacity calculations for changes in orientation in the modified area for 30 degrees fibre orientation around, based on formulas in the design codes.
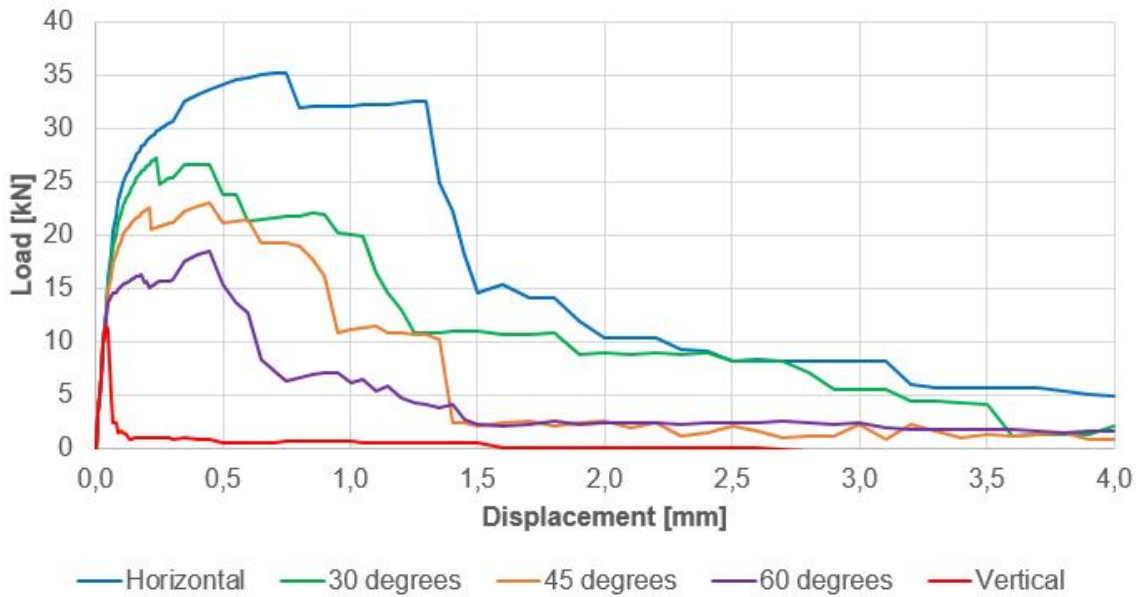
Figure 6.27: Load-displacement curves when the orientation is changing within modified area, 30 degrees fibre orientation in the rest of the beam.

6.6.3 Changes within 45 degrees fibre orientation

In these analysis the fibre orientation outside the modified area is 45 degrees.

The results are as expected for the maximum load-capacity. If there are horizontal fibre orientation in the middle the beam has the highest maximum load-capacity, but a lower value compared to horizontal or 30 degrees orientation in the rest.

For both 30 in and 45 degrees fibre orientation in the middle, the results for the load-bearing capacity up 0.3 mm loading, i.e. before the distance between load steps increase from 0.01 to 0.05 mm, are exactly the same if the orientation around is either 30 degrees or 45 degrees. That indicate that for FRC beams with quite similar properties in the rest of the beam as in the mid-section, the property outside the mid-section does not have any influence on low displacements.

When it comes to load-bearing capacity and the resistance at 2.2 mm displacement, the special thing in these analysis is that the vertical fibre orientation does not have any resistance at all. In addition, 30 and 45 degrees fibre orientation have a higher load-capacity than horizontal at this point. That may indicate that the properties for the residual tensile strength for these orientations fit each other well in the intersection between them. As for the analysis with 30 degrees, the curve for horizontal fibre orientation has a steep drop in the load-displacement curve. However, this time it happens at a lower displacement load, from 1.05 to 1.1 mm.

Interesting thing to observe in this case as that the load-carrying capacity for 30 degrees between 1 mm and 2 mm is significantly higher than for the case where it is a 30 degrees fibre orientation in the whole beam modeled.

Orientation	Load [kN]	Displacement [mm]	Load step	Load 2.2 mm [kN]
Horizontal	30.304	0.8	41	5.563
30 degrees	27.201	0.24	25	8.877
45 degrees	23.083	0.45	34	8.018
60 degrees	18.490	0.45	34	2.533
Vertical	11.498	0.04	5	-0.039

Table 6.15: 45 degrees, changes within modified area

Orientation	Horizontal	30 degrees	45 degrees	60 degrees	Vertical
f_{R3} [N/mm^2]	1.780	2.841	2.566	0.811	0
$f_{ftd.res2.5}$ [N/mm^2]	0.439	0.701	0.633	0.200	0
M_{Rd} [kNm]	0.593	0.946	0.854	0.270	0
V_{Rdcf} [kN]	5.928	9.459	8.544	2.699	0
$\rightarrow V_{Rd}$ [kN]	32.11	35.643	34.728	28.883	26.184

Table 6.16: Capacity calculations for changes in orientation in the modified area for 45 degrees fibre orientation around, based on formulas in the design codes.
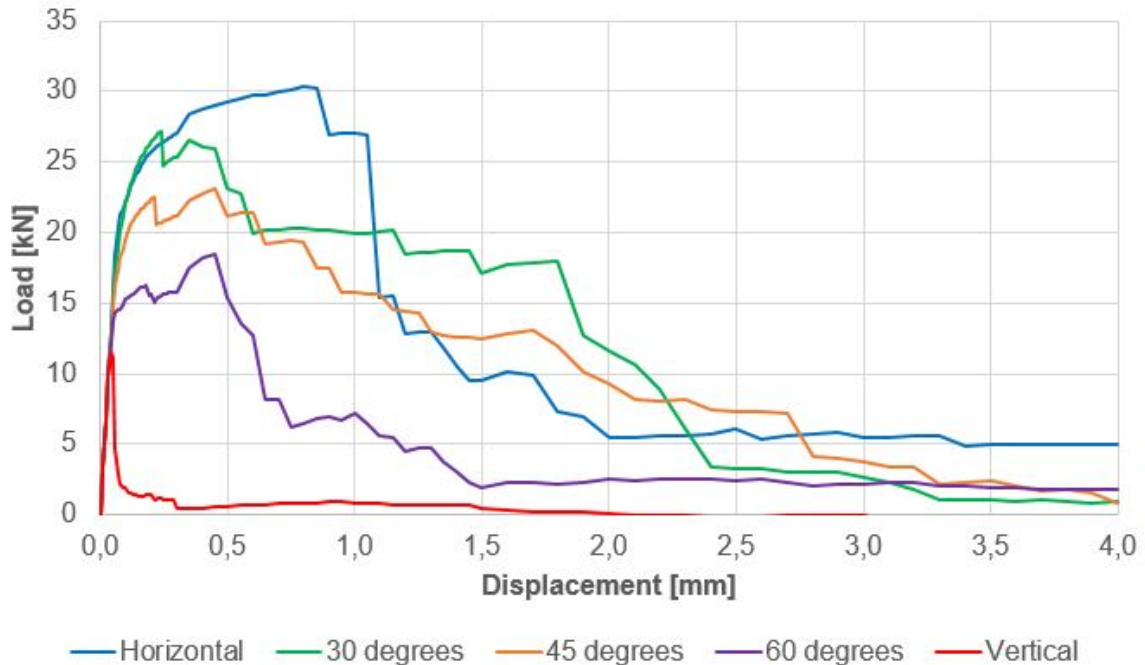
Figure 6.28: Load-displacement curves when the orientation is changing within modified area, 45 degrees fibre orientation in the rest of the beam.

6.6.4 Changes within 60 degrees fibre orientation

Here the fibre orientation outside the modified area is 60 degrees.

Also in this case the results for maximum loading for the other orientations than horizontal fibre orientation are astonishing similar as for the other fibre orientations outside the modified area. The horizontal fibre orientation still has decreasing maximum loading and a steep drop at an earlier stage than for a smaller degree for the orientation around.

Worth mentioning is the contribution from the 45 degrees fibre orientation to the shear capacity from the calculations. It gets its best result as the load-displacement curve evolves when the fibre orientation outside the mid-section is 60 degrees.

Orientation	Load [kN]	Displacement [mm]	Load step	Load 2.2 mm [kN]
Horizontal	22.463	0.45	34	4.187
30 degrees	27.201	0.24	25	6.297
45 degrees	23.083	0.45	34	8.680
60 degrees	18.490	0.45	34	2.122
Vertical	11.498	0.04	5	0.515

Table 6.17: 60 degrees, changes within modified area

Orientation	Horizontal	30 degrees	45 degrees	60 degrees	Vertical
f_{R3} [N/mm^2]	1.340	2.015	2.778	0.679	0.165
$f_{ftd.res2.5}$ [N/mm^2]	0.330	0.497	0.685	0.167	0.041
M_{Rd} [kNm]	0.446	0.671	0.925	0.226	0.055
V_{Rdcf} [kN]	4.462	6.710	9.249	2.261	0.549
$\rightarrow V_{Rd}$ [kN]	30.645	32.894	35.433	28.445	26.732

Table 6.18: Capacity calculations for changes in orientation in the modified area for 60 degrees fibre orientation around, based on formulas in the design codes.
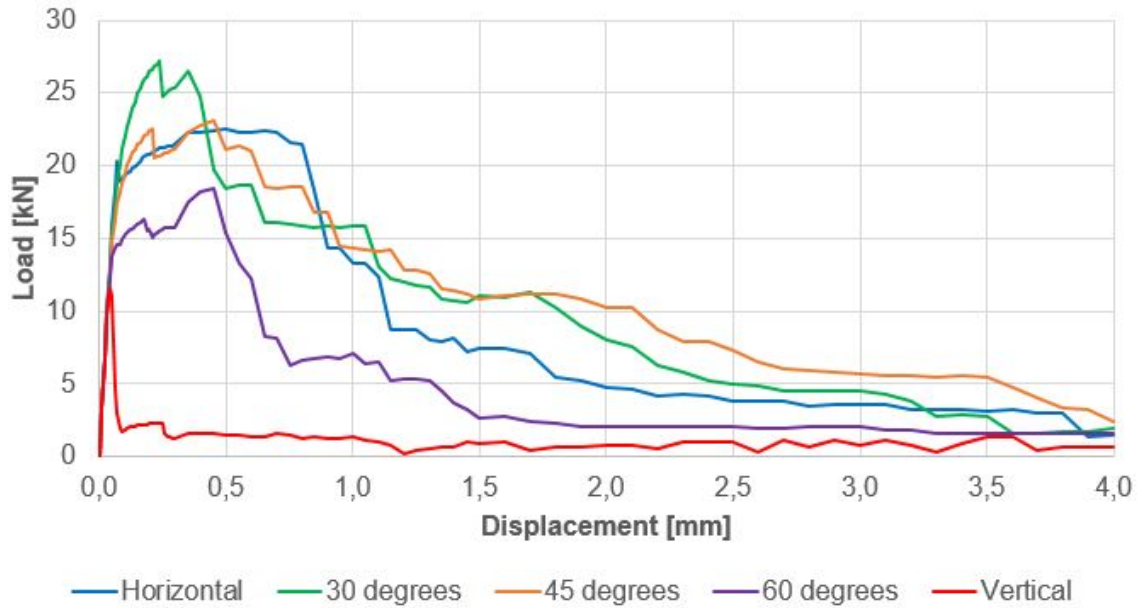
Figure 6.29: Load-displacement curves when the orientation is changing within modified area, 60 degrees fibre orientation in the rest of the beam.

6.6.5 Changes within vertical fibre orientation

Here the fibre orientation outside the modified area is vertical (90 degrees).

As expected, this has a larger impact on the capacity of the beams. Especially the load-bearing capacities when the displacement becomes larger than 1 mm are small compared with all the other beams for all orientations except the vertical fibre orientation itself.

Even though many of the fibre orientation have quite good maximum load-bearing capacities, all except 60 degrees fibre orientation have high drops corresponding to a brittle behaviour similar to non-reinforced concrete and vertical fibre orientation in the whole beam after reaching maximum capacity. That confirms the statement that the most important contribution from the orientation around the mid-section is the load-bearing ability with increasing displacements after reaching maximum capacity.

Orientation	Load [kN]	Displacement [mm]	Load step	Load 2.2 mm [kN]
Horizontal	21.364	0.08	9	2.104
30 degrees	27.161	0.24	25	4.529
45 degrees	23.188	0.55	36	2.732
60 degrees	18.335	0.45	34	2.635
Vertical	12.923	0.05	6	1.077

Table 6.19: Vertical, changes within modified area

Orientation	Horizontal	30 degrees	45 degrees	60 degrees	Vertical
f_{R3} [N/mm^2]	0.673	1.449	0.874	0.843	0.345
$f_{ftd.res2.5}$ [N/mm^2]	0.166	0.357	0.216	0.208	0.085
M_{Rd} [kNm]	0.224	0.483	0.291	0.281	0.115
V_{Rdcf} [kN]	2.242	4.826	2.911	2.808	1.148
$\rightarrow V_{Rd}$ [kN]	28.426	31.010	29.095	28.991	27.331

Table 6.20: Capacity calculations for changes in orientation in the modified area for vertical fibre orientation around, based on formulas in the design codes
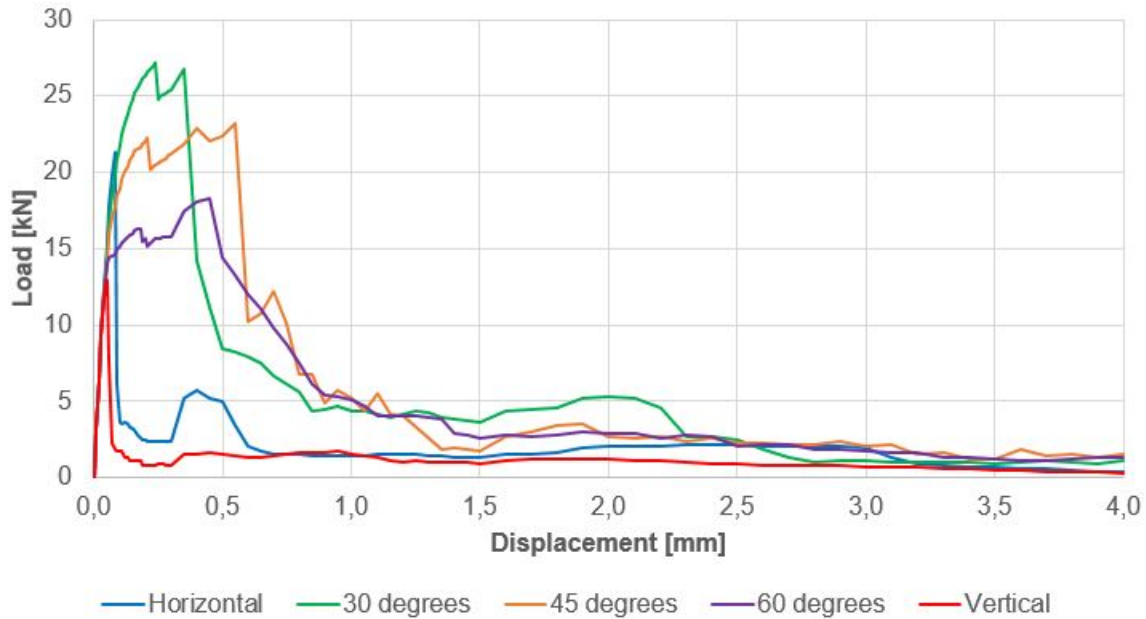
Figure 6.30: Load-displacement curves when the orientation is changing within modified area, vertical fibre orientation in the rest of the beam.

6.6.6 The influence of changing the property outside the mid-section for the different fibre orientations

To get a clearer overview over what influence the orientations outside the modified area in the mid-section has to say for the load-bearing capacity of the beams new load-displacement curves are made. In the presented diagrams, it is now the orientation outside the modified area that changes for the curves, not the one inside.

Horizontal are the one that behave the most as expected. Here, the lower the fibre orientation degree is, the higher the capacity. Similar for the other orientations than horizontal itself is the drop in capacity. The less favourable orientation clearly impact the load-bearing capacity of the beams.
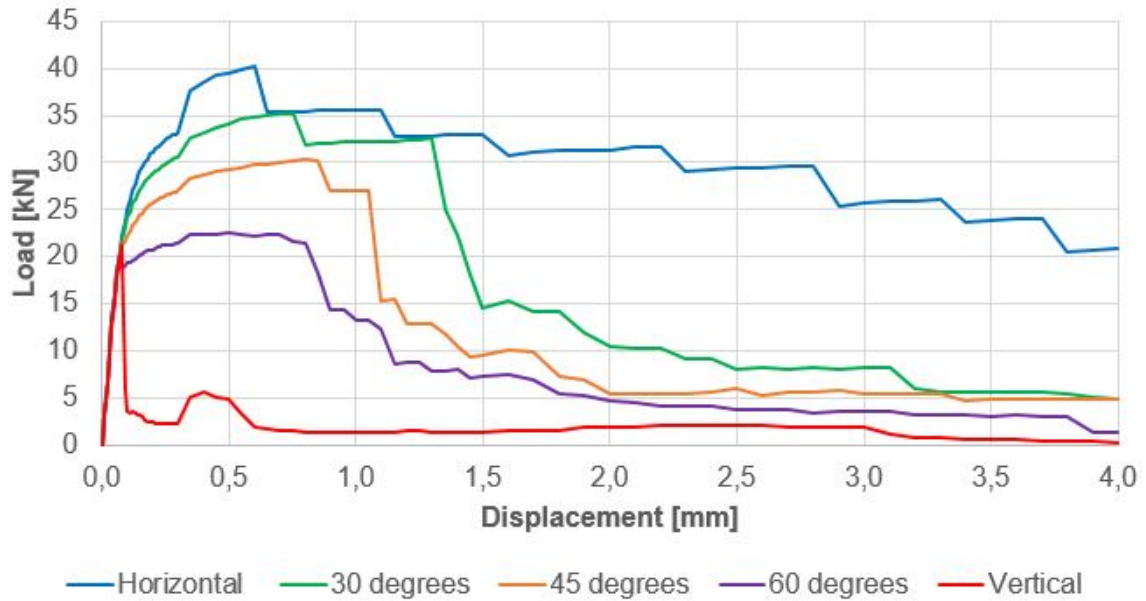
Figure 6.31: Horizontal fibre orientation in the mid-span with different properties in the rest of the beam.

30 degrees in the mid-section acts the same up to displacement of 0.3 mm for all cases. After this point, different developments start to evolve and the orientation in the rest of the beam begin to have an influence. Special for this analysis is that the load-bearing capacity for the beam with 45 degrees modeled in the rest has a much higher than the rest of the orientations between 1 and 2 mm displacement loading.
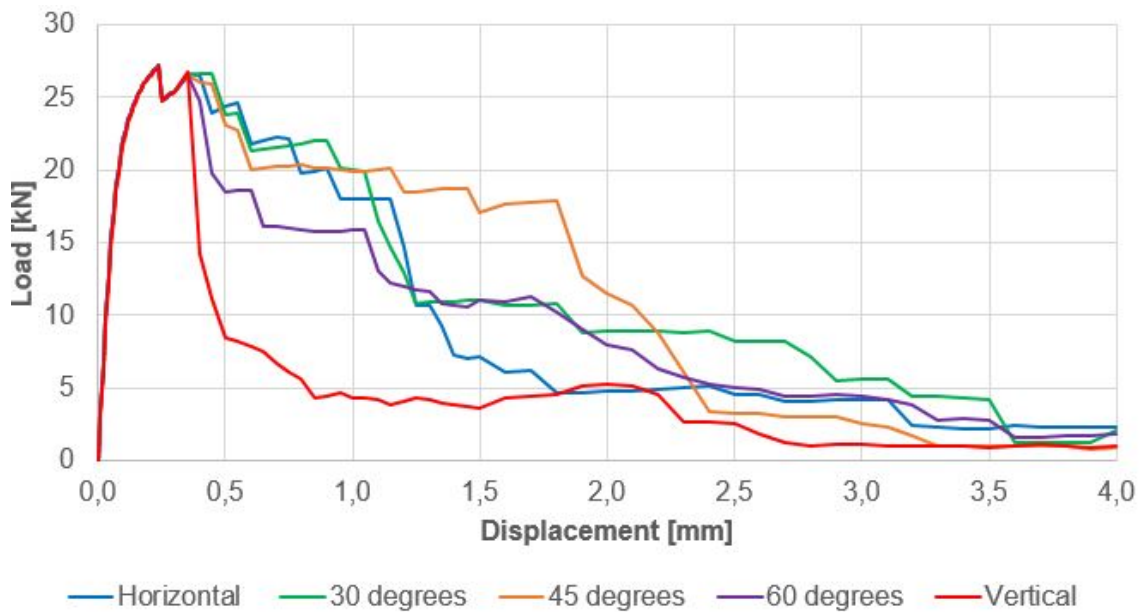
Figure 6.32: 30 degrees fibre orientation in the mid-span with different properties in the rest of the beam.

45 degrees fibre orientation has quite similar behaviour for horizontal, 45 degrees and 60 degrees fibre direction in the rest of the beam. With 30 degrees fibre orientation in the rest of the beam it behave similarly until 1.35 mm displacement before it get a second drop before reaching 1.4 mm displacement. Most certainly, a critical crack has been developed at this displacement loading, and the loss in capacity is caused by that. Another thing to notice is when it is vertical fibre orientation in the rest of the beam, the 45 degrees fibres in the middle try to counteract the influence and has a little bit higher capacity than for the other cases before the steep drop in load-capacity.
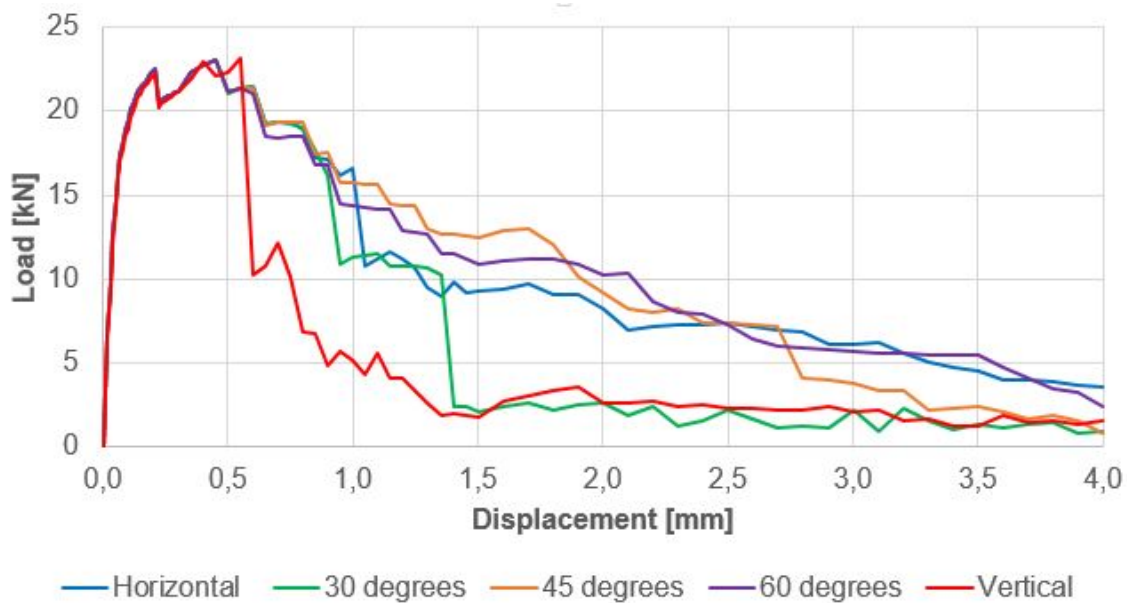
Figure 6.33: 45 degrees fibre orientation in the mid-span with different properties in the rest of the beam.

Looking at 60 degrees fibre orientation in the middle, the fibre orientation in the rest of the beam does not seem to have any impact at all. After reaching maximum load-capacity, some differences in the softening part of the curve can be seen up to 1.5 mm displacement, where the load-bearing capacity becomes similar for all the different orientations outside the mid-section.

As for 60 degrees orientation also the vertical orientation act similar for all cases. It reach a peak load of 11.5 kN for all, except the original one. When maximum is reached, the beams have a brittle failure and almost no residual load-bearing capacity afterwards. This was anyhow expected, since the fibres job is to withstand crack growth. Fibres acting in vertical 2D-direction does not affect this process much. The load-bearing capacity will therefore after the occurrence first crack become very low, since the crack will continue to develop without the fibres preventing it.
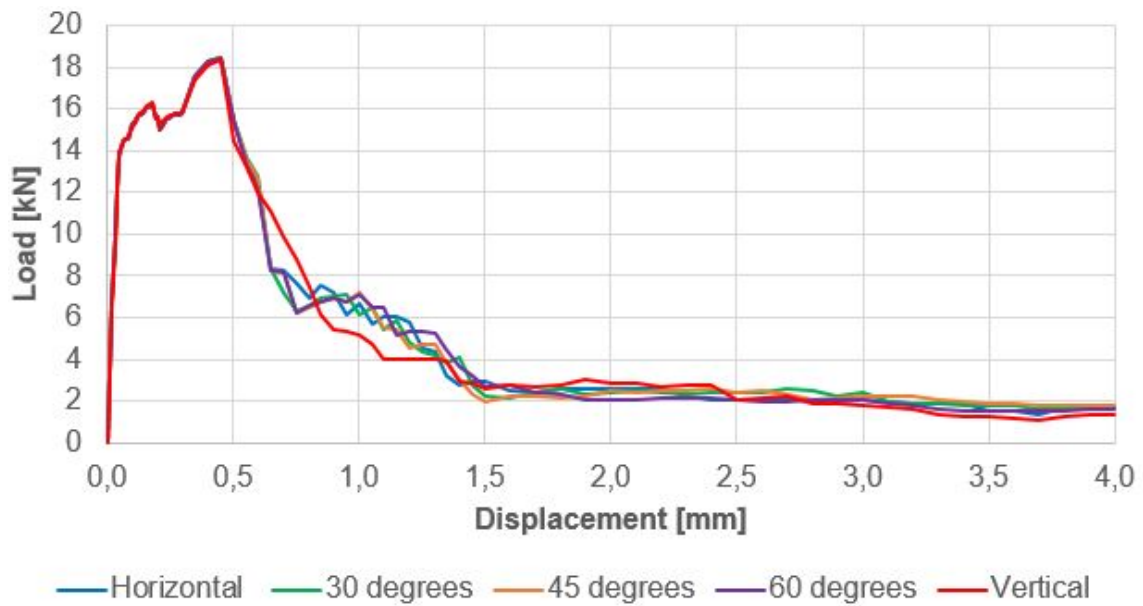
Figure 6.34: 60 degrees fibre orientation in the mid-span with different properties in the rest of the beam.
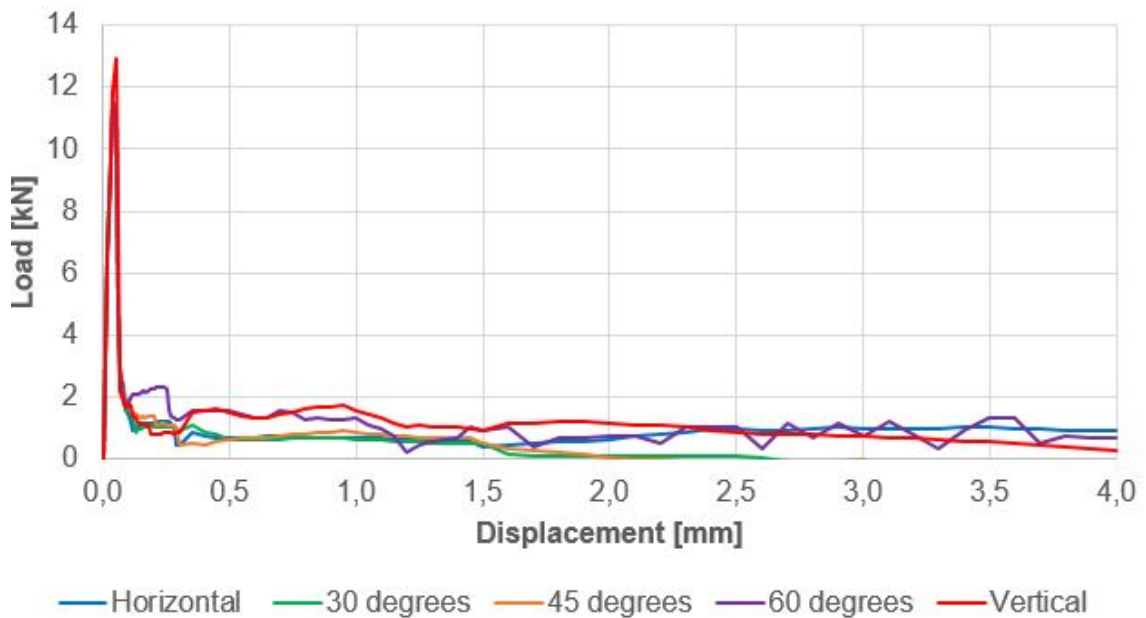
Figure 6.35: Vertical fibre orientation in the mid-span with different properties in the rest of the beam.

6.7   Exceeding the modified area in the mid-span

Since the lower angle on the fibre orientation did not have any considerable impact on the load-bearing ability for vertical fibre orientation in the mid-section a new, exceeded area, was modeled to see what effect that are going to have on the capacity. The new modified area is called MO2, and is shown in figure 6.36.
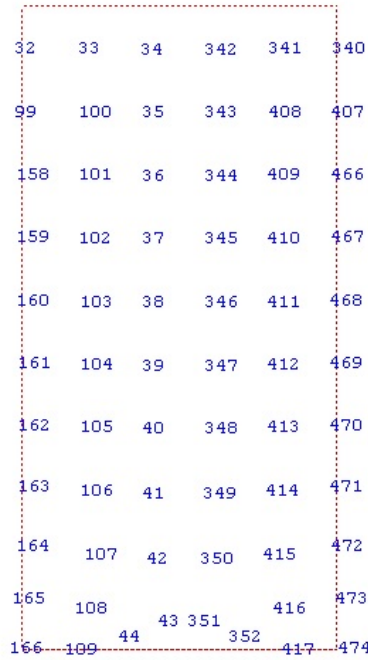
Figure 6.36: Modified area, MO2. Elements 33-44 100-109 159-163 341-352 408-417 467-471 represent MO2.

6.7.1   Results MO2

Orientation	Load [kN]	Displacement [mm]	Load step	Load 2.2 mm [kN]
Horizontal	30.452	0.22	23	1.406
30 degrees	26.817	0.23	24	7.097
45 degrees	23.343	0.55	36	5.337
60 degrees	17.923	0.4	33	4.802

Table 6.21: Load and displacement results from MO2-analysis

An interesting result from the changes in fibre direction within a modified area was that horizontal fibre direction did not have the highest maximum load capacity. Also for all cases, the load-bearing capacities were not especially high after reaching 1 mm displacement, and almost nothing after exceeding 2.5 mm displacement loading.

69

From table 6.21 one can see that the change has a clear impact on the maximum load-capacity for horizontal fibre direction in the modified mid-section. When exceeding the area where it is horizontal fibre orientation, the maximum load-capacity has increased with over 10 kN, is again greater than for 30 and 45 degrees and reached at a higher load step. A very steep brittle drop after reaching maximum load-capacity may indicate that for the horizontal fibre orientation, the vertical fibre orientation in the rest becomes more dominating than for other fibre orientations. Huge differences in their residual tensile strength could also be one of the reasons why they do not co-operate well together in the analysis. At 2.2 mm displacement, the load-capacity for the horizontal fibre orientation is quite similar to 1.077 kN from vertical fibre orientation in the whole beam. Even so, from the curve horizontal curve in figure 6.37 one can see how the horizontal fibres try to prevent the crack growth and actually increases the load-bearing capacity for a while. That also happened in the previous analysis with a smaller modified area, but at a lower scale.

For the other fibre orientations, the results are quite similarly when it comes to maximum load-capacity, and the point where it is reached. The load-bearing capacity at 2.2 mm displacement on the other hand is still very low for all cases, but for 30, 45 and 60 degrees the load-bearing capacity at 2.2 mm displacement have increased significantly compared to the results from the analysis of the smaller modified section. For 30 degrees, the capacity has gone from 4.529 to 7.097 kN, 45 degrees from 2.732 to 5.337 kN and 60 degrees from 2.635 to 4.802 kN. This shows that the exceeding modified area has an impact on the load-carrying capacity, especially between 0.5 and 1.5 mm displacement.
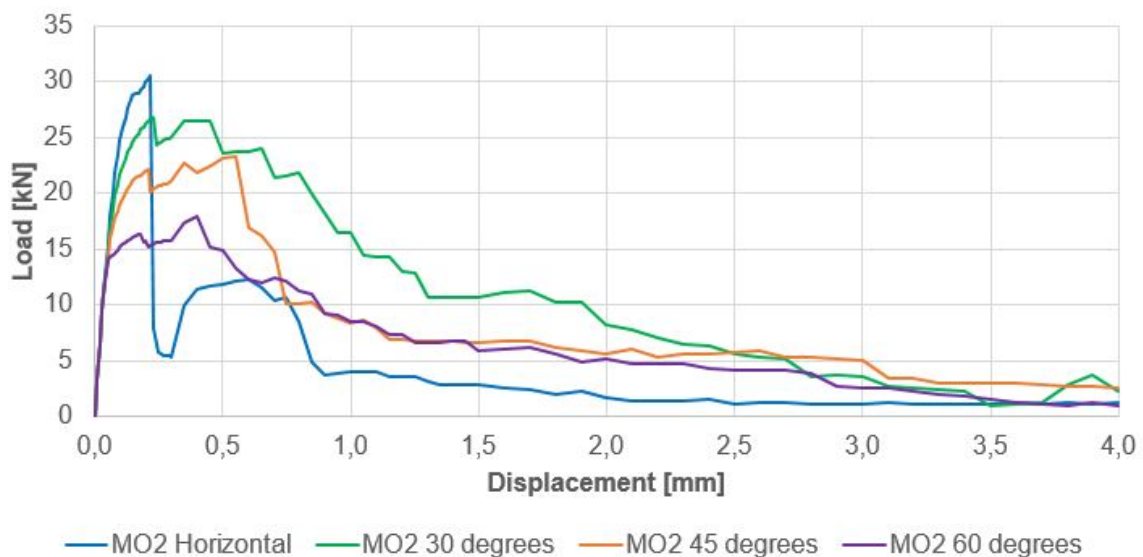
Figure 6.37: Load-displacement curves MO2

6.8   Analysis with 2 layers

In an attempt to make the modeling more close to reality, a 2-layer approach is introduced. The beam thickness of 150 mm is now divided into two layers with 75 mm thickness. To manage to do this in 2D, two layers were made based on the same points, before being merged together, creating two layers of element in top of each other based on the same nodes.
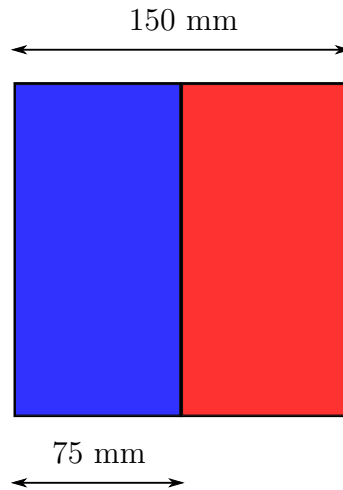
Figure 6.38: Illustration of modeling of the two layers from the side. Red symbolizes 30 degrees. Blue symbolize the other fibre orientation chosen

The material input given for the layers in this approach are shown in table 6.22. The physical properties are similar to one layer, except the change of thickness for the new layers. Table 6.23 shows the input.

Material name: MACONC		
Linear elasticity	→ Isotropic	
	Young's modulus	E= 38000 N/mm^2
	Poisson's ratio	$\nu = 0.2$
Static nonlinearity	→ Concrete and brittle materials	
	→ Total strain rotating crack	
	→ Direct input	
	→ Multi-lin. diagram in tension	
	→ Ideal in compression	
	→ No lateral confinement behav.	
	→ No lateral cracking reduction	
	→ No Poisson ratio	
	File stress-strain diagram	30DEGREESF1.dat
	Compressive strength	f$_{cm}$ = 65 N/mm^2

Material name: MACONC2		
Linear elasticity	→ Isotropic	
	Young's modulus	E= 38000 N/mm²
	Poisson's ratio	$\nu = 0.2$
Static nonlinearity	→ Concrete and brittle materials	
	→ Total strain rotating crack	
	→ Direct input	
	→ Multi-lin. diagram in tension	
	→ Ideal in compression	
	→ No lateral confinement behav.	
	→ No lateral cracking reduction	
	→ No Poisson ratio	
	File stress-strain diagram	HORIZONTALF1.dat
	Compressive strength	$f_{cm} = 65$ N/mm²

Table 6.22: Material properties for 2 layer-analysis

Physical property name: PHCONC		
Plane stress	→ Regular	
	Thickness	t = 75 mm
Physical property name: PHCONC2		
Plane stress	→ Regular	
	Thickness	t = 75 mm

Table 6.23: Physical properties 2 layers

2nd layer	Load [kN]	Displacement [mm]	Load step	Load 2.2 mm [kN]
Horizontal	27.201	0.24	25	7.603
30 degrees	27.201	0.24	25	8.945
45 degrees	27.201	0.24	25	10.338
60 degrees	27.201	0.24	25	16.134
Vertical	26.860	0.23	24	5.097

Table 6.24: Load-capacity - 2 layers

The result for the first four cases is the same as for 30 degrees fibre orientation in the whole beam. Maximum load-capacity is not very effected by these changes in the model. It is the same for all, except for vertical fibre orientation in one of the layers. As one can see in figure 6.39, the models begin to act differently after 0.3 mm displacement. Therefore, the capacities at 2.2 mm displacement is the most interesting. Here one can see that with a higher fibre orientation degree, the load-bearing capacity at a displacement of 2.2 mm is higher as well. So it becomes clear that with the two-layer modeling 30 degrees and 60 degrees fibre orientation co-operate very well together.

The gain of load-bearing capacity for the vertical fibre orientation as the second

layer is over twice as much for the maximum load-bearing capacity, and a residual capacity five times as high, compared to vertical fibre orientation in the whole beam. This is due to the introduction of 30 degrees in half of the beam. 30 degrees fibre orientation will prevent the crack from growing as it would for the original case with the same vertical properties in the whole beam.
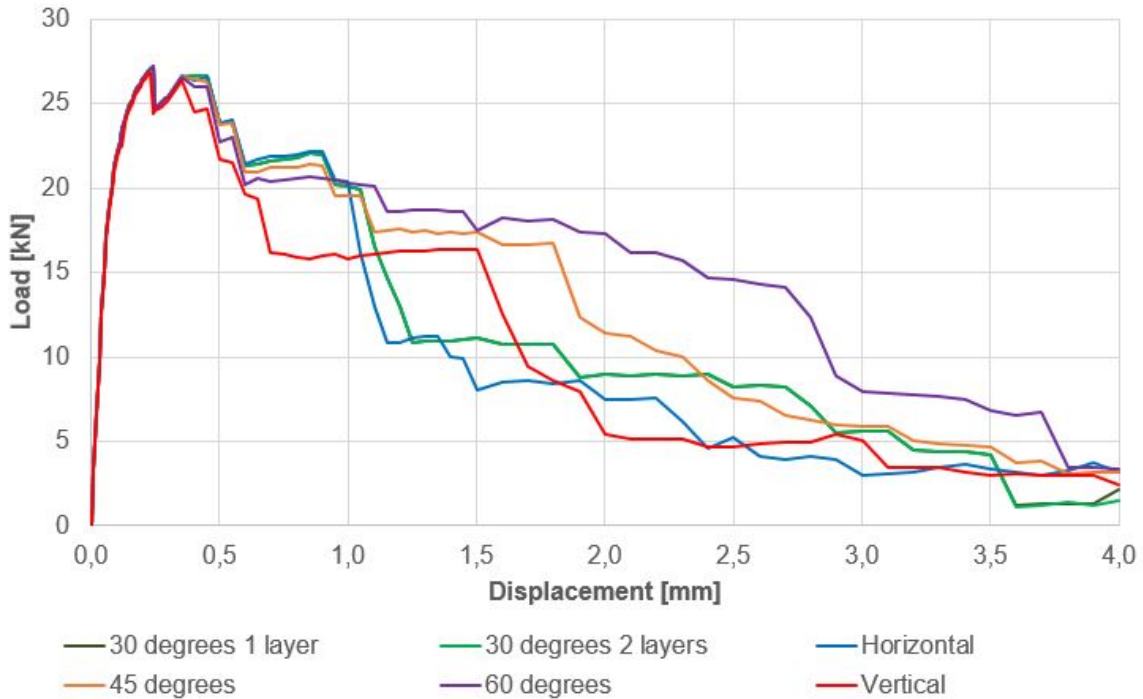
Figure 6.39: Load-displacement curves for analyses with 2 layers

6.8.1   Comparison with other orientation analysis

As already mentioned the increase in capacity for the one with second layer as 60 degrees is very large. Compared to the beam where the fibre orientation is 60 degrees is the whole beam the load-bearing capacity at 2.2 mm is almost eight(!) times as high. Same goes for the beam where it is 60 degrees in the modified area and 30 degrees in the rest of the beam. For these beams the load capacity at 2.2 mm were 2.122 kN and 2.395 kN respectively, compared to 16.134 kN from the two layer analysis.

Compared to the horizontal fibre direction within the modified area, MO1, and 30 degrees in the rest of the beam the results are as expected. A little decrease from 10.321 kN to 7.603 kN. This show the importance of the fibre orientation in the mid-span. The increase the contribution from 30 degrees give compared to having vertical fibre orientation in the mid-span and the whole beam, support upon this statement with an increased load-bearing ability at larger displacements.

6.9 Changes of density in the mid-span

Usually the amount of steel fibres in beams varies from 0.25 (20 kg/m^3) to 2.0 vol.-% (157 kg/m^3) [7]. Based on the values from the paper, the analysis up until now have assumed a fibre content of 0.5 vol.-%. Now three other fibre densities are considered in the mid-section, MO1; 0.3, 0.75 and 1 vol.-%. The goal is to see what influence local density changes have on the capacity through two different approaches for density analysis.

In the first approach, the densities are changed within the same orientation as in the rest of the beam. For example, for an analyze it is assumed that the fibre content in the middle is 0.75 vol.-% with a 60 degrees orientation, while in rest of the beam the volume fraction is 0.5 as for 60 degrees fibre orientation from earlier. In the second approach, the density is changed with different orientation within modified area, MO1, assuming horizontal fibre direction in the rest of the beam. These analyzes are shown in the next section.

The same fibre efficiency parameter as presented earlier is used, but since both orientation and density are considered, the values for w_1 and w_2 are now based on their respective, assumed influence on the load-capacity [3]:

$$w_1 = 0.7 \tag{6.19}$$

$$w_2 = 0.3 \tag{6.20}$$

which gives the following equation, where v_f represents the density in the mid-section:

$$\mu = w_1 \cdot \cos(\theta) + w_2 \cdot \frac{v_f}{\bar{v_f}} = 0.7\cos(\theta) + 0.3 \cdot \frac{v_f}{\bar{v_f}} \tag{6.21}$$

Based on the equation 6.21 the residual tensile strength has been calculated for the different volume fractions as shown in table 6.25.

Orientation	Fibre volume [%]	σ_2 [N/mm^2]
Horizontal	0.3	3.0
Horizontal	0.75	4.4
Horizontal	1.0	4.9
30 degrees	0.3	3.0
30 degrees	0.75	4.0
30 degrees	1.0	4.6
45 degrees	0.3	2.6
45 degrees	0.75	3.6
45 degrees	1.0	4.2
60 degrees	0.3	2.0
60 degrees	0.75	3.0
60 degrees	1.0	3.6
Vertical	0.3	0.7
Vertical	0.75	1.7
Vertical	1.0	2.3

Table 6.25: Residual tensile strength for different volume fractions

6.9.1 Horizontal fibre orientation
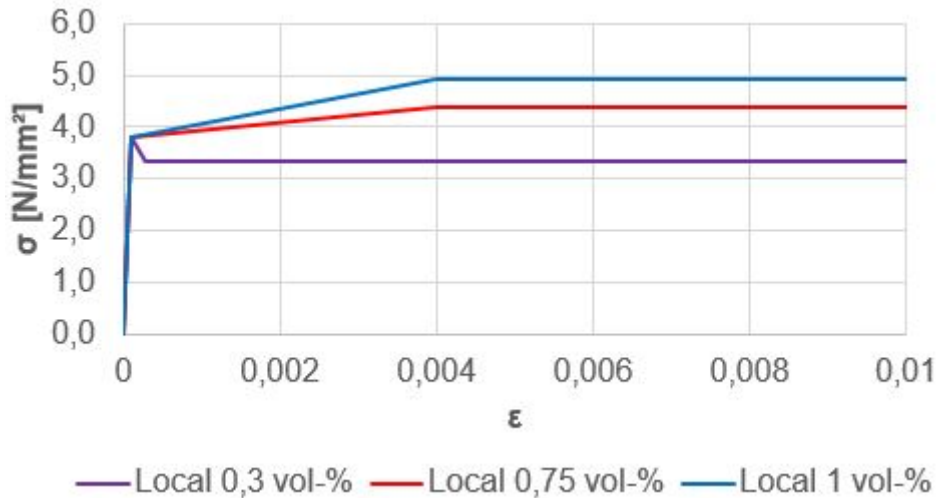
Figure 6.40: Tensile strength propagation for volume changes, horizontal

As one can see from the curves in figure 6.40 both 0.75 and 1.0 vol.-% have a strain hardening effect. The impact of this becomes very clear when looking at the load-displacement curves in figure 6.41. Both fibre contents have a very high load-bearing capacity. According to the analysis their load-bearing capacity at 4 mm displacement loading are 18.834 kN for 0.75 vol.-% and 16.339 kN for 1 vol.-%. These results are very good, but as expected since the load-bearing capacity for the horizontal fibre orientation with 0.5 vol.-% in the whole beam is high and has a similar shape in the load-displacement curve.

On the other side, it is remarkable that the 0.3 vol.-% has a such a low load-bearing ability compared to the rest when the displacement grows. Compared to same orientation, homogenous distributed in the whole beam the results are somewhat between 45 and 60 degrees fibre orientations. Based on its residual strength one would predicted that the capacity should been like for 30 degrees, but that is not the case.

Vol.-%	Load [kN]	Displacement [mm]	Load step	Load 2.2 mm [kN]
0.5	40.117	0.6	37	31.714
0.3	32.379	0.45	34	3.037
0.75	42.177	0.65	38	33.168
1.0	43.970	0.75	40	34.466

Table 6.26: Results from density changes, horizontal fibre direction

Volume fraction	0.3	0.75	1.0
f_{R3} [N/mm^2]	0.972	10.614	11.029
$f_{ftd.res2.5}$ [N/mm^2]	0.240	2.618	2.721
M_{Rd} [kNm]	0.324	3.534	3.673
V_{Rdcf} [kN]	3.236	35.344	36.727

Table 6.27: Capacity calculations for changes in density in the modified area for horizontal fibre orientation, based on formulas from the design codes
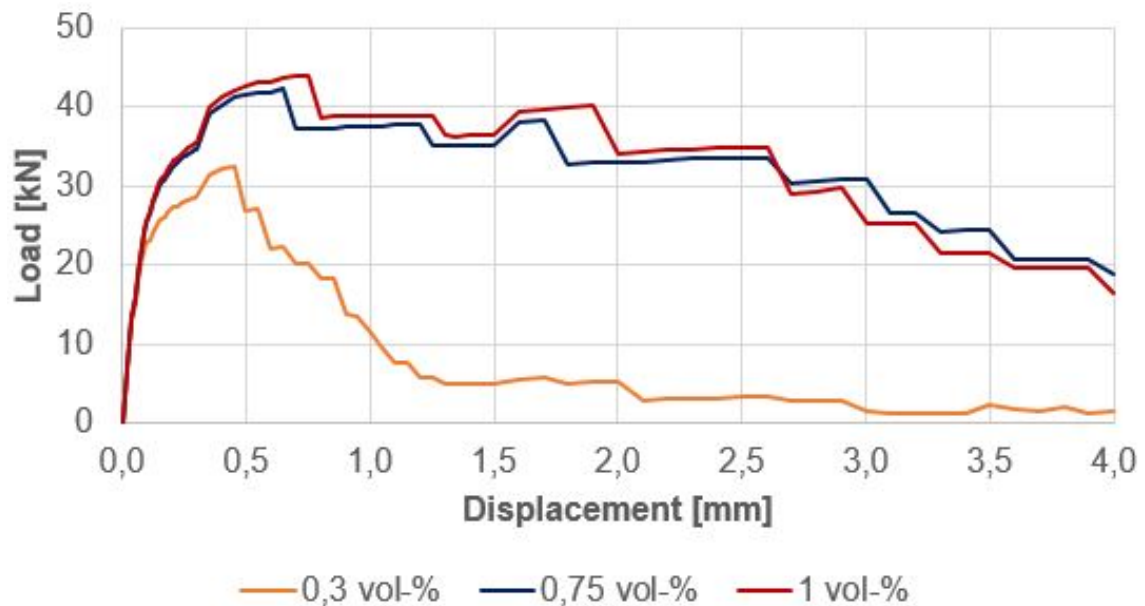
Figure 6.41: Load-displacement curves for changes of density in the mid-span, horizontal

6.9.2   30 degrees fibre orientation
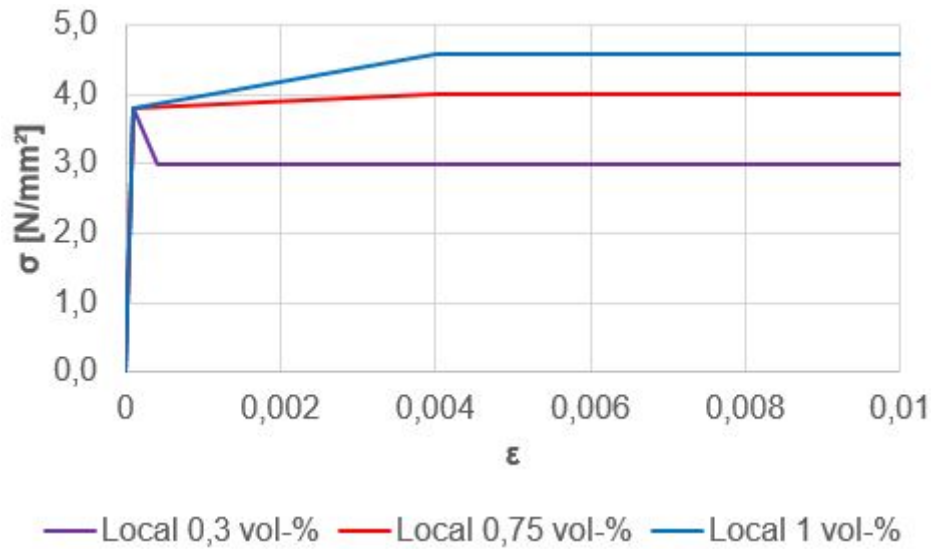
Figure 6.42: Tensile strength propagation for volume changes, 30 degrees

Also here two of the fibre contents gain a strain hardening effect. As one can see in figure 6.43 the cases with strain hardening reaches maximum loading in the same area of displacement and also have a similar load-displacement curves. An interesting aspect here is that from around 2.5 mm displacement all cases have small differences (only a few kN) in the load-bearing capacity up to 4 mm displacement. At horizontal fibre orientation, the differences were large when the displacement became increased as well.

Vol.-%	Load [kN]	Displacement [mm]	Load step	Load 2.2 mm [kN]
0.5	27.201	0.24	25	8.945
0.3	24.922	0.23	24	6.406
0.75	35.896	0.8	41	9.936
1.0	36.463	0.85	42	9.090

Table 6.28: Results from density changes, 30 degrees fibre orientation

Volume fraction	0.3	0.75	1.0
f_{R3} [N/mm^2]	2.050	3.180	2.909
$f_{ftd.res2.5}$ [N/mm^2]	0.506	0.784	0.718
M_{Rd} [kNm]	0.683	1.059	0.967
V_{Rdcf} [kN]	6.826	10.588	9.686

Table 6.29: Capacity calculations for changes in density in the modified area for 30 degrees fibre orientation, based on formulas from the design codes
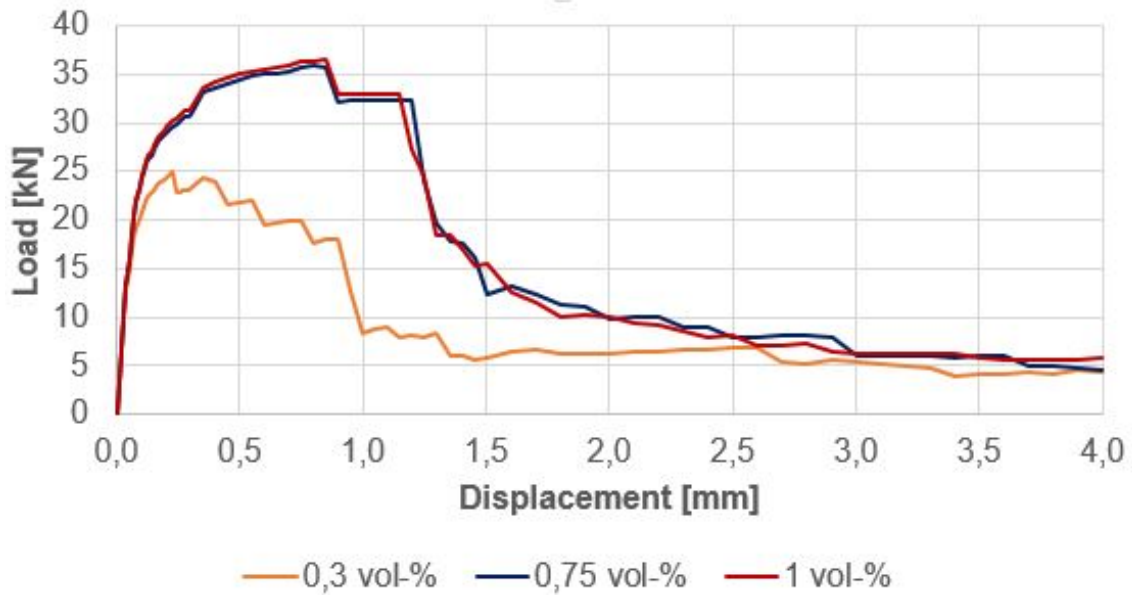
Figure 6.43: Load-displacement curves for changes of density in the mid-span, 30 degrees

6.9.3 45 degrees fibre orientation
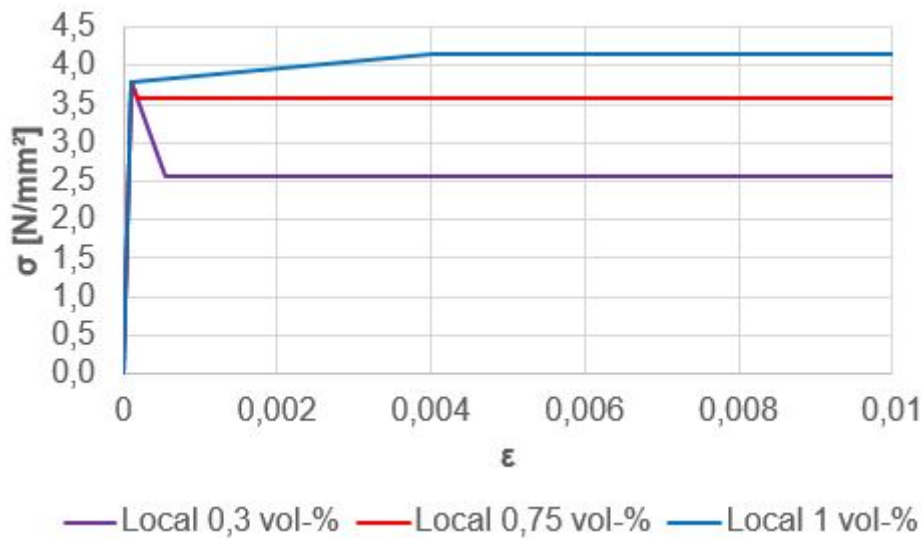
Figure 6.44: Tensile strength propagation for volume changes, 45 degrees

In a difference to the two previous cases, here only 1 vol.-% has a strain hardening effect. Even so, the differences in the development of the load-bearing capacity between 0.75 and 1 vol.-% are not as large as one might expect. The difference is that 1 vol.-% is able carry a higher loading at a larger displacement then 0.75 vol.-%. After the critical cracks start to occur for both cases (drop in load-capacity), their load-displacement development are similar.

Vol.-%	Load [kN]	Displacement [mm]	Load step	Load 2.2 mm [kN]
0.5	23.083	0.45	34	8.018
0.3	22.300	0.45	34	3.044
0.75	30.044	0.85	42	7.382
1.0	31.007	0.95	44	5.886

Table 6.30: Results from density changes, 45 degrees fibre orientation

Volume fraction	0.3	0.75	1.0
f_{R3} [N/mm^2]	0.974	2.362	1.884
$f_{ftd.res2.5}$ [N/mm^2]	0.240	0.583	0.465
M_{Rd} [kNm]	0.324	0.787	0.627
V_{Rdcf} [kN]	3.244	7.866	6.272

Table 6.31: Capacity calculations for changes in density in the modified area for 45 degrees fibre orientation, based on formulas from the design codes
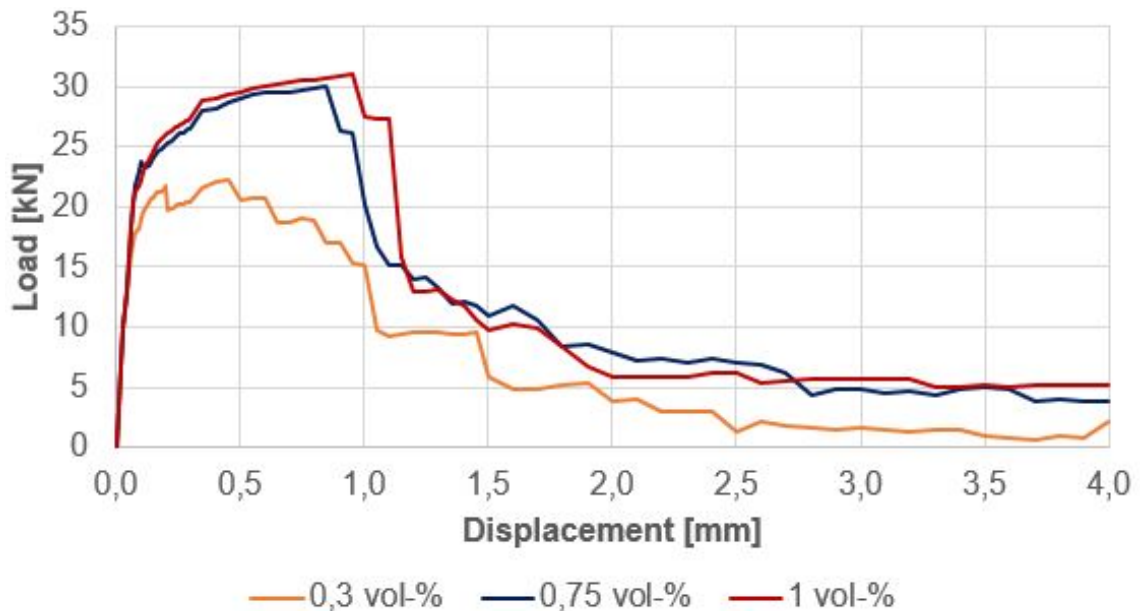
Figure 6.45: Load-displacement curves for changes of density in the mid-span, 45 degrees

79

6.9.4 60 degrees fibre orientation
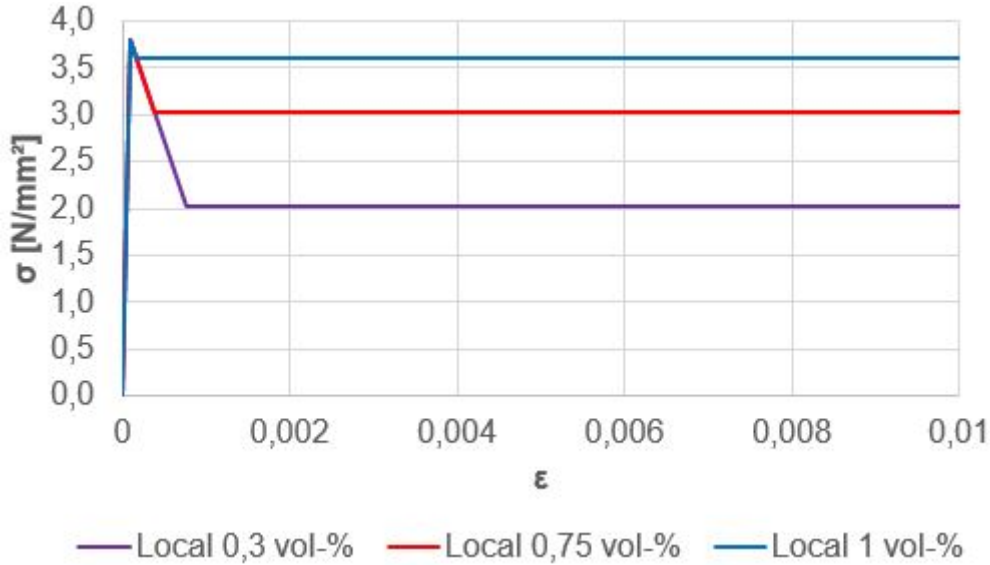
Figure 6.46: Tensile strength propagation for volume changes, 60 degrees

In these analysis all fibre contents reach their residual tensile strength after a tension softening behaviour, as shown in figure 6.46. As difference to what to expect the 0.75 vol.-% give the highest maximum capacity in the analysis. Up to 0.5 mm displacement and between 1 mm and 1.6 mm displacement it has a greater load-bearing capacity than for 1 vol.-%. The behaviour after these areas in the curve, on the other hand, is what to expect based on their given strength. 1 vol.-% gives a stable load-bearing capacity between 4 and 5 kN from 2 to 4 mm displacement loading.

Vol.-%	Load [kN]	Displacement [mm]	Load step	Load 2.2 mm [kN]
0.5 (original)	18.490	0.45	34	2.122
0.3	18.949	0.55	36	2.629
0.75	24.890	0.23	24	3.485
1.0	22.892	0.09	10	4.956

Table 6.32: Results from density changes, 60 degrees fibre orientation

Volume fraction	0.3	0.75	1.0
f_{R3} [N/mm^2]	0.841	1.115	1.586
$f_{ftd.res2.5}$ [N/mm^2]	0.208	0.275	0.391
M_{Rd} [kNm]	0.280	0.371	0.528
V_{Rdcf} [kN]	2.801	3.714	5.281

Table 6.33: Capacity calculations for changes in density in the modified area for 60 degrees fibre orientation, based on formulas from the design codes
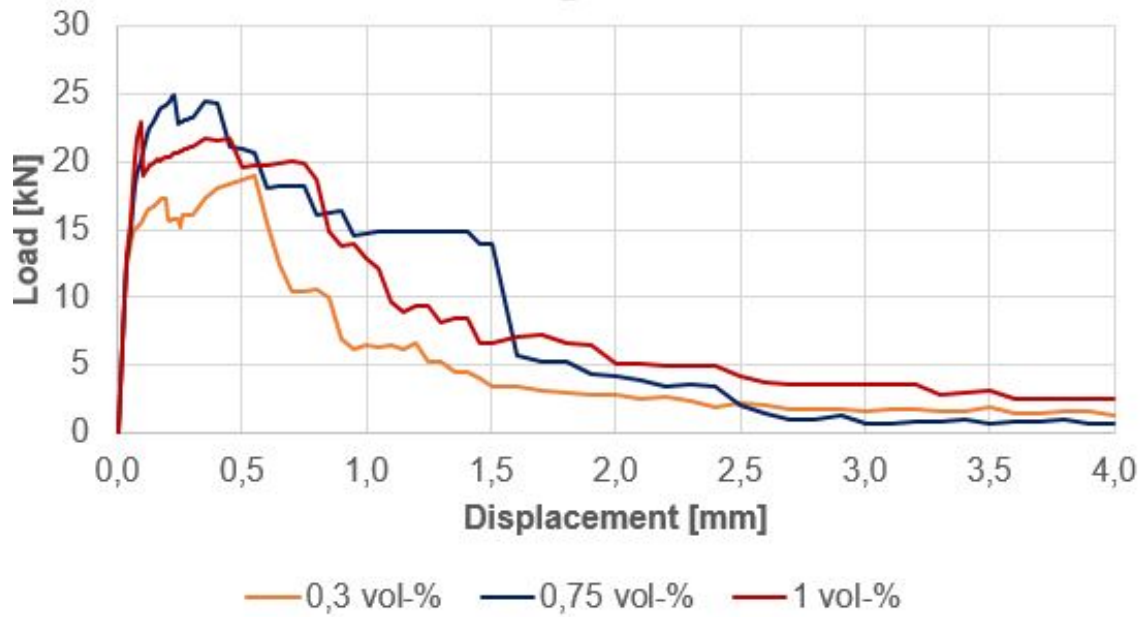
Figure 6.47: Load-displacement curves for changes of density in the mid-span, 60 degrees

6.9.5 Vertical fibre orientation
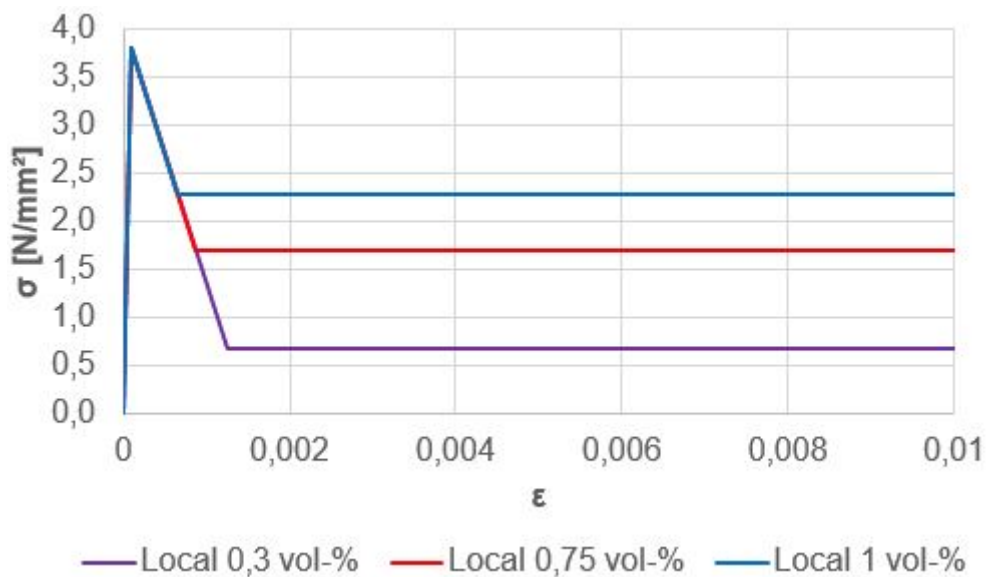
Figure 6.48: Tensile strength propagation for volume changes, vertical

In these analysis the problem when consider only the orientation and when considering both orientation and density becomes clear. When only considering orientation the tensile strength follows the linear curve(it softens) down to the point where the line reach failure at ε'_2, as shown in figure 6.11. The values for the residual tensile strength are therefore overestimated, but can still give an indication of the behaviour when the fibre orientation is vertical and fibre volume in the mid-section changes.

81

Vol.-%	Load [kN]	Displacement [mm]	Load step	Load 2.2 mm [kN]
0.5	12.923	0.05	6	1.077
0.3	13.389	0.05	6	1.060
0.75	16.609	0.55	36	2.299
1.0	20.209	0.45	34	0.990

Table 6.34: Results from density changes, vertical fibre orientation

Volume fraction	0.3	0.75	1.0
f_{R3} [N/mm^2]	0.339	0.736	0.317
$f_{ftd.res2.5}$ [N/mm^2]	0.084	0.181	0.078
M_{Rd} [kNm]	0.113	0.245	0.105
V_{Rdcf} [kN]	1.130	2.450	1.055

Table 6.35: Capacity calculations for changes in density in the modified area for vertical fibre orientation based on formulas from the design codes

As one can see, when the fibre density is increased in the modified area the maximum load becomes higher and is reached at a larger displacement. Similarly for all vertical orientation analysis is a drop in the load-bearing capacity after reaching this point which indicate that for vertical fibre orientations the beam has critical cracks at maximum loading. That leads to a low load-bearing capacity at larger displacement, illustrated in figure 6.49. The only one with an increase worth mentioning is 0.75 vol.-%, which are twice as high capacity as the rest at 2.2 mm displacement.
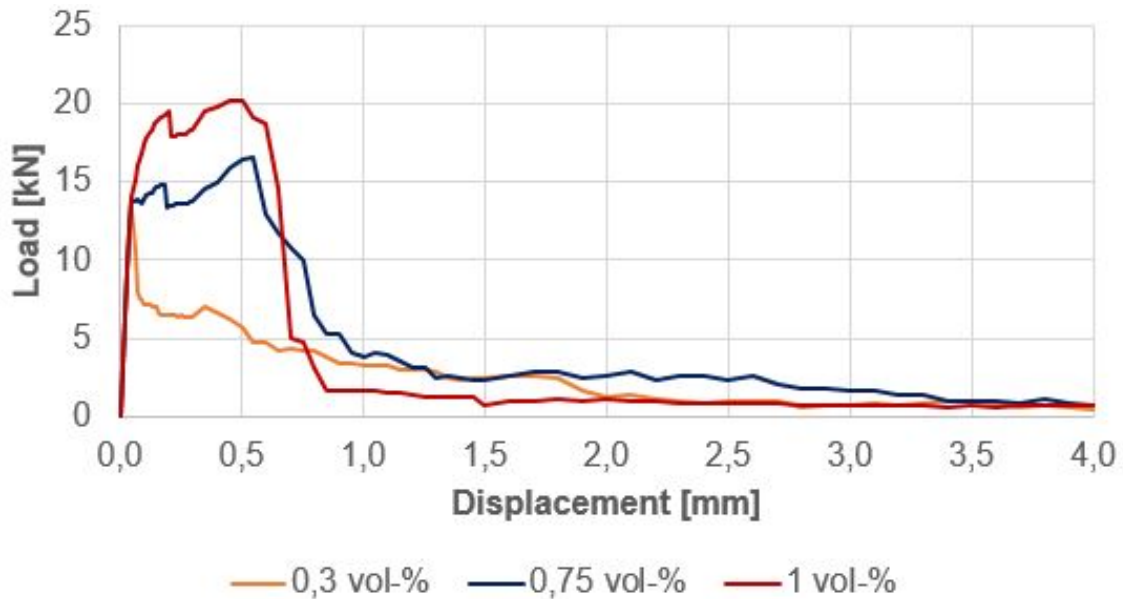
Figure 6.49: Load-displacement curves for changes of density in the mid-span, vertical

6.10 Changes in orientation and density in the mid-span

In these analysis both the orientations and the densities are changing within the modified area MO1, keeping horizontal fibre orientation(optimal) with a density of 0.5 vol.-% in the rest of the beam. This was chosen because the horizontal fibre orientation had the same residual tensile properties with and without density included in the fibre efficiency parameter.

6.10.1   30 degrees fibre orientation

Vol.-%	Load [kN]	Displacement [mm]	Load step	Load 2.2 mm [kN]
0.5 (orientation)	27.201	0.24	25	4.928
0.3	24.746	0.22	23	4.637
0.75	40.858	0.6	37	32.058
1.0	43.132	0.7	39	33.742

Table 6.36: Displacement and loading, 30 degrees fibre orientation

Volume fraction	0.3	0.75	1.0
f_{R3} [N/mm^2]	1.484	10.259	10.797
$f_{ftd.res2.5}$ [N/mm^2]	0.366	2.530	2.663
M_{Rd} [kNm]	0.494	3.416	3.596
V_{Rdcf} [kN]	4.941	34.161	35.955

Table 6.37: Capacity calculations for changes in density in the modified area for 30 degrees fibre orientation, with horizontal fibre orientation in the rest of the beam, based on formulas from the design codes.

As the displacement increases the beams are still able to have a high load-bearing ability for the beams with strain hardening properties, 0.75 and 1 vol.-%. Figure 6.50 clearly shows what the properties in the mid-span have of impact on the load-bearing capacity. Compared to the model with 30 degrees in the rest of the beam this analysis show significant improvements in keeping the load-bearing capacity high at 0.75 and 1 vol.-%. That leads to very high contributions to the shear capacity for the beam. The drop from a crack occurrence does not happen in these cases. The curves have the same development as for the horizontal curves with increased fibre content from the previous analysis, but at a lower load level.
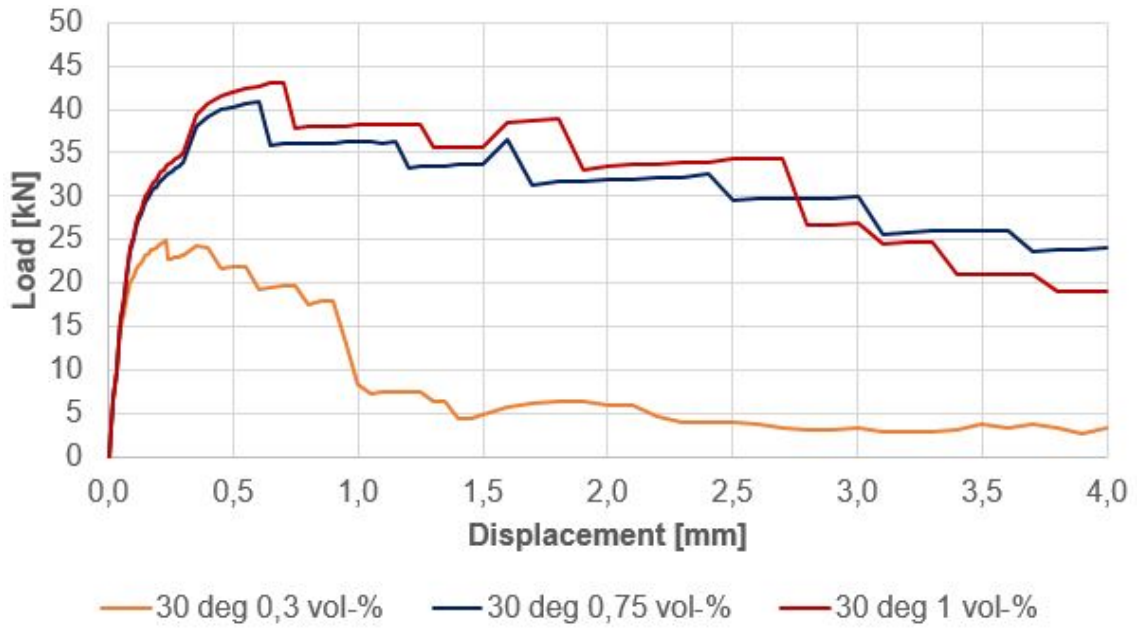
Figure 6.50: Load-displacement curves for 30 degrees fibre orientation and density in modified area.

6.10.2   45 degrees fibre orientation

Vol.-%	Load [kN]	Displacement [mm]	Load step	Load 2.2 mm [kN]
0.5 (orientation)	23.051	0.45	34	7.174
0.3	22.305	0.45	34	7.5
0.75	34.825	0.5	35	9.33
1.0	41.592	0.65	38	32.549

Table 6.38: Displacement and loading, 45 degrees fibre orientation

Volume fraction	0.3	0.75	1.0
f_{R3} [N/mm^2]	2.4	2.986	10.416
$f_{ftd.res2.5}$ [N/mm^2]	0.592	0.736	2.569
M_{Rd} [kNm]	0.799	0.994	3.468
V_{Rdcf} [kN]	7.992	9.942	34.684

Table 6.39: Capacity calculations for changes in density in the modified area for 45 degrees fibre orientation, with horizontal fibre orientation in the rest of the beam, based on formulas from the design codes.

An interesting thing to observe from these analyzes is what impact the horizontal fibre orientation have on 1.0 vol.-%. From the previous chapter, where the properties were in the same orientation(45 degrees) as the mid-span, the load-displacement curve for 0.75 and 1 vol.-% were quite similar. Here the impact from the horizontal properties in the rest of the beam keeps the load-bearing capacity at very good level with increasing displacement. The results from the load-displacement curve

84

are similar to the one where it is horizontal fibre orientation and 0.5 vol.-% in the whole beam, which is special. The distribution around the modified area seems, in this particular case, to have a huge impact on the load-bearing ability of the beam, since this result is the one standing out from the rest in tensile behaviour. Similarly huge contribution to the shear capacity as for 0.75 and 1 vol.-% in 30 degrees are calculated for 1 vol.-% here as well.
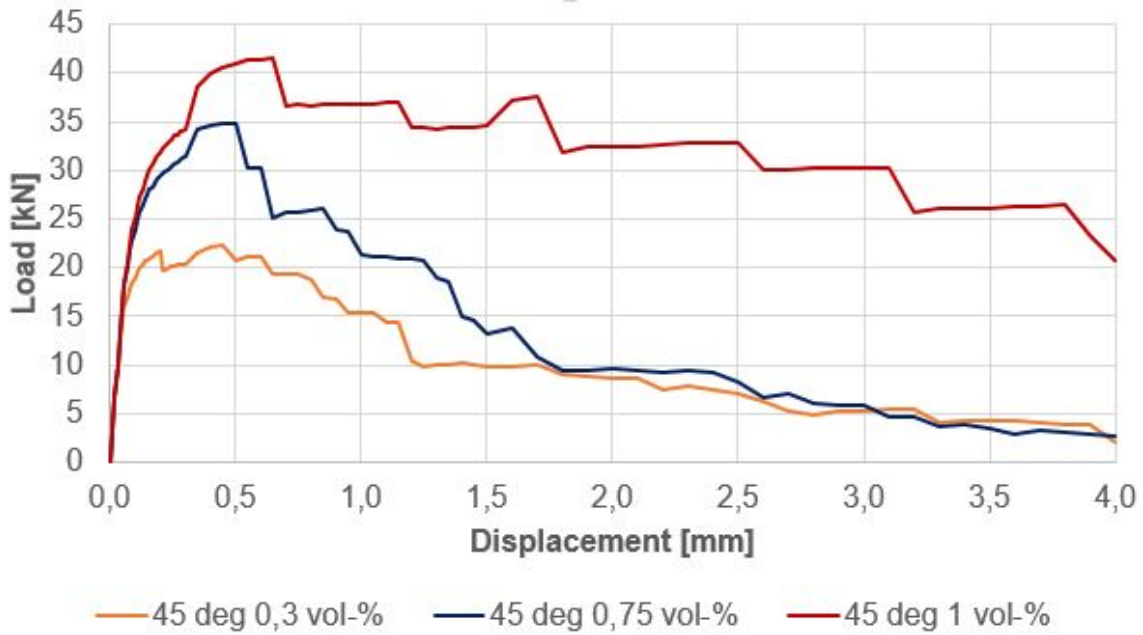
Figure 6.51: Load-displacement curves for 45 degrees fibre orientation and density in modified area.

6.10.3 60 degrees fibre orientation

Vol.-%	Load [kN]	Displacement [mm]	Load step	Load 2.2 mm [kN]
0.5	18.498	0.45	34	2.695
0.3	17.842	0.5	35	5.323
0.75	24.928	0.23	24	5.776
1.0	34.797	0.5	35	9.63

Table 6.40: Displacement and loading, 60 degrees fibre orientation

Volume fraction	0.3	0.75	1.0
f_{R3} [N/mm^2]	1.703	1.848	3.082
$f_{ftd.res2.5}$ [N/mm^2]	0.42	0.456	0.760
M_{Rd} [kNm]	0.567	0.615	3.468
V_{Rdcf} [kN]	5.672	6.155	10.262

Table 6.41: Capacity calculations for changes in density in the modified area for 60 degrees fibre orientation, with horizontal fibre orientation in the rest of the beam, based on formulas from the design codes.

The results for the maximum load-bearing here are somewhat as predicted on the forehand. In difference to the case where the fibre orientation around was the same (60 degrees), the fibre volumes have a larger effect on the load-bearing capacity. Especially for the case with 1 vol.-% the impact of having horizontal fibres in the rest of the beam are significantly. Interesting aspect from the load-displacement curve is also the increased load-bearing capacity from 2.5 mm to 2.8 mm displacement. There are none other cases that have a somewhat similar effect at a displacement at this level. Similarly behaviour from other beams with horizontal fibres may indicate that the fibres try to strengthen the beam, and prevent a new crack from exceeding. As for the calculations the shear capacities are around twice as much for all beams compared to the analysis with 60 degrees, 0.5 vol.-% in the rest.
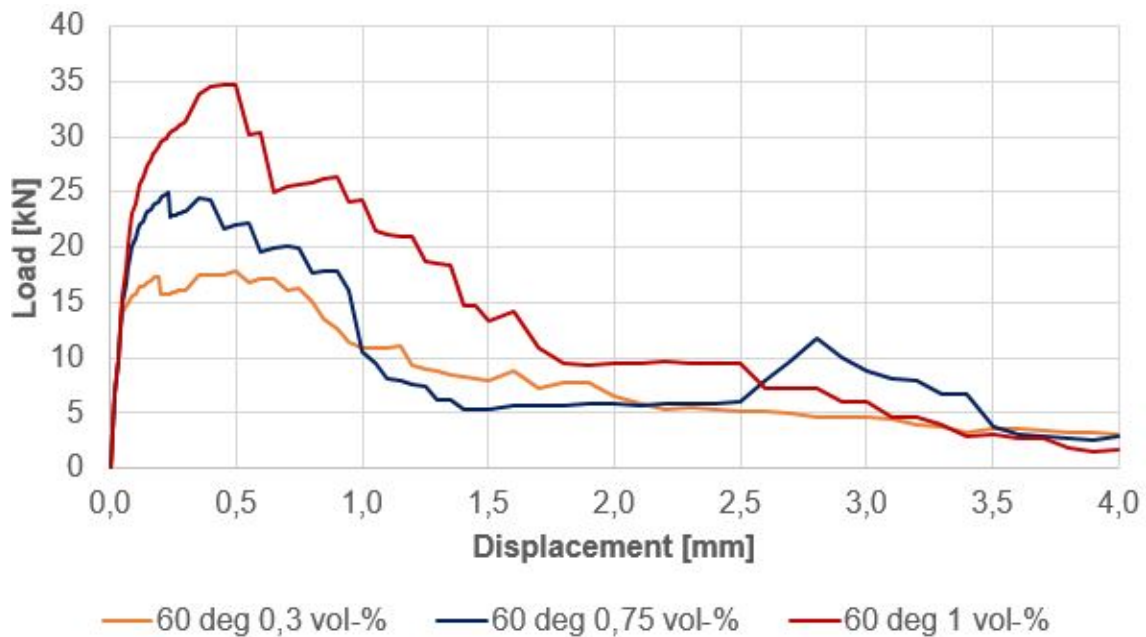
Figure 6.52: Load-displacement curves for 60 degrees fibre orientation and density in modified area.

6.10.4 Vertical fibre orientation

Vol.-%	Load [kN]	Displacement [mm]	Load step	Load 2.2 mm [kN]
0.5	11.498	0.04	5	0.804
0.3	13.635	0.05	6	1.094
0.75	16.051	0.5	35	2.967
1.0	20.183	0.5	35	2.907

Table 6.42: Displacement and loading, vertical fibre orientation

Volume fraction	0.3	0.75	1.0
f_{R3} [N/mm^2]	0.35	0.949	0.930
$f_{ftd.res2.5}$ [N/mm^2]	0.086	0.234	0.229
M_{Rd} [kNm]	0.117	0.316	0.310
V_{Rdcf} [kN]	1.166	3.162	3.098

Table 6.43: Capacity calculations for changes in density in the modified area for vertical fibre orientation, with horizontal fibre orientation in the rest of the beam, based on formulas from the design codes.

The first thing to observe is that the maximum load-capacity is reached for the cases where the fibre density is increased at a larger displacement than earlier. In addition, a big differences from the previous cases with vertical fibre orientation is the load-bearing capacity for 0.75 and 1 vol.-% up to 2 mm displacement. None of the other cases with vertical fibre orientation in the mid-span are somewhere close to getting the same capacities.
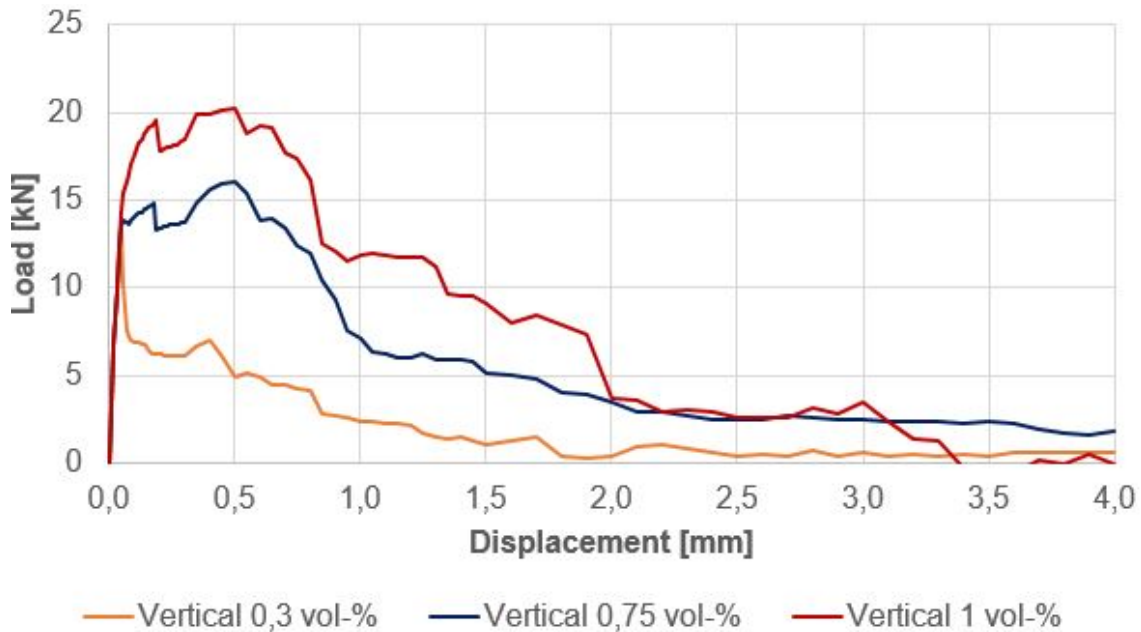
Figure 6.53: Load-displacement curves for vertical fibre orientation in modified area.

Chapter 7

Discussion

Compared to non-reinforced concrete, for all cases, except vertical fibre orientation, the load-bearing capacity after 0.05 mm displacement were significantly higher in the analysis with FRC. The FRC beams reach the maximum load-capacity at ten times as large displacement.

7.1 Comparison of orientation analysis

When the orientation is the same and distribution is homogenous in the whole beam, the results were similar to the expectations. Lower fibre orientation degree give higher capacity. Since the capacities from the paper had a maximum capacity just over 20 kN, the load-displacement curves for 30, 45 and 60 degrees shows that usually the fibre reinforced concrete would give a maximum load capacity from the bending tests around this level from lab-results.

For horizontal fibre orientation in the modified area in the mid-span the maximum load capacity is effected by the changes in the rest of the beam. For 30 and 45 degrees fibre orientations, it is the load-bearing abilities that are effected for changed properties. For 60 degrees and vertical fibre orientation, the results are similar for all cases. In the analysis with a modified area in the middle the orientation around influences the horizontal fibre orientation the most with a steep drop where the other properties outside the area become active. Then, the beam can no longer interact crack development at the same scale as before, since the stresses from the force start affecting the areas with less preferable properties.

All analysis with a vertical fibre orientation included go through a drop in load-capacity shortly after reaching the maximum load-bearing capacity. Since fibres in vertical orientation is 90 degrees from the normal vector of the crack, they will not have any influence in preventing the cracks from growing, as other orientations would.

7.2 Comparison of density analysis

From horizontal and up to 45 degrees fibre orientation, an increased density made the maximum load-capacity occur at a larger displacement. A good indication that those types of FRC beams are the strongest ones. Increased density from the original 0.5 vol.-% give similar load-displacement for all of these three orientations.

From the second variation, compared to the density analysis with same orientation in the rest of the beam, the biggest advantage when adding horizontal fibre orientation are seen for the beams with 1 vol.-%. For all orientation, they had a higher load-bearing capacity when the displacement was increased. For example, for 30 degrees, which had the highest capacity, horizontal fibre orientation gave an increased maximum load-capacity with over 7 kN. It can also be seen that the typical steep drop when critical crack occurs when orientations was the same, is not that apparent with the change of properties to horizontal fibre orientation outside the modified area. The horizontal fibres in the rest of the beam prevent the crack from growing, and therefore the beams get this increase in load-bearing capacity for all cases. For the most, the horizontal fibre orientation in the rest of the beam give a positive effect for the load-bearing capacity after 0.5 mm displacement. In those cases, the FRCs with higher fibre content than 0.5 vol.-% in the middle have gained some increase in load-bearing capacity in the curves, which symbolizes the horizontal fibres preventing the growth of a new crack.

From 0 to 60 degrees an increased density in the mid-section from the original 0.5 vol.-% gave considerable contributions to the shear capacity from the COIN-calculations.

7.3 Comparison of both orientation and density analysis

Especially the load-bearing capacities after 0.5 mm displacement loading were of interest. When the density was included, it was clear that the types of FRC that had a strain hardening behaviour got significantly good load-bearing abilities at large displacements. Typical increases before a drop in the load-displacement curve symbolizes that the fibres try to prevent a new crack from growing, but after a while cannot keep preventing the crack growth any longer.

Chapter 8

Conclusions and Suggestions for further work

8.1 Conclusions

The object with this report was to investigate by nonlinear analysis how variations, both globally and locally, in orientations and density influence the capacity of FRC beams. This was done through the FEM-program DIANA, and the thesis shows that it is possible to get good results from modeling and analyzing fibre reinforced concrete in DIANA.

The analysis show huge advantages when adding fibres to the concrete. The contributions to increased shear capacity, especially from the lower angles between the normal vector of the crack and the fibre orientation, are considerable.

From the orientation analysis, 30 and 45 degrees gave a shear contribution that increased the calculated shear capacity from EC2 with around 20-25%. Most of the analysis show a brittle drop after reaching their peak in load-displacement diagram. This drop indicate that the first critical crack has developed. The capacity after is the residual capacity where the fibres keep preventing crack growth.

From the density analysis all beams with horizontal fibre orientation outside the modified area show that the fibres help the concrete by giving a load-bearing capacity worth considering after the occurrence of the first crack. For 60 degrees fibre orientation in the mid-section, the contribution to the shear capacity was around doubled for all fibre volume contents when horizontal fibres were added.

1 vol.-% horizontal fibre orientation in the mid-section and 0.5 vol.-% in the rest gave the best result with a maximum capacity of 43.97 kN, almost four times as high as for non-reinforced. Not a surprising result since this was the strongest FRC modeled.

When the fibres have properties that give it a strain hardening effect the analysis show a significantly increase in load-bearing capacity when the displacement increases. Since the load-displacement is similar for horizontal and 30 degrees that indicate that the 4 ‰ strain-value need to be checked.

8.2   Suggestions for further work

Modeling fibre reinforced concrete is a difficult and complicated process because of the random distribution of the fibres in the mix. The analysis done in this thesis give a good indication that it is possible to make changes and model fibre reinforced concrete in DIANA. However, more models should be developed with other approaches. One of them is varying properties for each element. Also, in this report the analysis were done in 2D. It will be beneficial to do 3D-analysis to get results closer to reality.

An area that need to be worked on is the values for strain softening and hardening. The fracture energy from the model code (fib) overestimated the capacity based on the one from the paper when the failure strain was considered. Moreover, as pointed out in the conclusions, the value where the FRC was assumed to have reached strain hardening should be checked. A more explored and solid definition for the softening and hardening part of the stress-strain curves is recommendable.

Another suggestion is to try to recreate test results from the lab in analysis. This can be done through DIANA-analysis where properties change from element to element. By doing this the fibre efficiency parameter can be investigated and improved.

Since the object of this report was to investigate the influence from orientation and density on load-bearing capacity, mostly the analysis were run with displacement-control. A later study should run more analysis with force-control to give more stabilized load-displacement curves.

Bibliography

[1] N. Banthia. Fibre reinforced concrete. *ACI SP-142ACI, Detroit, MI*, 1994.

[2] TNO DIANA. DIANA User manual.

[3] M. A. N. Hendriks T. Kanstad E. V. Sarmiento. Accounting for the fibre orientation on the structural performance of flowable fibre reinforced concrete, 2013.

[4] Terje Kanstad (NTNU) et al. Forslag til retningslinjer for dimensjonering, utførelse og kontroll av fiberarmerte konstruksjoner. coin project report 29-2011. Technical report, NTNU, Trondheim, Norge, 2011.

[5] International Federation for Structural Concrete. Model code for concrete structures, 2010.

[6] Stefan Jacobsen and more. *Concrete Technology 1.* NTNU, Trondheim, Norge, 2013.

[7] Anja Birgitta Estensen Klausen. Steel fibres in load-carrying concrete structures. guideline survey and practical examples. coin project report 17-2009. Technical report, NTNU, Trondheim, Norge, 2009.

[8] Ingemar Löfgren. *Fibre-reinforced Concrete for Industrial Construction.* PhD thesis, Chalmers University of Technology, Göteborg, Sweden, Göteborg, Sweden, 2005.

[9] Kjell Mathisen. Adaptive solution algorithms - lecture notes TKT4197.

[10] Håvard Nedrelid. Structural fibre-reinforced concrete - design approaches and experimental results.

[11] Standard Norge. NS-EN 1990, Eurokode: Grunnlag for prosjektering av konstruksjoner, 2002.

[12] Standard Norge. NS-EN 1992-1-1:2004 + NA:2008, Eurokode 2: Prosjektering av betongkonstruksjoner, del 1-1: Almenne regler of regler for bygninger, 2004.

[13] Standard Norge. NS-EN12390-4: Prøving av herdnet betong - del 4: Trykkfasthet - krav til prøvingsmaskinen, 2004.

[14] Standard Norge. NS-EN 14651: Prøvingsmetode for betong med metalliske fibere. måling av bøyestrekkfasthet, 2007.

[15] Standard Norge. NS-EN 12390-2: Prøving av herdnet betong - del 2: Støping og herdning av prøvelegemer for fasthetsprøving, 2009.

[16] Standard Norge. NS-EN 12390-1: Prøving av herdnet betong - del 1: Form, mål og andre krav til prøvelegemer og former, 2012.

[17] Department of Structural Engineering. *Concrete Structures 3*. NTNU, Trondheim, Norge, 2013.

[18] Ane Marte Olimb. Testing of fibre reinforced concrete structures. Master's thesis, NTNU, Trondheim, Norge, 2012.

[19] Torstein Oma. Numerical simulation of reinforced concrete beam with web opening, 2013.

[20] Michael E. Plesha Robert D. Cook, David S. Malkus and Robert J. Witt. *Concepts and Applications of Finite Element Analysis*. John Wiley and Sons. Inc, 2002.

[21] Sindre Sandbakk. *Fibre Reinforced Concrete - Evalutation of Test Methods and Material Development*. PhD thesis, NTNU, Trondheim, Norge, 2011.

[22] Elena Vidal Sarmiento. Modelling of tension behaviour in fibre reinforced concrete beams, 2012.

[23] Chote Soranakom. Multi-scale modeling of fiber and fabric reinforced cement based composites, 2008.

[24] Svein Ivar Sørensen. *Betongkonstruksjoner*. Tapir akademiske forlag, Trondheim, Norge, 2010.

[25] Dr. J. G. M. van Mier. RILEM TC 148-SSC: Strain softening of concrete - test methods for compressive softening, 2000.

[26] Wikipedia.org. Concrete fracture analysis.

Appendix A

BASISFILE.FGC

```
!|----------------------------------------------------------------------|
!| DATE        :               | Description:                          |
!|----------------------------------------------------------------------|
!| CREATED BY : Øyvind Trygge   |Main input file:                       |
!|        Moltubakk             |Create geometry and investigate beam   |
!|                              |from paper                             |
!|----------------------------------------------------------------------|
!| REVISION MARKS:                                                      |
!|------|-----------|-----------------------------------------------------|
!| REV. |   DATE    | DESCRIPTION                               |Sign    |
!|------|-----------|-----------------------------------------------|-------|
!| 1    |     2014  | Start modelling                           |       |
!|------|-----------|-----------------------------------------------|-------|


! SETTINGS
! FILE CLOSE; NO
UTILITY SETUP DIRECTORY
"C:\Users\ØyvindTrygge\Documents\NTNU\Masteroppgave\DIANA\Masterbeammodel"
FEMGEN BEAM
PROPERTY FE-PROG DIANA STRUCT_2D  ; YES
UTILITY SETUP UNITS LENGTH MILLIMETER
UTILITY SETUP UNITS MASS KILOGRAM
UTILITY SETUP UNITS FORCE NEWTON
UTILITY SETUP UNITS TIME SECOND
UTILITY SETUP UNITS TEMP KELVIN
UTILITY SETUP UNDO ON
UTILITY SETUP BINSET OFF
MESHING OPTIONS CHECK STRUCTURED OFF
UTILITY SETUP OPTIONS ANALYSIS SOLVER-COMMAND diana_w



!+++++++++++++++++++++++++++++++++++++++++++++++++++++++++++++++++++++++++
!                        Structure
!+++++++++++++++++++++++++++++++++++++++++++++++++++++++++++++++++++++++++

! POINTS ----------------------------------------------------------------
 GEOMETRY POINT COORD P1 0 0
 GEOMETRY POINT COORD P2 50 0
 GEOMETRY POINT COORD P3 297.5 0
 GEOMETRY POINT COORD P4 297.5 25
 GEOMETRY POINT COORD P5 300 25
 GEOMETRY POINT COORD P6 300 150
 GEOMETRY POINT COORD P7 0 150

 EYE FRAME
 LABEL GEOMETRY POINTS



 ! LINES AND SURFACES ---------------------------------------------------
 GEOMETRY LINE STRAIGHT L1 P1 P2
 GEOMETRY LINE STRAIGHT L2 P2 P3
 GEOMETRY LINE STRAIGHT L3 P3 P4
 GEOMETRY LINE STRAIGHT L4 P4 P5
 GEOMETRY LINE STRAIGHT L5 P5 P6
 GEOMETRY LINE STRAIGHT L6 P6 P7
 GEOMETRY LINE STRAIGHT L7 P7 P1

 CONSTRUCT SET LEFT APPEND LINES ALL

 GEOMETRY SURFACE REGION S1 LEFT
 VIEW GEOMETRY CURRENT RED
 LABEL GEOMETRY LINES ALL RED
```

```
! MESHING ------------------------------------------------------------------
 MESHING OPTIONS ALGORITHM PAVING S1
 MESHING DIVISION ELSIZE ALL 6.25
 MESHING TYPES ALL QU8 CQ16M
 MESHING DIVISION AUTOMATIC
 MESHING GENERATE
 VIEW MESH


! MIRROR TO FULL MODEL ------------------------------------------------------
 GEOMETRY COPY S1 S2 MIRROR X 300
 VIEW GEOMETRY ALL RED
 LABEL GEOMETRY POINTS ALL BLUE
 EYE FRAME
 MESHING GENERATE
 VIEW MESH



! MERGE MESH ----------------------------------------------------------------
! MESHING MERGE ALL



! MATERIAL AND PHYSICAL PROPERTIES ------------------------------------------
! PROPERTY MATERIAL MACONC ELASTIC ISOTROP 38000 0.2
! PROPERTY MATERIAL MACONC STATNONL CONCBRIT CRACK CONSTA TENSIO1 ULTIMATE
! TAUCRI1 NONE 3.8 0.015 0.001
! PROPERTY MATERIAL MACONLIN ELASTIC ISOTROP 38000 0.2

PROPERTY PHYSICAL PHCONCRE GEOMETRY PLANSTRS THREGULR 150

PROPERTY MATERIAL MACONC STATNONL CONCBRIT TOTCRKRO DIRECT MULTILIN CONSTA
NOCNFC NOREDC NOPOIS "HORIZONTALF1.dat" 65
! PROPERTY MATERIAL MACONC2 STATNONL CONCBRIT TOTCRKRO DIRECT MULTILN
! CONSTA NOCNFC NOREDC NOPOIS "FIBREHOR075.dat" 65

! ASSIGNMENT ----------------------------------------------------------------
! PROPERTY ATTACH ALL MACONLIN PHCONC
PROPERTY ATTACH ALL MACONC PHCONC
CONSTRUCT PMODIFIER MO1 CENTROID CUBOID 289 24 -1 311 151 1
! CONSTRUCT PMODIFIER MO2 CENTROID CUBOID 269 24 -1 331 151 1
PROPERTY ATTACH MO1 MACONC2 PHCONC
! PROPERTY ATTACH MO2 MACONC2 PHCONC

! PROPERTY ATTACH S1 MACONC PHCONC
! PROPERTY ATTACH S2 MACONC PHCONC
! PROPERTY ATTACH S3 MACONC2 PHCONC2
! PROPERTY ATTACH S4 MACONC2 PHCONC2

! SUPPORTS ------------------------------------------------------------------
 PROPERTY BOUNDARY CONSTRAINT CO1 P2 X Y
 PROPERTY BOUNDARY CONSTRAINT CO2 P9 Y
 LABEL MESH CONSTRNT

! LOADS ---------------------------------------------------------------------
 PROPERTY LOADS DISPLACE LO1 P6 -1.0 Y
 LABEL MESH OFF
 LABEL MESH LOADS



! ANALYSE -------------------------------------------------------------------
! UTILITY WRITE DIANA
! yes
```

Appendix B

HORIZONTALMLTSCQ16M.DAT

```
FEMGEN MODEL      : HORIZONTALMLTS-CQ16M
ANALYSIS TYPE     : Structural 2D
'DIRECTIONS'
    1  1.00000E+000   0.00000E+000   0.00000E+000
    2  0.00000E+000   1.00000E+000   0.00000E+000
    3  0.00000E+000   0.00000E+000   1.00000E+000
'COORDINATES'
    1  0.00000E+000   0.00000E+000   0.00000E+000
    2  5.00000E+000   0.00000E+000   0.00000E+000
    3  1.00000E+001   0.00000E+000   0.00000E+000
    4  1.50000E+001   0.00000E+000   0.00000E+000
    5  2.00000E+001   0.00000E+000   0.00000E+000
    6  2.50000E+001   0.00000E+000   0.00000E+000
    7  3.00000E+001   0.00000E+000   0.00000E+000
    8  3.50000E+001   0.00000E+000   0.00000E+000
    9  4.00000E+001   0.00000E+000   0.00000E+000
   10  4.50000E+001   0.00000E+000   0.00000E+000
--------------------------------------------------
 1968  3.87690E+002   7.32420E+001   0.00000E+000
 1969  4.00461E+002   7.39436E+001   0.00000E+000
 1970  4.13073E+002   7.42863E+001   0.00000E+000
 1971  4.25570E+002   7.44190E+001   0.00000E+000
 1972  4.38021E+002   7.44530E+001   0.00000E+000
 1973  4.50465E+002   7.44703E+001   0.00000E+000
 1974  4.62909E+002   7.44905E+001   0.00000E+000
 1975  4.75356E+002   7.45362E+001   0.00000E+000
 1976  4.87821E+002   7.46584E+001   0.00000E+000
 1977  5.00288E+002   7.49159E+001   0.00000E+000
'MATERI'
    1 YOUNG   3.80000E+004
      POISON  2.00000E-001
    2 YOUNG   3.80000E+004
      POISON  2.00000E-001
      TOTCRK ROTATE
      TENCRV MULTLN
      TENPAR  0.00000E+000   0.00000E+000   4.50000E+000   1.18000E-004
              4.50000E+000   1.18100E-004   4.50000E+000   6.79000E-003
              0.00000E+000   6.79100E-003
      COMCRV CONSTA
      COMSTR  6.30000E+001
'GEOMET'
    1 THICK   1.50000E+002
'ELEMENTS'
CONNECT
    1 CQ16M   213  490  149  422  145  146  147  421
    2 CQ16M   149  491  150  423  143  144  145  422
    3 CQ16M   150  492  151  424  141  142  143  423
    4 CQ16M   151  493  152  425  139  140  141  424
    5 CQ16M   152  494  153  426  137  138  139  425
    6 CQ16M   153  495  154  427  135  136  137  426
    7 CQ16M   154  496  155  428  133  134  135  427
    8 CQ16M   155  497  156  429  131  132  133  428
    9 CQ16M   156  498  157  430  129  130  131  429
   10 CQ16M   157  499  158  431  127  128  129  430
   --------------------------------------------------
  601 CQ16M  1395 1963 1396 1938 1369 1908 1368 1937
  602 CQ16M  1396 1964 1397 1939 1370 1909 1369 1938
  603 CQ16M  1397 1965 1398 1940 1371 1910 1370 1939
  604 CQ16M  1398 1966 1373 1912 1372 1911 1371 1940
  605 CQ16M  1398 1967 1375 1942 1374 1941 1373 1966
  606 CQ16M  1385 1968 1388 1955 1387 1954 1386 1953
  607 CQ16M  1384 1969 1389 1956 1388 1968 1385 1952
  608 CQ16M  1383 1970 1390 1957 1389 1969 1384 1951
  609 CQ16M  1382 1971 1391 1958 1390 1970 1383 1950
```

```
  610 CQ16M   1381 1972 1392 1959 1391 1971 1382 1949
  611 CQ16M   1380 1973 1393 1960 1392 1972 1381 1948
  612 CQ16M   1379 1974 1394 1961 1393 1973 1380 1947
  613 CQ16M   1378 1975 1395 1962 1394 1974 1379 1946
  614 CQ16M   1377 1976 1396 1963 1395 1975 1378 1945
  615 CQ16M   1376 1977 1397 1964 1396 1976 1377 1944
  616 CQ16M   1398 1965 1397 1977 1376 1943 1375 1967
MATERI
/ 1-33 45-341 353-616 / 1
/ 34-44 342-352 / 2
GEOMET
/ 1-616 / 1
'LOADS'
CASE 1
DEFORM
77   TR 2 -1.00000E+000
'GROUPS'
NODES
   1 LEFT / 1-148 /
   2 SE1 / 57-77 1000-1126 /
'SUPPOR'
11   TR 1
/ 11 77 1010 / TR 2
'UNITS'
LENGTH MM
TIME SEC
TEMPER KELVIN
FORCE N
MASS  1.00000E+003
'END'
```

Appendix C

HORIZONTAL30DEG.DAT

```
FEMGEN MODEL      : HORIZONTAL30DEG
ANALYSIS TYPE     : Structural 2D
'DIRECTIONS'
   1  1.00000E+000   0.00000E+000   0.00000E+000
   2  0.00000E+000   1.00000E+000   0.00000E+000
   3  0.00000E+000   0.00000E+000   1.00000E+000
'COORDINATES'
   1  0.00000E+000   0.00000E+000   0.00000E+000
   2  5.00000E+000   0.00000E+000   0.00000E+000
   3  1.00000E+001   0.00000E+000   0.00000E+000
   4  1.50000E+001   0.00000E+000   0.00000E+000
   5  2.00000E+001   0.00000E+000   0.00000E+000
   6  2.50000E+001   0.00000E+000   0.00000E+000
   7  3.00000E+001   0.00000E+000   0.00000E+000
   8  3.50000E+001   0.00000E+000   0.00000E+000
   9  4.00000E+001   0.00000E+000   0.00000E+000
  10  4.50000E+001   0.00000E+000   0.00000E+000
---------------------------------------------------
1968  3.87690E+002   7.32420E+001   0.00000E+000
1969  4.00461E+002   7.39436E+001   0.00000E+000
1970  4.13073E+002   7.42863E+001   0.00000E+000
1971  4.25570E+002   7.44190E+001   0.00000E+000
1972  4.38021E+002   7.44530E+001   0.00000E+000
1973  4.50465E+002   7.44703E+001   0.00000E+000
1974  4.62909E+002   7.44905E+001   0.00000E+000
1975  4.75356E+002   7.45362E+001   0.00000E+000
1976  4.87821E+002   7.46584E+001   0.00000E+000
1977  5.00288E+002   7.49159E+001   0.00000E+000
'MATERI'
   1 YOUNG   3.80000E+004
     POISON  2.00000E-001
   2 YOUNG   3.80000E+004
     POISON  2.00000E-001
     TOTCRK ROTATE
     TENCRV MULTLN
     TENPAR  0.00000E+000   0.00000E+000   3.80000E+000   1.00000E-004
             3.80000E+000   1.10000E-004   3.80000E+000   4.00000E-002
             0.00000E+000   4.01000E-002
     COMCRV CONSTA
     COMSTR  6.30000E+001
   3 YOUNG   3.80000E+004
     POISON  2.00000E-001
     TOTCRK ROTATE
     TENCRV MULTLN
     TENPAR  0.00000E+000   0.00000E+000   3.80000E+000   1.00000E-004
             3.30000E+000   2.83800E-004   3.30000E+000   4.00000E-002
             0.00000E+000   4.01000E-002
     COMCRV CONSTA
     COMSTR  6.50000E+001
'GEOMET'
   1 THICK   1.50000E+002
'ELEMENTS'
CONNECT
   1 CQ16M  213 490 149 422 145 146 147 421
   2 CQ16M  149 491 150 423 143 144 145 422
   3 CQ16M  150 492 151 424 141 142 143 423
   4 CQ16M  151 493 152 425 139 140 141 424
   5 CQ16M  152 494 153 426 137 138 139 425
   6 CQ16M  153 495 154 427 135 136 137 426
   7 CQ16M  154 496 155 428 133 134 135 427
   8 CQ16M  155 497 156 429 131 132 133 428
   9 CQ16M  156 498 157 430 129 130 131 429
  10 CQ16M  157 499 158 431 127 128 129 430
---------------------------------------------------
```

```
 600 CQ16M  1394 1962 1395 1937 1368 1907 1367 1936
 601 CQ16M  1395 1963 1396 1938 1369 1908 1368 1937
 602 CQ16M  1396 1964 1397 1939 1370 1909 1369 1938
 603 CQ16M  1397 1965 1398 1940 1371 1910 1370 1939
 604 CQ16M  1398 1966 1373 1912 1372 1911 1371 1940
 605 CQ16M  1398 1967 1375 1942 1374 1941 1373 1966
 606 CQ16M  1385 1968 1388 1955 1387 1954 1386 1953
 607 CQ16M  1384 1969 1389 1956 1388 1968 1385 1952
 608 CQ16M  1383 1970 1390 1957 1389 1969 1384 1951
 609 CQ16M  1382 1971 1391 1958 1390 1970 1383 1950
 610 CQ16M  1381 1972 1392 1959 1391 1971 1382 1949
 611 CQ16M  1380 1973 1393 1960 1392 1972 1381 1948
 612 CQ16M  1379 1974 1394 1961 1393 1973 1380 1947
 613 CQ16M  1378 1975 1395 1962 1394 1974 1379 1946
 614 CQ16M  1377 1976 1396 1963 1395 1975 1378 1945
 615 CQ16M  1376 1977 1397 1964 1396 1976 1377 1944
 616 CQ16M  1398 1965 1397 1977 1376 1943 1375 1967
MATERI
/ 1-33 45-341 353-616 / 2
/ 34-44 342-352 / 3
GEOMET
/ 1-616 / 1
'LOADS'
CASE 1
DEFORM
77   TR 2 -1.00000E+000
'GROUPS'
NODES
    1 LEFT / 1-148 /
    2 SE1 / 57-77 1000-1126 /
'SUPPOR'
11   TR 1
/ 11 77 1010 / TR 2
'UNITS'
LENGTH MM
TIME SEC
TEMPER KELVIN
FORCE N
MASS  1.00000E+003
'END'
```

Appendix D

2LAYERS30DEGHOR.DAT

```
FEMGEN MODEL      : 2LAYERS30HOR
ANALYSIS TYPE     : Structural 2D
'DIRECTIONS'
    1  1.00000E+000   0.00000E+000   0.00000E+000
    2  0.00000E+000   1.00000E+000   0.00000E+000
    3  0.00000E+000   0.00000E+000   1.00000E+000
'COORDINATES'
    1  0.00000E+000   0.00000E+000   0.00000E+000
    2  5.00000E+000   0.00000E+000   0.00000E+000
    3  1.00000E+001   0.00000E+000   0.00000E+000
    4  1.50000E+001   0.00000E+000   0.00000E+000
    5  2.00000E+001   0.00000E+000   0.00000E+000
    6  2.50000E+001   0.00000E+000   0.00000E+000
    7  3.00000E+001   0.00000E+000   0.00000E+000
    8  3.50000E+001   0.00000E+000   0.00000E+000
    9  4.00000E+001   0.00000E+000   0.00000E+000
   10  4.50000E+001   0.00000E+000   0.00000E+000
------------------------------------------------
 1968  3.87690E+002   7.32420E+001   0.00000E+000
 1969  4.00461E+002   7.39436E+001   0.00000E+000
 1970  4.13073E+002   7.42863E+001   0.00000E+000
 1971  4.25570E+002   7.44190E+001   0.00000E+000
 1972  4.38021E+002   7.44530E+001   0.00000E+000
 1973  4.50465E+002   7.44703E+001   0.00000E+000
 1974  4.62909E+002   7.44905E+001   0.00000E+000
 1975  4.75356E+002   7.45362E+001   0.00000E+000
 1976  4.87821E+002   7.46584E+001   0.00000E+000
 1977  5.00288E+002   7.49159E+001   0.00000E+000
'MATERI'
    1 YOUNG   3.80000E+004
      POISON  2.00000E-001
    2 YOUNG   3.80000E+004
      POISON  2.00000E-001
      TOTCRK ROTATE
      TENCRV MULTLN
      TENPAR  0.00000E+000   0.00000E+000   3.80000E+000   1.00000E-004
              3.30000E+000   2.83800E-004   3.30000E+000   4.00000E-002
              0.00000E+000   4.01000E-002
      COMCRV CONSTA
      COMSTR  6.50000E+001
    3 YOUNG   3.80000E+004
      POISON  2.00000E-001
      TOTCRK ROTATE
      TENCRV MULTLN
      TENPAR  0.00000E+000   0.00000E+000   3.80000E+000   1.00000E-004
              3.80000E+000   1.10000E-004   3.80000E+000   4.00000E-002
              0.00000E+000   4.01000E-002
      COMCRV CONSTA
      COMSTR  6.50000E+001
'GEOMET'
    1 THICK   7.50000E+001
    2 THICK   7.50000E+001
'ELEMENTS'
CONNECT
    1 CQ16M   213 490 149 422 145 146 147 421
    2 CQ16M   149 491 150 423 143 144 145 422
    3 CQ16M   150 492 151 424 141 142 143 423
    4 CQ16M   151 493 152 425 139 140 141 424
    5 CQ16M   152 494 153 426 137 138 139 425
    6 CQ16M   153 495 154 427 135 136 137 426
    7 CQ16M   154 496 155 428 133 134 135 427
    8 CQ16M   155 497 156 429 131 132 133 428
    9 CQ16M   156 498 157 430 129 130 131 429
   10 CQ16M   157 499 158 431 127 128 129 430
```

```
--------------------------------------------------
1217 CQ16M  1395 1963 1396 1938 1369 1908 1368 1937
1218 CQ16M  1396 1964 1397 1939 1370 1909 1369 1938
1219 CQ16M  1397 1965 1398 1940 1371 1910 1370 1939
1220 CQ16M  1398 1966 1373 1912 1372 1911 1371 1940
1221 CQ16M  1398 1967 1375 1942 1374 1941 1373 1966
1222 CQ16M  1385 1968 1388 1955 1387 1954 1386 1953
1223 CQ16M  1384 1969 1389 1956 1388 1968 1385 1952
1224 CQ16M  1383 1970 1390 1957 1389 1969 1384 1951
1225 CQ16M  1382 1971 1391 1958 1390 1970 1383 1950
1226 CQ16M  1381 1972 1392 1959 1391 1971 1382 1949
1227 CQ16M  1380 1973 1393 1960 1392 1972 1381 1948
1228 CQ16M  1379 1974 1394 1961 1393 1973 1380 1947
1229 CQ16M  1378 1975 1395 1962 1394 1974 1379 1946
1230 CQ16M  1377 1976 1396 1963 1395 1975 1378 1945
1231 CQ16M  1376 1977 1397 1964 1396 1976 1377 1944
1232 CQ16M  1398 1965 1397 1977 1376 1943 1375 1967
MATERI
/ 1-616 650-660 958-968 / 2
/ 617-649 661-957 969-1232 / 3
GEOMET
/ 1-616 650-660 958-968 / 1
/ 617-649 661-957 969-1232 / 2
'LOADS'
CASE 1
DEFORM
77   TR 2 -1.00000E+000
'GROUPS'
NODES
   1 LEFT / 1-148 /
   2 SE1 / 57-77 1000-1126 /
   3 LEFT3 / 1-148 /
   4 SE3 / 57-77 1000-1126 /
'SUPPOR'
11   TR 1
/ 11 77 1010 / TR 2
'UNITS'
LENGTH MM
TIME SEC
TEMPER KELVIN
FORCE N
MASS  1.00000E+003
'END'
```

Appendix E

.DAT FILES FOR FIBRES

- HorizontalF1.dat
- 30degreesF1.dat
- 45degreesF1.dat
- 60degreesF1.dat
- VerticalF1.dat
- Fibre30deg1.dat

```
HORIZONTALF1.dat

        TENPAR 0.0 0.0
                3.8 1.0E-04
                3.8 1.1E-04
                3.8 0.04
                0.0 0.0401


30DEGRESSF1.dat

        TENPAR 0.0 0.0
                3.8 1.0E-04
                3.3 2.838E-04
                3.3 0.04
                0.0 0.0401


45DEGRESSF1.dat

        TENPAR 0.0 0.0
                3.8 1.0E-04
                2.7 5.048E-04
                2.7 0.04
                0.0 0.0401


60DEGREESF1.dat

        TENPAR 0.0 0.0
                3.8 1.0E-04
                1.9 8.0E-04
                1.9 0.04
                0.0 0.0401


VERTICALF1.dat

        TENPAR 0.0 0.0
                3.8 1.18E-04
                0.0 1.5E-03
                0.0 0.04
                0.0 0.0401


FIBRE30DEG1.dat

        TENPAR 0.0 0.0
                3.8 1.0E-04
                4.6 4.0E-03
                4.6 0.04
                0.0 0.0401
```

Appendix F

DISPLACEMENT.DCF

```
*FILOS
 INITIA
*NONLIN
 BEGIN EXECUT
   LOAD  STEPS  EXPLIC  SIZES 1e-005 0.01(30) 0.05(24) 0.1(25)
   ITERAT  MAXITE 100
 END EXECUT
 BEGIN OUTPUT
   FILE "horizontalmltscq16m4"
   DISPLA  TOTAL  TRANSL  GLOBAL
   FORCE  REACTI  TRANSL  GLOBAL
   STRAIN  TOTAL  GREEN  GLOBAL
   STRAIN  TOTAL  GREEN  PRINCI
   STRESS  TOTAL  CAUCHY  GLOBAL
 END OUTPUT
*END
```

Appendix G

HORIZONTALFORCE.DCF

```
   *FILOS
    INITIA
   *NONLIN
    BEGIN EXECUT
       BEGIN LOAD
          BEGIN STEPS
             BEGIN EXPLIC
                ARCLEN
                SIZES 1e-005 10(10) 5(30) 2(40)
             END EXPLIC
          END STEPS
       END LOAD
       ITERAT  MAXITE 150
    END EXECUT
    BEGIN OUTPUT
       FILE "horizontalforce"
       DISPLA  TOTAL  TRANSL  GLOBAL
       FORCE   REACTI  TRANSL  GLOBAL
       STRAIN  TOTAL   GREEN   GLOBAL
       STRESS  TOTAL   CAUCHY  GLOBAL
    END OUTPUT
   *END
```

Appendix H

MOMENT AND SHEAR CALCULATIONS

- Orientation
- Density changing within the same orientation
- Density changing in MO1, horizontal fibre orientation in the rest

Shear in the Eurocode, clause 6.2.2 (1)

CRdc	0,12	
d	135	0,9xh
k	2	
ρ	0,02	Assumed
f.ck	57	

1,16371382 >   vmin   0,41946153

V.Rdc   26,184   Non-reinforced

Changes within MO1 orientaion

Horizontal

	Horizontal	30 degrees	45 degrees	60 degrees	Vertical
Load	31,714	4,928	7,174	2,629	0,804
f.R3	10,148	1,577	2,296	0,841	0,257
f.ftk.res.2,5	3,7549376	0,5834752	0,8494016	0,3112736	0,0951936
f.ftd.res2,5	2,503	0,389	0,566	0,208	0,063
MRd	3,379	0,525	0,764	0,280	0,086
VRdcf	33,794	5,251	7,645	2,801	0,857
VRd	59,978	31,435	33,828	28,985	27,040

30 degrees

	Horizontal	**30 degrees**	45 degrees	60 degrees	Vertical
Load	10,321	8,945	2,377	2,395	0,1
f.R3	3,303	2,862	0,761	0,766	0,032
f.ftk.res.2,5	1,2220064	1,059088	0,2814368	0,283568	0,01184
f.ftd.res2,5	0,815	0,706	0,188	0,189	0,008
MRd	1,100	0,953	0,253	0,255	0,011
VRdcf	10,998	9,532	2,533	2,552	0,107
VRd	37,182	35,715	28,716	28,736	26,290

60 degrees

	Horizontal	30 degrees	45 degrees	**60 degrees**	Vertical
Load	4,187	6,297	8,68	2,122	0,515
f.R3	1,340	2,015	2,778	0,679	0,165
f.ftk.res.2,5	0,4957408	0,7455648	1,027712	0,2512448	0,060976
f.ftd.res2,5	0,330	0,497	0,685	0,167	0,041
MRd	0,446	0,671	0,925	0,226	0,055
VRdcf	4,462	6,710	9,249	2,261	0,549
VRd	30,645	32,894	35,433	28,445	26,732

45 degrees

	Horizontal	30 degrees	**45 degrees**	60 degrees	Vertical
Load	5,563	8,877	8,018	2,533	0
f.R3	1,780	2,841	2,566	0,811	0,000
f.ftk.res.2,5	0,6586592	1,0510368	0,9493312	0,2999072	0
f.ftd.res2,5	0,439	0,701	0,633	0,200	0,000
MRd	0,593	0,946	0,854	0,270	0,000
VRdcf	5,928	9,459	8,544	2,699	0,000
VRd	32,111	35,643	34,728	28,883	26,184

Vertical

	Horizontal	30 degrees	45 degrees	60 degrees	**Vertical**
Load	2,104	4,529	2,732	2,635	1,077
f.R3	0,673	1,449	0,874	0,843	0,345
f.ftk.res.2,5	0,2491136	0,5362336	0,3234688	0,311984	0,1275168
f.ftd.res2,5	0,166	0,357	0,216	0,208	0,085
MRd	0,224	0,483	0,291	0,281	0,115
VRdcf	2,242	4,826	2,911	2,808	1,148
VRd	28,426	31,010	29,095	28,991	27,331

Shear in the Eurocode, clause 6.2.2 (1)

CRdc	0,12			
d	135		0,9xh	
k	2			
ρ	0,02		Assumed	
f.ck	57			

1,163713821 >   vmin   0,41946153

V.Rdc   26,184   Non-reinforced

Horizontal	0,5 (orientation)	0,3 vol-%	0,75 vol-%	1 vol-%
Load	31,714	3,037	33,168	34,466
f.R3	10,148	0,972	10,614	11,029
f.ftk.res.2,5	3,7549376	0,3595808	3,9270912	4,0807744
f.ftd.res2,5	2,503	0,240	2,618	2,721
MRd	3,379	0,324	3,534	3,673
VRdcf	33,794	3,236	35,344	36,727
VRd	59,978	29,420	61,527	62,911

30 degrees	0,5 (orientation)	0,3 vol-%	0,75 vol-%	1 vol-%
Load	8,495	6,406	9,936	9,09
f.R3	2,718	2,050	3,180	2,909
f.ftk.res.2,5	1,005808	0,7584704	1,1764224	1,076256
f.ftd.res2,5	0,671	0,506	0,784	0,718
MRd	0,905	0,683	1,059	0,969
VRdcf	9,052	6,826	10,588	9,686
VRd	35,236	33,010	36,771	35,870

45 degrees	0,5 (orientation)	0,3 vol-%	0,75 vol-%	1 vol-%
Load	8,018	3,044	7,382	5,886
f.R3	2,566	0,974	2,362	1,884
f.ftk.res.2,5	0,9493312	0,3604096	0,8740288	0,6969024
f.ftd.res2,5	0,633	0,240	0,583	0,465
MRd	0,854	0,324	0,787	0,627
VRdcf	8,544	3,244	7,866	6,272
VRd	34,728	29,427	34,050	32,456

60 degrees	0,5 (orientation)	0,3 vol-%	0,75 vol-%	1 vol-%
Load	2,122	2,629	3,485	4,956
f.R3	0,679	0,841	1,115	1,586
f.ftk.res.2,5	0,2512448	0,3112736	0,412624	0,5867904
f.ftd.res2,5	0,167	0,208	0,275	0,391
MRd	0,226	0,280	0,371	0,528
VRdcf	2,261	2,801	3,714	5,281
VRd	28,445	28,985	29,897	31,465

Vertical	0,5 (orientation)	0,3 vol-%	0,75 vol-%	1 vol-%
Load	1,077	1,06	2,299	0,99
f.R3	0,345	0,339	0,736	0,317
f.ftk.res.2,5	0,1275168	0,125504	0,2722016	0,117216
f.ftd.res.2,5	0,085	0,084	0,181	0,078
MRd	0,115	0,113	0,245	0,105
VRdcf	1,148	1,130	2,450	1,055
VRd	27,331	27,313	28,633	27,239

Shear in the Eurocode, clause 6.2.2 (1)

CRdc	0,12	
d	135	0,9xh
k	2	
ρ	0,02	Assumed
f.ck	57	

1,16371382 >   vmin   0,41946153

V.Rdc   26,184   Non-reinforced

Changes within MO1, horizontal in the rest

30 degrees	0,3 vol-%	0,75 vol-%	1 vol-%
Load	4,637	32,058	33,742
f.R3	1,484	10,259	10,797
f.ftk.res.2,5	0,5490208	3,7956672	3,9950528
f.ftd.res2,5	0,366	2,530	2,663
MRd	0,494	3,416	3,596
VRdcf	4,941	34,161	35,955
VRd	31,125	60,345	62,139

45 degrees	0,3 vol-%	0,75 vol-%	1 vol-%
Load	7,5	9,33	32,549
f.R3	2,400	2,986	10,416
f.ftk.res.2,5	0,888	1,104672	3,8538016
f.ftd.res2,5	0,592	0,736	2,569
MRd	0,799	0,994	3,468
VRdcf	7,992	9,942	34,684
VRd	34,176	36,126	60,868

60 degrees	0,3 vol-%	0,75 vol-%	1 vol-%
Load	5,323	5,776	9,63
f.R3	1,703	1,848	3,082
f.ftk.res.2,5	0,6302432	0,6838784	1,140192
f.ftd.res2,5	0,420	0,456	0,760
MRd	0,567	0,615	1,026
VRdcf	5,672	6,155	10,262
VRd	31,856	32,338	36,445

Vertical	0,3 vol-%	0,75 vol-%	1 vol-%
Load	1,094	2,967	2,907
f.R3	0,350	0,949	0,930
f.ftk.res.2,5	0,1295296	0,3512928	0,3441888
f.ftd.res2,5	0,086	0,234	0,229
MRd	0,117	0,316	0,310
VRdcf	1,166	3,162	3,098
VRd	27,349	29,345	29,281

Appendix I

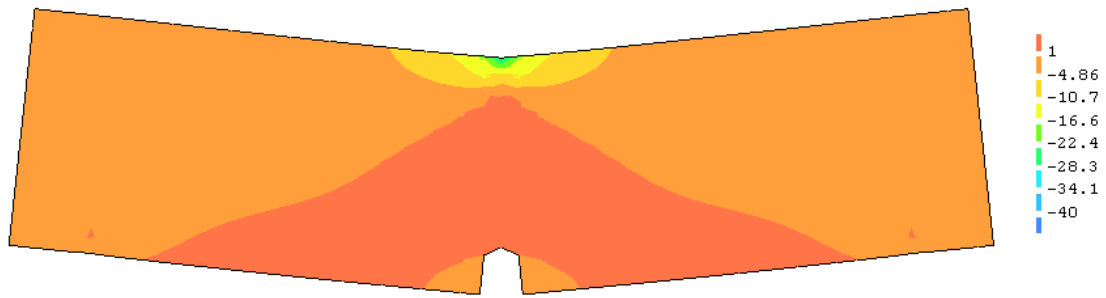# PLOT FROM FORCE-CONTROLLED ANALYSIS
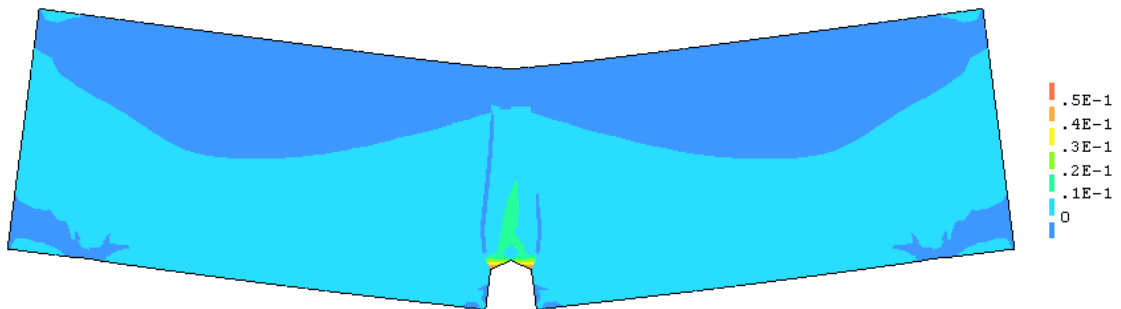
- Stress
- Strain

Figure I.1: Load step 80 - Force - Stress - σ_{xx}

Figure I.2: Load step 80 - Force - Strain ε_{xx}